

The hadronic final state at HERA

Paul R. Newman*

*School of Physics and Astronomy, University of Birmingham,
Birmingham B15 2TT, United Kingdom*

Matthew Wing†

*Department of Physics and Astronomy, University College London,
Gower Street, London WC1E 6BT, United Kingdom
and DESY, Notkestrasse 85, 22607 Hamburg, Germany*

(published 22 August 2014)

The hadronic final state in electron-proton collisions at HERA has provided a rich testing ground for development of the theory of the strong force, QCD. In this review, over 200 publications from the H1 and ZEUS Collaborations are summarized. Short distance physics, the measurement of processes at high-energy scales, has provided rigorous tests of perturbative QCD and constrained the structure of the proton as well as allowing precise determinations of the strong coupling constant to be made. Nonperturbative or low-energy processes have also been investigated and results on hadronization interpreted together with those from other experiments. Searches for exotic QCD objects, such as pentaquarks, glueballs, and instantons, have been performed. The subject of diffraction has been reinvigorated through its precise measurement, such that it can now be described by perturbative QCD. After discussion of HERA, the H1 and ZEUS detectors, and the techniques used to reconstruct differing hadronic final states, the above subject areas are elaborated on. The major achievements are then condensed further in a final section summarizing what has been learned.

DOI: [10.1103/RevModPhys.86.1037](https://doi.org/10.1103/RevModPhys.86.1037)

PACS numbers: 12.38.–t, 13.60.–r, 13.87.–a

CONTENTS

I. Introduction	1038	A. Charged-particle distributions	1060
II. Reconstruction of Final States at HERA	1039	B. Bose-Einstein correlations	1062
A. The H1 and ZEUS detectors	1039	C. Charm fragmentation	1062
B. Charged particles	1039	D. Inelastic J/ψ production	1063
C. Electrons, photons, and muons	1040	E. Exotic and unusual QCD	1064
D. Heavy flavor identification	1040	1. Pentaquark states	1065
E. Hadronic jets	1041	2. Instanton searches	1065
F. Photoproduction and DIS and how to tell them apart	1042	3. Search for glueball states	1066
G. Very-forward taggers	1043	4. Deuteron and antideuteron production	1066
H. Triggering	1043	V. Exclusive and Semi-inclusive Processes	1067
III. Hadronic Final States and Short Distance Physics	1043	A. Introduction	1067
A. Perturbative QCD theory of the hadronic final state	1044	B. Exclusive production of 1^{--} states	1069
B. Comparisons with data	1046	1. Kinematics and experimental selection	1069
1. Jet production	1046	2. General characteristics of vector meson production	1069
2. Jet substructure	1048	3. Vector meson production in QCD	1070
3. Prompt photon production	1049	4. Deeply virtual Compton scattering and generalized parton densities	1072
4. Heavy quark production	1050	5. Exclusive processes in dipole models and low- x saturation	1073
C. Extracting information from the data	1051	C. Inclusive diffractive dissociation	1073
D. Pushing the boundaries of applicability	1053	1. Kinematics and experimental selection of diffraction	1073
1. Higher orders	1054	2. Inclusive diffraction data	1074
2. New low- x phenomena	1055	3. Factorization studies	1075
3. Virtual photon structure	1056	4. Energy dependences and soft phenomenology	1076
4. The underlying event	1057	5. QCD phenomenology and diffractive parton densities	1077
5. Discussion	1058	6. Applications of diffractive parton densities	1078
E. Event shapes	1058	7. Limitations of diffractive parton densities	1080
IV. Nonperturbative Aspects and Hadronization	1060	8. Diffractive DIS in dipole models	1081

*p.r.newman@bham.ac.uk

†m.wing@ucl.ac.uk

D. Leading protons and neutrons beyond the Pomeron region	1081
E. Very hard diffraction and the BFKL Pomeron	1082
VI. Summary and Outlook	1083
Acknowledgments	1084
References	1084

I. INTRODUCTION

HERA (the Hadron Elektron Ringanlage) (Voss and Wiik, 1994) at the DESY laboratory in Hamburg, Germany, was, to date, the only example of a storage ring devoted to producing collisions between leptons and hadrons. It was located in a tunnel of length 6.3 km, housing two independent beam pipes, the first storing electrons or positrons, here generically referred to as electrons, and the second protons. In an initial phase of operation (HERA-I, 1992–2000), the electron beam energy was predominantly 27.5 GeV and the protons were at 820 GeV (1992–1997) or 920 GeV (1998–2000). In its second, higher-luminosity phase (HERA-II, 2002–2007), the electrons remained at the same energy, but were longitudinally polarized, and the proton energy also remained at 920 GeV except for the last few months, when lower energies (575 and 460 GeV) were used primarily for a measurement of the longitudinal proton structure function. Experiments were located at up to four points around the ring, of which this review is concerned with the two, H1 and ZEUS, where the electrons and the protons were brought to collision, yielding an ep center-of-mass energy $\sqrt{s} \leq 318$ GeV.

For the bulk of the kinematic region accessible at HERA, the electron-proton collisions proceed via the exchange of a photon, as shown in Fig. 1. The possible processes are conveniently subdivided into two categories according to the photon virtuality Q^2 . The region with $Q^2 \gg 1$ GeV² corresponds to the short distance deep inelastic scattering (DIS) regime, where the photon is usually considered as a structureless t -channel exchange. In contrast, in the “photo-production” regime $Q^2 \rightarrow 0$, the photon can be thought of

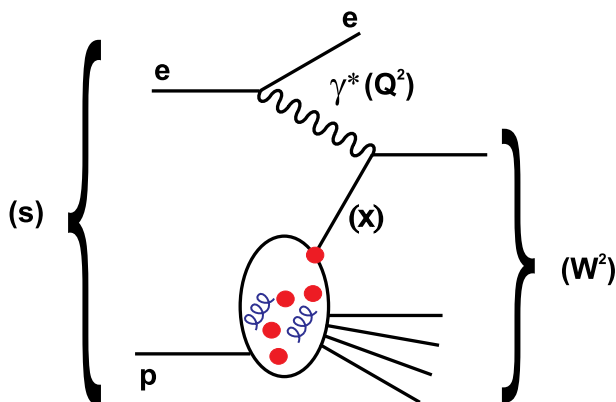


FIG. 1 (color online). Schematic illustration of a generic electron-proton DIS process, in which an exchanged photon of virtuality Q^2 couples to a quark carrying a fraction x of the proton’s longitudinal momentum. The electron-proton center-of-mass energy is denoted as \sqrt{s} and the photon-proton center-of-mass energy (equivalently the invariant mass of the hadronic final state) is denoted as W .

as a distinct object, decoupling from the electron well in advance of the proton target and interacting as a separate entity, often through its own partonic structure (see Sec. III.A). To a large extent, analyses at HERA have treated these two kinematic regions separately, although particularly where there are other hard scales in the problem, this is a largely artificial distinction.

Conventionally, the term “hadronic final state” is taken to mean the full final state after the removal of the scattered beam lepton and any electroweak radiation clearly associated with it. It therefore includes any further leptons or gauge bosons produced in the photon-proton interaction. As illustrated in Fig. 1, the invariant mass of the hadronic final state is denoted by W and is equivalent to the center-of-mass energy of the $\gamma^{(*)}p$ collision. Expressed in terms of the commonly used “inelasticity” invariant y , $W^2 \approx ys - Q^2$. When a hard scale is present, the photon couples to a single quark, which carries a fraction x of the proton’s momentum, where $x \approx Q^2/(sy)$ is the Bjorken variable. For a more formal introduction to deep inelastic scattering, see, for example, Devenish and Cooper-Sarkar (2004).

The asymmetric beam energies and near-hermetic instrumentation of the HERA experiments were well suited to the study of the hadronic final state over a wide range of W , Q^2 , and x values. These favorable kinematics allowed, for the first time, a detailed exploration of the dynamics of the excitations of a single hadron under a multitude of different circumstances. The vast majority of the processes under study are driven by the strong interaction, such that where hard scales are present, the theory of quantum chromodynamics (QCD) (Gross and Wilczek, 1973a, 1973b; Politzer, 1973, 1974) and our understanding of proton and photon structure were tested with unique precision. This has led to new insights and a deeper understanding of QCD in general, as well as providing the stimulus for ever-more sophisticated calculations.

HERA hadronic final state data provide a very wide range in the energy scale of the process. The softest processes are governed by hadronic mass scales of $\mathcal{O}(1)$ GeV. Increasing the scale from this starting point allows the closely controlled study of the transition from a regime which must be described in terms of hadronic objects to one which can be described perturbatively in terms of partons. At the other extreme, the highest transverse energy jets provide scales of $\mathcal{O}(100)$ GeV, resolving the structure of electron-parton interactions at the 10^{-18} m level. The corresponding kinematic range in the Bjorken variable is approximately $10^{-4} < x < 0.5$. Together with a new window on fragmentation and hadronization phenomena, these aspects of HERA data have provided a laboratory of unprecedented precision and kinematic range for the elucidation of the QCD dynamics of standard DIS processes, which has led to a vastly improved understanding of the structure of the proton and improved measurements of fundamental parameters of the standard model such as the coupling constant of the strong force.

Beyond the best understood domain, HERA data have provided access to new kinematic regions and processes with which to test QCD and extend the range of applicability of existing predictions. Many hadronic final-state problems have contained multiple hard scales, provided by large transverse momenta and heavy quark masses as well as Q^2 . Understanding

the delicate interplay between these different scales has provided exacting challenges to theory. In photoproduction, HERA data scan the transition from the classic ep scattering picture, where the photon interacts in a pointlike manner, to the situation where the photon interacts via its own distinct partonic structure, more reminiscent of hadron-hadron scattering, facilitating a controlled study of the differing characteristics of the two extremes. Diffractive and related processes in which the proton stays intact or converts to a neutron via a charge-exchange reaction imply more complex interactions in which no net color is exchanged. HERA has provided an explosion of precise and eclectic measurements of these hard exclusive and semi-inclusive processes with cleanly identified experimental signatures, leading to a detailed understanding in the framework of QCD. As discussed and illustrated in more detail in the following, the multitude of hadronic final-state processes studied in ep collisions at HERA has thus led to something of a revolution in the development and testing of QCD.

II. RECONSTRUCTION OF FINAL STATES AT HERA

A. The H1 and ZEUS detectors

To visualize the physics processes and reconstruction requirements, displays of a neutral and a charged current DIS event are shown in Fig. 2 for the ZEUS (ZEUS Collaboration, 1993) and H1 (Abt *et al.*, 1997a, 1997b) detectors, respectively. In a neutral current event, where a photon, or at high Q^2 a Z^0 , is exchanged, a deposit of energy in the calorimeter consistent with an electron, matched to a track, can be seen back to back in azimuth with a hadronic jet. In a charged current event, where a W^\pm is exchanged, there is no activity to balance the hadronic jet, indicating the presence of an undetected neutrino. The figures also show the key parts of the central detectors. In both cases, the electron beam enters the detector from the left and the proton beam from the right; due to the significantly larger energy of the protons there is more instrumentation in the direction of the outgoing proton beam.¹

Other than the forward-backward asymmetry in instrumentation, the detectors were similar to other general-purpose detectors at high-energy colliders such as those at LEP, the Tevatron, and the LHC. Both H1 and ZEUS detectors had microvertex detectors for measuring weak decays, surrounded by a central drift chamber for the precise tracking of charged particles. Forward and rear tracking detectors gave additional charged-particle information with the rear detectors particularly useful for measuring low-angle scattered electrons at small Q^2 where the DIS cross section is largest. Beyond the tracking detectors were calorimeters in which a single technology was used for the ZEUS detector with the H1 detector also including a dedicated higher-precision electron

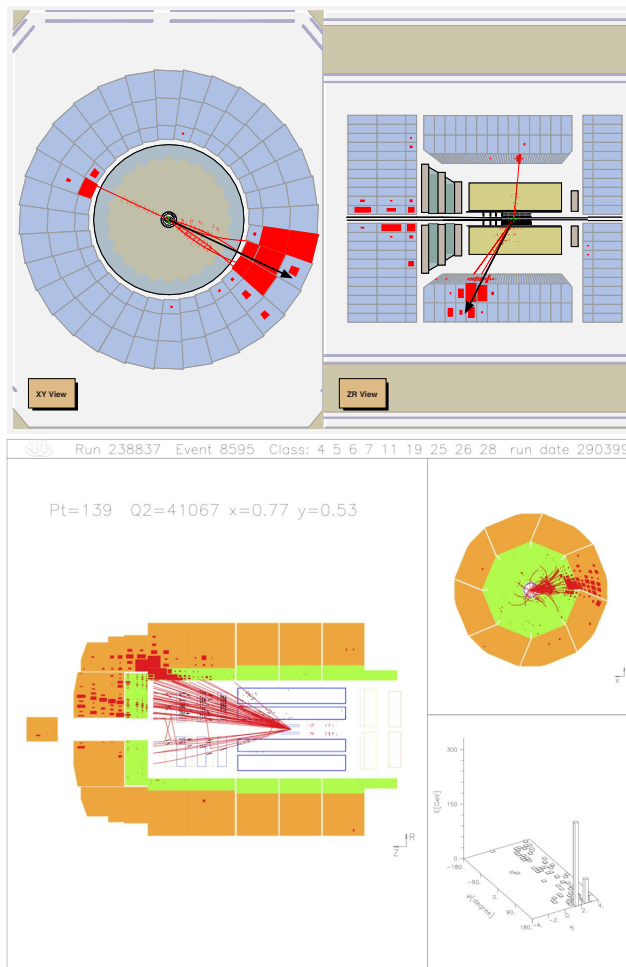


FIG. 2 (color online). Event displays of the (top) ZEUS and (bottom) H1 detectors showing a neutral current and a charged current DIS event, respectively.

calorimeter in the rear direction. Finally, large muon detectors surrounded the calorimeters. Further, smaller detectors with dedicated purposes, such as for electron or proton tagging, were placed along the beam pipe in both directions. These detectors are described in the context of hadronic final-state reconstruction methods in Secs. II.B–II.H.

B. Charged particles

Tracks from charged particles were primarily reconstructed by cylindrical drift chambers surrounding the interaction point: central jet chambers (CJC1 and CJC2) (Burger *et al.*, 1989; Abt *et al.*, 1997a, 1997b) in H1 and the central tracking detector (Harnew *et al.*, 1989; Foster *et al.*, 1993, 1994) in ZEUS. These were supplemented by silicon vertex detectors (Eick *et al.*, 1997; Pitzl *et al.*, 2000; Polini *et al.*, 2007) placed between the beam pipe and the drift chambers and in front of forward and rear tracking devices. The H1 and ZEUS drift chambers covered polar-angle regions of $20^\circ < \theta < 160^\circ$ and $15^\circ < \theta < 164^\circ$, respectively, and were operated in uniform axial magnetic fields of 1.16 and 1.43 T. The high magnetic fields ensured excellent charge separation up to about 20 GeV. The tracking resolutions were both $\sigma(p_T)/p_T \approx (0.002 - 0.003)p_T$, with p_T in GeV.

¹A right-handed Cartesian coordinate system is used throughout this review, with the Z axis pointing in the proton beam direction, referred to as the “forward” direction, and the X axis pointing toward the center of HERA. The coordinate origin is at the nominal interaction point. The pseudorapidity is defined as $\eta = -\ln[\tan(\theta/2)]$, where the polar angle θ is measured with respect to the proton-beam direction.

Pulse height measurements from the sense wires were also used to calculate the specific energy loss due to ionization dE/dx . The resolutions of the dE/dx measurements for well-reconstructed tracks were under 10% (Steinhart, 1999; Bartsch, 2007). The dE/dx measurements were used as a method of particle identification, using likelihood tests to distinguish between electrons, pions, kaons, protons, and deuterons.

C. Electrons, photons, and muons

Both detectors had large general-purpose sampling calorimeters which covered most of the solid angle for the measurement of electromagnetic (EM) objects. The H1 Collaboration had a finely segmented liquid argon (LAr) (Andrieu *et al.*, 1993) calorimeter with a lead or stainless steel absorber, complemented by a lead-scintillating fiber spaghetti calorimeter (SpaCal) (Appuhn *et al.*, 1997) which covered polar-angle ranges of $4^\circ < \theta < 153^\circ$ and $153^\circ < \theta < 177^\circ$, respectively. Under test beam conditions, the energy resolutions were $\sigma(E)/E \approx 11\%/\sqrt{E}$ and $\approx 7\%/\sqrt{E}$ for electrons in the LAr calorimeter and SpaCal, respectively, with E in GeV. The ZEUS detector had a uranium-scintillator calorimeter (Andresen *et al.*, 1991; Derrick *et al.*, 1991; Caldwell *et al.*, 1992; Bernstein *et al.*, 1993) which covered a polar-angle range of $2.5^\circ < \theta < 178.5^\circ$. Under test beam conditions, the single-particle energy resolution for the ZEUS calorimeter was $18\%/\sqrt{E}$ for electrons, with E in GeV.

One of the primary design considerations of the experiments was the accurate reconstruction of the scattered electrons, which should display the signature of isolated high-energy deposits in the EM calorimeter. Various requirements were made on the EM clusters and the isolation, usually including a matching of the clusters of energy to a charged-particle track, such that DIS events were selected with high purity and high efficiency (Abramowicz, Caldwell, and Sinkus, 1995; Glazov, 1998). A typical minimum energy requirement on the scattered electron was 10 GeV for the H1 LAr and ZEUS calorimeters and 6.5 GeV for the SpaCal. In order to make the best measurements of the longitudinal structure function at high y , these minimum energy requirements were reduced in dedicated analyses to 3.4 GeV (Aaron *et al.*, 2008c) in the SpaCal and 6 GeV (Chekanov *et al.*, 2009h) in the ZEUS calorimeter.

The variables Q^2 , x , and y can be reconstructed from the energy and polar angle of the scattered electron only, using the so-called “electron method,” which arises from simple consideration of the DIS kinematics. Several other reconstruction methods exist which make use of combinations of the measurements of the scattered electron and the hadronic final state (Jacquet and Blondel, 1979; Bentvelsen, Engelen, and Kooijman, 1992; Hoeger, 1992; Bassler and Bernardi, 1995). The reconstruction method used depends on the analysis and the regions in which particles are measured; e.g., for charged current events where there is no isolated high-energy electron, the Jacquet-Blondel method was used. Typical relative resolutions in Q^2 were between about 2% and 10%, depending on the reconstruction method.

Photon candidates, typically above 5 GeV in transverse energy, were identified in the central calorimeters by

reconstructing narrow clusters in the EM calorimeter with no track pointing to them. Backgrounds from π^0 and η particles were removed by considering the shape of the cluster and of the calorimeter shower; example quantities were the transverse radius of the cluster and the ratio of the highest energy EM cell to the total cluster energy (Aaron *et al.*, 2010i; Chekanov *et al.*, 2010d). Photons of lower energy could be identified in Compton scattering processes ($ep \rightarrow e\gamma p$) in which the final state consists only of the photon, an electron, and a lack of hadronic activity.

Muons were identified by a combination of tracking, calorimetry, and the large muon chambers surrounding the calorimeters. Depending on the given analysis and kinematic cuts and whether a highly pure or highly efficient sample was required, different algorithms were used to combine information from the various subdetectors. Wherever possible, a track matched with a muon signature in another subdetector was used for the momentum measurement. A minimum ionizing particle (mip) signal in the calorimeters was also used as a high efficiency, but low purity, signal for a muon. Finally, the clearest signal for a muon was provided by the muon chambers. In the case of H1, the return yoke of the magnetic coil was the outermost part of the detector and was equipped with streamer tubes forming the central muon detector (Abt *et al.*, 1997b) and tail catcher ($4^\circ < \theta < 171^\circ$). In the forward region ($3^\circ < \theta < 17^\circ$), a set of drift chamber layers formed the forward muon detector (Biddulph *et al.*, 1994), which allowed a momentum measurement, together with an iron toroidal magnet. The ZEUS central and rear muon chambers (Abbiendi *et al.*, 1993) consisted of limited-streamer tube chambers placed behind the calorimeter, inside and outside a magnetized iron yoke, covering a polar-angle region of $34^\circ < \theta < 171^\circ$. The forward muon detector (Abbiendi *et al.*, 1993) consisted of six trigger planes of limited-streamer tubes and four planes of drift chambers covering the angular region $5^\circ < \theta < 32^\circ$. The efficiency of muon reconstruction depended on the method used, with the detection of a mip signal having almost 100% efficiency and isolated muons above 2 GeV being detected 90% and 55% of the time in the H1 and ZEUS muon systems, respectively (Aaron *et al.*, 2009g).

D. Heavy flavor identification

As in other high-energy physics experiments, heavy quarks were identified by several means such as reconstructing a given meson mass, requiring a large momentum of a lepton perpendicular to the axis of an associated jet, or reconstructing displaced vertices using a silicon detector placed close to the interaction point.

All ground state charm mesons have been reconstructed by combining tracking information from potential decay products. When only considering this information and no further particle identification or measurements of secondary vertices, the decay $D^* \rightarrow D^0 \pi_s \rightarrow K \pi \pi_s$ has the purest signal; an example is shown in Fig. 3. No beauty mesons have been fully reconstructed due to the significantly smaller statistical sample.

Before the use of silicon microvertex detectors, the principal way to identify beauty events was to reconstruct leptons

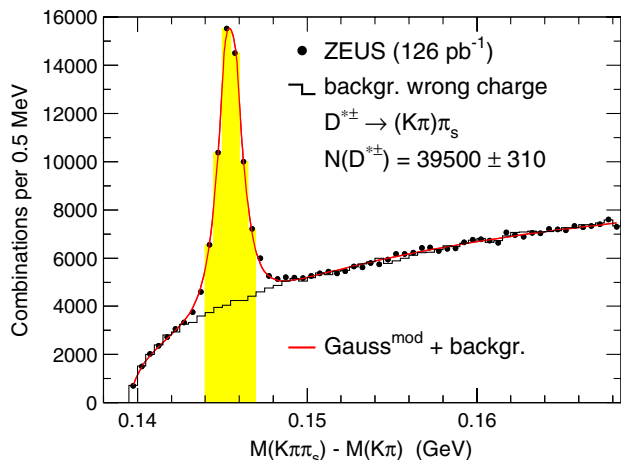


FIG. 3 (color online). The distribution of the mass difference $m(D^*) - m(D^0)$ for D^* candidates and a background estimate. From Chekanov *et al.*, 2009i.

and measure their momentum p_T^{rel} perpendicular to the axis of an associated jet. This gave a large sample due to a 10% branching ratio which is much higher than any given meson's branching fraction to easily usable hadronic decays. Because of the quark's larger mass, leptons from beauty decays are concentrated at higher values of p_T^{rel} than leptons from charm decays or in events initiated by light quarks. Typical purities achieved for beauty events by this method were about 20%.

The reconstruction of secondary vertices, using a microvertex detector, from the weak decay of heavy quarks, provides a method for tagging charm and beauty with high efficiency or, by applying stringent requirements, with high purity. The H1 central silicon tracker (Pitzl *et al.*, 2000) consisted of two layers of double-sided silicon strips, covering an angular range of $30^\circ < \theta < 150^\circ$ for tracks passing through both layers. The ZEUS microvertex detector (MVD) (Polini *et al.*, 2007) consisted of barrel (BMVD) and forward (FMVD) sections with, respectively, three cylindrical layers and four vertical planes. The BMVD provided polar-angle coverage for tracks with three measurements from 30° to 150° . The FMVD extended the coverage to 7° . A commonly used variable is the impact parameter δ of a track which is the transverse distance of closest approach of the track to the primary vertex; see Fig. 4. If the angle α is less than 90° , δ is defined as positive; otherwise, δ is defined as negative. Negative values only arise due to imperfect resolution and hence events initiated by light quarks are symmetric about $\delta = 0$. An asymmetry to high positive values occurs due to heavy quark decays. A more powerful discriminator is the significance S_L at which the transverse distance between the primary and secondary vertices L_{xy} is nonzero. Thus S_L is defined as $L_{xy}/\sigma(L_{xy})$, where $\sigma(L_{xy})$ is the uncertainty on L_{xy} . An example distribution is shown in Fig. 5, where a strong asymmetry is observed.

To achieve the most precise measurements for beauty and also charm production, the above and other discriminating variables were combined in a neural network (Aaron *et al.*, 2010h) or a discriminating test function (Chekanov *et al.*, 2008a).

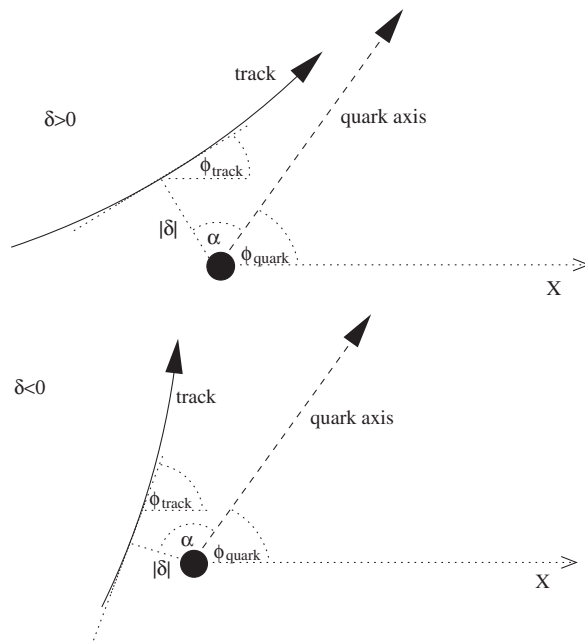


FIG. 4. Diagrams of a track in the X - Y plane. The direction of the struck quark, experimentally approximated as a jet axis, is used to define the impact parameter δ .

E. Hadronic jets

In the first results on jet production from H1 and ZEUS, jets were reconstructed from the calorimeter cells using the JADE clustering (Bartel *et al.*, 1986; Bethke *et al.*, 1988) or cone algorithms. Because of the theoretical problems with cone algorithms, such as ambiguity in the seed finding and overlapping jets, both collaborations switched to the inclusive k_T clustering algorithm (Catani *et al.*, 1993; Ellis and Soper, 1993) for the vast majority of their publications.

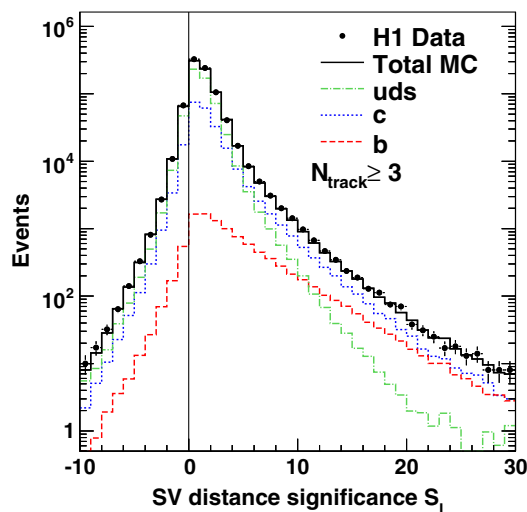


FIG. 5 (color online). Distribution of the significance at which the transverse distance between the primary and secondary vertices is nonzero. Included is a decomposition of the data by fitting Monte Carlo templates for light, c , and b quarks. From Aaron *et al.*, 2010h.

Calorimeter cells alone have continued to be used for some publications, due to the finer granularity achieved in the forward parts of the detector compared with the results of using some preclustering before the jet finding. However, energy flow objects (EFOs) have also been in common use by both collaborations. These objects are based on an algorithm which combines tracking and calorimeter information in order to optimize the resolution. In a typical jet at HERA, the amount of tracking information used, and hence the improvement in the jet energy resolution when including tracks, is about 10%–20%. In certain situations, when several tracks are explicitly reconstructed in a jet, such as a heavy flavor meson (Chekanov *et al.*, 2009g), the fraction of tracking information used in the EFO input to a jet reaches about 50% and leads to a significant reduction in the systematic uncertainties such as that due to the calorimeter hadronic energy scale.

The single-hadron energy resolutions, as measured in test beams, are $\sigma(E)/E \approx 50\%/\sqrt{E} \oplus 2\%$ and $35\%/\sqrt{E}$, with E in GeV, for the H1 and ZEUS calorimeters, respectively. A detailed parametrization of the jet energy resolution has not been performed. However, a transverse energy resolution of 9% has been achieved at H1 for $E_T^{\text{jet}} > 25$ GeV (Caron, 2002) and at ZEUS for $E_T^{\text{jet}} > 14$ GeV (Chekanov *et al.*, 2002a).

The precision of initial measurements of jet cross sections was limited by the uncertainty in the relative jet energy scale between data and Monte Carlo simulations. Since the cross section falls rapidly with increasing energy, a 1% uncertainty in the determination of the scale led to about a 5% uncertainty in the cross section. Therefore, a reduction in the energy scale uncertainty from initial estimates of about 5% (25% uncertainty in the cross section) was necessary to be able to fully exploit the data, for example, in precise extractions of parton densities or the strong coupling constant (see Sec. III.C).

In order to precisely determine the hadronic jet energy scale, various methods were employed by, e.g., using tracking information in a jet or cross-calibrating jets reconstructed in different parts of the calorimeters. However, the use of neutral current DIS events provided the most powerful calibration tool based on the momentum balance between an outgoing jet and the scattered electron. This relied on an accurate reconstruction of the electron and a precise determination of the EM energy scale uncertainty. For the most precise calibrations, closely related techniques exploiting the double-angle kinematic reconstruction method (Bentvelsen, Engelen, and Kooijman, 1992; Hoeger, 1992) were employed. The differences between the jet and electron transverse energies for data and Monte Carlo simulations are shown for the ZEUS data in Fig. 6 versus the pseudorapidity and transverse energy of the jet. This demonstrates that the uncertainty on the determination of the jet energy scale is 1% (Chekanov *et al.*, 2002a, 2002d; Wing, 2002). H1 followed similar procedures and achieved an uncertainty of 1.5% (Aktas *et al.*, 2006h).

F. Photoproduction and DIS and how to tell them apart

Results from HERA are often (somewhat arbitrarily) classified as pertaining to either photoproduction or DIS. In a DIS event, the exchanged photon is virtual, with a

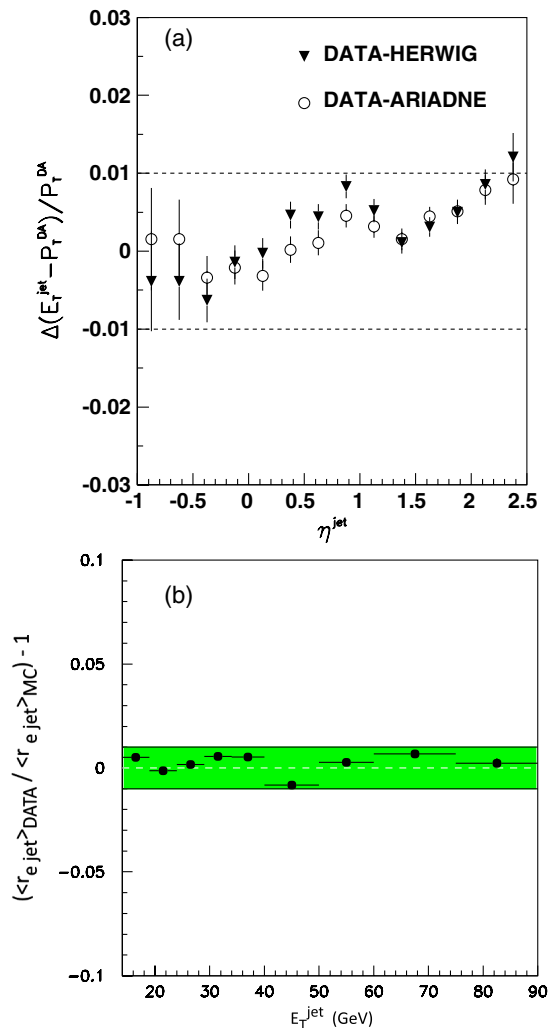


FIG. 6 (color online). ZEUS jet energy scale uncertainty as a function of (a) η^{jet} and (b) E_T^{jet} , showing that the scale is known to 1%. In (a), the relative difference between the hadronic jet transverse energy E_T^{jet} and the transverse momentum of the scattered electron, calculated using the double-angle method P_T^{DA} is shown as a function of the jet pseudorapidity η^{jet} . In (b), the relative difference between the data and Monte Carlo simulation is shown for the quantity $\langle r_{e\text{jet}} \rangle$ as a function of the jet transverse energy, where $r_{e\text{jet}}$ is the ratio of the jet to electron transverse energies.

squared four momentum typically larger than about 1 GeV^2 , and a high-energy scattered electron observed in the main calorimeters. Photoproduction is usually defined by the absence of the scattered electron in the main calorimeters, implying a virtuality $Q^2 < 1 \text{ GeV}^2$ and a median value of $10^{-4} - 10^{-3} \text{ GeV}^2$. The value of 1 GeV^2 is operational and depends on the exact coverage of the calorimeter. In photoproduction, the photon is quasisreal and the concept of a photon structure is introduced.

Small calorimeters were placed along the direction of the outgoing electron beam at distances up to 40 m from the interaction point; see Fig. 7. These were used to tag the electrons in photoproduction events over a narrower range in Q^2 and y . For example, in the case of the H1 calorimeter at $Z = -33$ m, values of Q^2 were smaller than 0.01 GeV^2 and

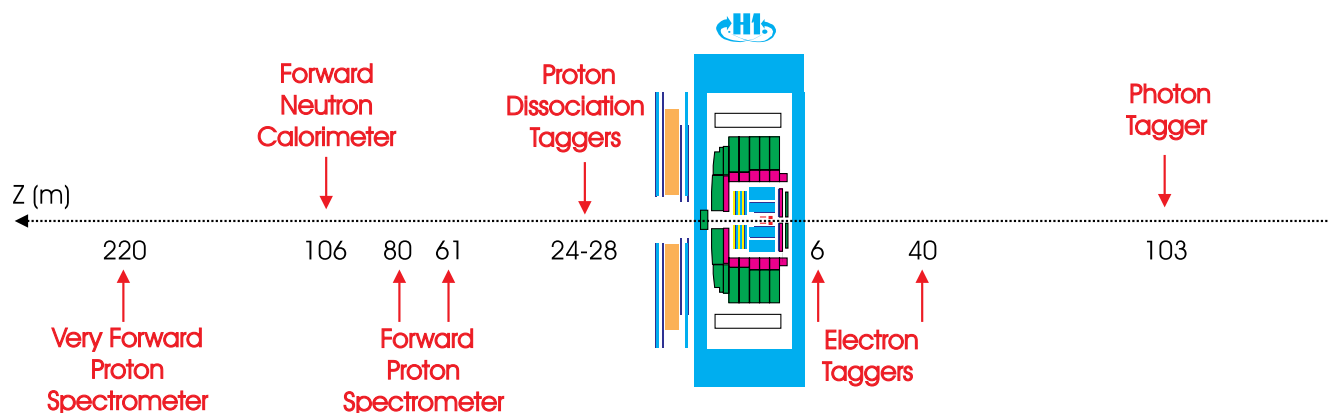


FIG. 7 (color online). Schematic illustration of the beam line instrumentation for the example of the H1 experiment. The detector components shown are all described in the text with the exception of the 103 m photon tagger which was used for luminosity determination via the Bethe-Heitler $ep \rightarrow e\pi\gamma$ process and the proton dissociation taggers which were used to identify forward rapidity gaps (see Sec. V).

the acceptance range was approximately $0.3 < y < 0.7$. This naturally led to smaller samples compared with those obtained via the antitag of an electron in the main calorimeters, but improved the reconstruction resolution.

G. Very-forward taggers

Both experiments had very-forward particle taggers to detect low-angle protons and neutrons, particularly for measurements of diffractive production (see Sec. V).

The H1 forward proton spectrometer (FPS) (Adloff *et al.*, 1999d; Van Esch *et al.*, 2000) and ZEUS leading proton spectrometer (LPS) (Derrick *et al.*, 1997) detected positively charged particles carrying a substantial fraction of the incoming proton energy. The particle trajectories were measured using a system of detectors that could be inserted very close (typically a few mm) to the proton beam, positioned between 64 and 80 m and 24 and 90 m from the interaction point for the FPS and LPS, respectively. The leading proton detectors approached the beam in both the horizontal and vertical planes, with complementary acceptances in scattered proton energy. Despite providing a pure sample of protons, the acceptance was only around 2%. The effective transverse momentum resolution was dominated by the intrinsic transverse momentum spread of the proton beam at the interaction point, which was about 40–45 MeV in the horizontal plane and about 100 MeV in the vertical plane.

Both H1 and ZEUS had forward neutron calorimeters (Bhadra *et al.*, 1995, 1997a, 1997b; Adloff *et al.*, 1999d) installed in the HERA tunnel at $\theta = 0$ and at $Z = 106$ m from the interaction point in the proton-beam direction. Both devices consisted of a main calorimeter, with hadronic energy resolution of $\sigma(E)/E \approx (60 - 70)\%/\sqrt{E}$, with E in GeV, supplemented by a preshower calorimeter in the case of H1 and a scintillator hodoscope in the case of ZEUS. The forward neutron calorimeters had a limited angular coverage, being sensitive to neutrons of less than about 0.05° or 0.8 mrad. Both devices achieved spatial resolutions of about 2 mm.

Figure 7 shows an illustration, for the example of the H1 experiment, of the layout of the additional components along the beam line in both directions away from the main detector.

H. Triggering

Both H1 (Sefkow *et al.*, 1995; Nicholls *et al.*, 1998; Baird *et al.*, 2001) and ZEUS (Smith, Tokushuku, and Wiggers, 1992; Allfrey *et al.*, 2007) experiments mainly used a three-level trigger system of progressive sophistication in order to select the most interesting events on-line and remove background from beam-gas interactions and low-energy ep collisions in which additional statistics would not improve any measurement. The H1 trigger consisted of two hardware levels and a software filter farm, whereas ZEUS had one hardware level and two software filters. The first two levels often considered simple energy sums in the calorimeter or the reconstructed vertex position. At the third level, a simplified and fast version of much of the offline reconstruction code, such as jet and tracking algorithms, was used. From a nominal HERA bunch crossing rate of 10 MHz, the trigger system reduced the rate such that data were written to storage at a rate of ≈ 10 Hz.

Trigger filters which selected events with a high-energy electron candidate were very efficient selectors of DIS events. Because of bandwidth restrictions, these were often prescaled or were combined with additional requirements, such as a jet or a reconstructed meson in the event, depending on the physics motivation. Several hundred different combinations of triggers existed to try and cover all interesting physics channels, while remaining within the limits dictated by data transfer rates and processing speeds.

The principal trigger chains in the H1 and ZEUS experiments, in terms of both bandwidth and frequency of use in physics analyses, were designed to select inclusive DIS and jet events. The information to select an electron or jet candidate was often supplemented in the trigger with tracking information and, in the case of the photoproduction selection at H1, with an electron tag in the beam-pipe calorimeters.

III. HADRONIC FINAL STATES AND SHORT DISTANCE PHYSICS

In this section, measurements are presented which characterize the hadronic final state in the presence of a hard scale,

typically the virtuality Q^2 of the exchanged boson, the transverse energy of a jet, or the mass of a heavy quark in the event. A high or hard scale implies that the reaction occurs at short distance and hence allows perturbative calculations to be performed. Almost all processes and cross sections at HERA, both DIS and photoproduction, involving a jet of high transverse energy or a heavy quark have been calculated in the DGLAP (Gribov and Lipatov, 1972; Lipatov, 1975; Altarelli and Parisi, 1977; Dokshitzer, 1977) approximation to next-to-leading order (NLO) in QCD perturbation theory. In many cases, several different approaches to the NLO QCD calculations are available for a given process and input parameters such as the strong coupling constant can also be varied. Comparisons between the calculations and with data have led to improvements in the predictions. Various other approximations to QCD are also available which emphasize different aspects of parton cascade dynamics and evolution. These include the Balitsky-Fadin-Kuraev-Lipatov (BFKL) (Kuraev, Lipatov, and Fadin, 1976, 1977; Balitsky and Lipatov, 1978) and Ciafalini-Catani-Fiorani-Marchesini (CCFM) (Ciafaloni, 1988; Catani, Fiorani, and Marchesini, 1990a, 1990b; Marchesini, 1995) approaches. A thorough review of non-DGLAP predictions of standard short distance processes is not carried out here since NLO corrections are not usually available. However, these approaches are considered later in the context of low- x physics (Sec. III.D) and diffraction (Sec. V).

Measurements of jet and heavy flavor production are directly sensitive to the gluon density in the proton and have hence been used in QCD fits to constrain the parton densities in the proton. Heavy quark data in DIS are also used to extract the beauty $F_2^{b\bar{b}}$ and charm $F_2^{c\bar{c}}$ contributions to the proton structure F_2 . These results are reviewed in detail elsewhere (Klein and Yoshida, 2008; Perez and Rizvi, 2013). Measurements of photoproduction are also sensitive to the structure of the photon and the data can in principle be used in fits to constrain the parton densities in the photon. A more detailed review of photoproduction and its constraints on photon structure can also be found elsewhere (Butterworth and Wing, 2005); however, new results since that review are discussed here.

A. Perturbative QCD theory of the hadronic final state

A brief description of perturbative QCD (pQCD) related to the hadronic final state is given in this section. More detailed accounts can be found elsewhere (Brock *et al.*, 1995; Ellis, Stirling, and Webber, 2003; Dissertori, Knowles, and Schmelling, 2003).

Given that the lowest order DIS process, a quark-parton model (QPM) event (see Fig. 1), contains a scattered electron recoiling against a jet, it may seem trivial to describe jet cross sections in DIS. However, once the sizable phase space for parton radiation is considered in the context of the wide range of possible jet algorithms, the situation becomes far more subtle. Jet cross sections are generally presented in the Breit frame (Feynman, 1972; Streng, Walsh, and Zerwas, 1979) in which the exchanged virtual boson is purely spacelike, with 3-momentum $q = (0, 0, Q)$, and is collinear with the incoming parton, such that QPM events do not contribute at large

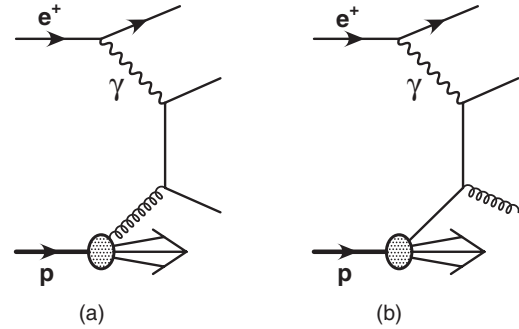


FIG. 8. (a) Boson-gluon-fusion and (b) u -channel QCD Compton processes. Along with s -channel QCD Compton scattering, these are the LO QCD processes in DIS and direct photoproduction, i.e., the lowest order process involving at least one power (or vertex) of α_s .

transverse energies. Therefore leading-order (LO) QCD processes dominate jet cross sections in DIS (see Fig. 8).

From the diagrams, it can be seen that the boson-gluon-fusion process is related to the gluon density in the proton. This is dominant at low Q^2 , where low- x partons are most important, whereas the QCD Compton process becomes more important with increasing Q^2 since it is related to the quark density in the proton. Measurements of jet cross sections are therefore sensitive to the strong coupling constant α_s . When combined with inclusive DIS cross-section measurements, they allow its precise extraction simultaneously with the parton densities in the proton, as discussed in Sec. III.C. This can be seen from a general schematic formula for perturbative QCD calculations of DIS jet processes:

$$d\sigma_{ep \rightarrow e + \text{jets} + X} = \sum_a \int_0^1 d\hat{\sigma}_{ea \rightarrow cd}(x, \alpha_s(\mu_R), \mu_F, \mu_R) f_{a/P}(x, \mu_F) dx, \quad (1)$$

where the sum is over the possible partons a in the proton given by the parton density function (PDF) $f_{a/P}$. The factorization and renormalization scales are denoted by μ_F and μ_R and may be given by $\sqrt{Q^2}$, the jet transverse energy, or a combination of the two. The short distance cross section $d\hat{\sigma}_{ea \rightarrow cd}$ depends on x , the strong coupling, α_s , μ_F , and μ_R .

In photoproduction, where the electron escapes detection and continues down the beam pipe, the virtuality Q^2 is low and the hard scale is given instead by the transverse energy of the jets. The diagrams shown in Fig. 8 also apply to the LO direct jet photoproduction process where direct-photon events are classified as those in which all of the photon's momentum participates in the hard interaction. Equation (1) is modified to

$$d\sigma_{ep \rightarrow e + \text{jets} + X} = \sum_a \int_0^1 d\hat{\sigma}_{\gamma a \rightarrow cd}(x, \alpha_s(\mu_R), \mu_F, \mu_R) f_{\gamma/e} f_{a/P}(x, \mu_F) dx, \quad (2)$$

where the term $f_{\gamma/e}$ represents the probability of the electron radiating a photon and is given by the Weizsäcker-Williams

formula (Williams, 1934; von Weizsacker, 1934; Frixione *et al.*, 1993). Another class of events, resolved-photon processes, also contribute to the photoproduction cross section. At LO, such processes are classified as those in which only a fraction of the photon's momentum participates in the hard interaction. For such events, the photon can be considered as developing a structure, the parton densities of which are probed by the hard scale of the interaction. This means that the ep collision can be viewed as a hadron-hadron collision in which partons from both the photon and the proton participate in the hard process. Therefore many extra diagrams contribute in LO QCD to the photoproduction cross section; an example is shown in Fig. 9, in which a quark from the photon collides with a gluon from the proton.

A general schematic formula for perturbative QCD calculations of photoproduction processes is given by

$$d\sigma_{ep \rightarrow e + \text{jets} + X} = \sum_{a,b} \int_0^1 dx_\gamma \int_0^1 dx_p f_{\gamma/e} f_{b/\gamma}(x_\gamma, \mu_{F\gamma}) f_{a/p}(x_p, \mu_{Fp}) d\hat{\sigma}_{ab \rightarrow cd}(x_\gamma, x_p, \alpha_s(\mu_R), \mu_{F\gamma}, \mu_{Fp}, \mu_R), \quad (3)$$

where x_p and x_γ are the longitudinal momentum fractions of the parton a in the proton and the parton b in the photon, respectively. The term $f_{a/p}$ ($f_{b/\gamma}$) represents the PDFs of partons with flavor a (b) in the proton (photon). The factorization scale for the proton (photon) is denoted by μ_{Fp} ($\mu_{F\gamma}$), and μ_R is the renormalization scale. The factorization and renormalization scales are often assumed to have the same value in calculations, although this is not necessarily the case and hence for generality, they are here treated separately. The term $d\hat{\sigma}_{ab \rightarrow cd}$ is the hard (partonic) cross section. In the case where parton b is the entire photon, $f_{b/\gamma}(x_\gamma, \mu_{F\gamma})$ is $\delta(1 - x_\gamma)$ and Eq. (3) describes direct photoproduction and reduces to Eq. (2).

The separation between resolved and direct processes has more to do with the limitations of our ability to calculate QCD cross sections than with fundamental physics. The separations are not unique beyond LO. For example, the LO resolved-photon process in Fig. 9 can also be considered as a direct-photon process in NLO QCD. Nevertheless, the labels “direct” and “resolved” are useful tools for exploring the world of photon physics.

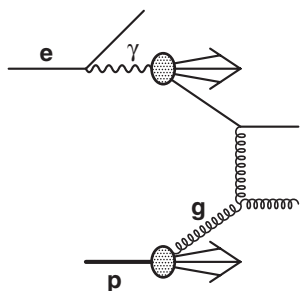


FIG. 9. An example of a LO resolved jet photoproduction process, containing a hard scattering between a quark from the photon and a gluon from the proton.

The NLO corrections for the production of two hard partons at HERA, in both photoproduction and DIS, were calculated in the 1990s (see below), thereby allowing comparisons with inclusive-jet and dijet measurements, by applying a jet algorithm to the partons in the final state of an NLO parton-level event generator. These NLO QCD calculations generally give an accurate prediction of the normalization and the shapes of basic kinematic distributions. However, in order to compare with observables measurable from the data, corrections for hadronization using Monte Carlo models are necessary. A multiplicative hadronization correction factor is determined from the ratio of the cross sections at the hadron and parton levels in the Monte Carlo simulation. As the simulations are based only on LO matrix elements with parton showering, their applicability is questionable. However, some level of control over the procedure can be assured by checking the compatibility of the dependences on important variables such as jet transverse energy and angle between the NLO calculation and the parton-level Monte Carlo simulation. For some event properties and kinematic configurations, the NLO QCD calculations are not very reliable, due to the fact that they allow at most one parton to be radiated in addition to the primary jet pair. Calculations at the next order, next-to-next-to-leading order (NNLO) in QCD (Jimenez-Delgado and Reya, 2009; Martin *et al.*, 2009; Alekhin *et al.*, 2010), have been performed for inclusive DIS but not with final-state objects such as jets or heavy quarks present.

In DIS, NLO QCD calculations are available for the production of jets in neutral current (Mirkes and Zeppenfeld, 1996; Catani and Seymour, 1997; Graudenz, 1997; Potter, 1999; Nagy and Trocsanyi, 2001) and charged current (Mirkes and Zeppenfeld, 1996) processes. The NLO corrections have also been calculated for $2 \rightarrow 3$ scattering (i.e., three-jet cross sections) in DIS (Nagy and Trocsanyi, 2001) and can in principle be extended to photoproduction. Inclusive hadron production has also been calculated to NLO (Kniehl, Kramer, and Potter, 2000; Kretzer, 2000; Albino, Kniehl, and Kramer, 2005; de Florian, Sassot, and Stratmann, 2007a, 2007b; Albino, Kniehl, and Kramer, 2008), whereas prompt photon production has been calculated to $\mathcal{O}(\alpha^3)$ (Gehrmann-De Ridder, Kramer, and Spiesberger, 2000; Gehrmann-De Ridder, Gehrmann, and Poulsen, 2006a, 2006b).

In photoproduction, NLO QCD calculations are available for the production of jets (Gordon and Storrow, 1992; Frixione, Kunszt, and Signer, 1996; Frixione, 1997; Frixione and Ridolfi, 1997; Harris and Owens, 1997; Klasen and Kramer, 1997; Aurenche *et al.*, 2000), hadrons (Binnewies, Kniehl, and Kramer, 1995; Fontannaz, Guillet, and Heinrich, 2002), and prompt photons (Gordon and Storrow, 1994; Fontannaz, Guillet, and Heinrich, 2001; Krawczyk and Zembruski, 2001; Zembruski and Krawczyk, 2003; Fontannaz and Heinrich, 2004).

The above perturbative calculations all require some choices of input parameters and also need to be corrected for hadronization, which lead to uncertainties in the predictions. The renormalization and factorization scales, the proton and photon PDFs, the value of α_s , and, where appropriate, fragmentation functions all need to be chosen. The uncertainties are usually dominated by varying the renormalization

scale by a factor of 2. However, they vary depending on the phase space and distribution measured; the precision of the predictions are discussed where appropriate in Sec. III.B. It should be noted that the scale variation by a factor of 2 is merely convention and bears no relation to, e.g., a one-sigma uncertainty. This should therefore be treated with caution. In one example fit to data (Chekanov *et al.*, 2005a), the variation produced unacceptable χ^2 values and so a variation of $\sqrt{2}$ was chosen. Measurements in which variation of the scale by a factor of 2 appear to be an underestimation are discussed in Sec. III.D.

The above parton-level calculations for jet production assume massless partons, which is also a possible procedure when calculating heavy quark production [the so-called “massless” scheme (Binnewies, Kniehl, and Kramer, 1997, 1998; Kniehl, Kramer, and Spira, 1997)]. These calculations are for photoproduction; no heavy flavor calculations exist using this scheme for DIS. Here charm and beauty are regarded as active flavors in the PDFs of the proton and photon and are fragmented from massless partons into massive hadrons after the hard process. This scheme should be applicable at high transverse momenta. For momenta of the outgoing heavy quark of the order of the quark mass, the fixed order or “massive” scheme in photoproduction (Frixione, Mangano *et al.*, 1995; Frixione, Nason, and Ridolfi, 1995) and in DIS (Harris and Smith, 1995a, 1995b, 1998) is more appropriate. In the massive scheme, u , d , and s are the only active flavors in the structure functions of the proton and charm and beauty are produced only in the hard subprocess. Compared with inclusive jet production, these calculations are subject to significant additional uncertainties from the mass of the heavy quark and, where appropriate, the transition of the quark to a hadron. More details of the different schemes and, in particular, their relevance for determination of PDFs is given in Abramowicz *et al.* (2013a), and references therein.

In addition to NLO calculations, data are also often compared with predictions from Monte Carlo models which incorporate LO matrix elements matched with leading-logarithm parton showers. The Monte Carlo models generally give a more complete and realistic final state, but are unreliable in normalization due to the fact that the matrix elements are currently only LO. The approaches (Frixione and Webber, 2002; Nason, 2004) of matching matrix elements calculated at NLO with parton showers are widely used for LHC processes. This has been extended to HERA physics but only for heavy flavor production (Toll, 2010).

B. Comparisons with data

1. Jet production

A measurement of the inclusive-jet cross section is shown as a function of the jet transverse energy in the Breit frame $E_{T,B}^{\text{jet}}$ in Fig. 10. The cross section falls by 3 orders of magnitude as $E_{T,B}^{\text{jet}}$ increases from 9 to 50 GeV and the uncertainty on the measurement remains below 5% for $E_{T,B}^{\text{jet}} < 30$ GeV, dominated by the uncertainty on the jet energy scale. The statistical uncertainties become dominant only above 30 GeV. The excellent description of these data is a triumph of QCD. The theoretical uncertainties are of broadly

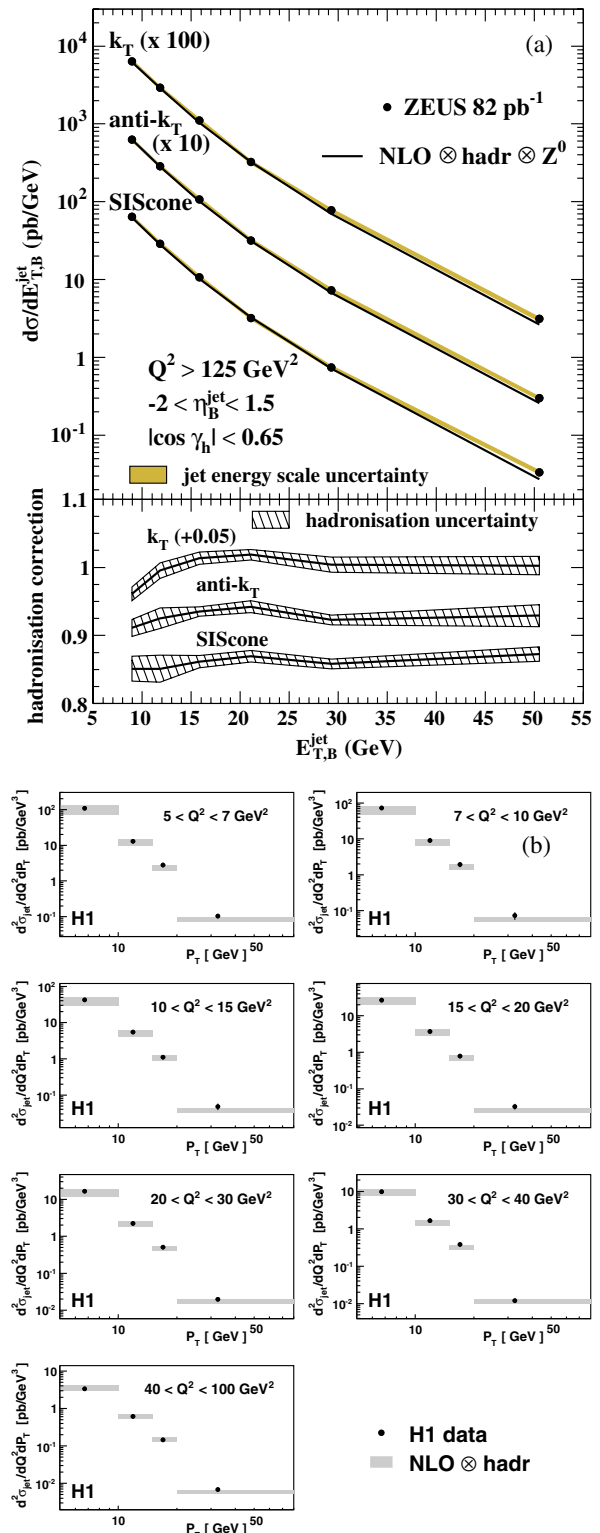


FIG. 10 (color online). (a) Measurement of $d\sigma/dE_{T,B}^{\text{jet}}$ for inclusive-jet production in the Breit frame in DIS for different jet algorithms. The lower part shows the hadronization corrections applied to the NLO calculations. (b) Measurement of $d^2\sigma/dQ^2 dP_T$ in different regions of Q^2 for inclusive-jet production in the Breit frame in DIS using the k_T jet algorithm. Note that P_T is equivalent to $E_{T,B}^{\text{jet}}$. The data in (a) and (b) are compared with NLO QCD predictions (corrected for hadronization and Z^0 effects). (a) From Abramowicz *et al.*, 2010b and (b) from Aaron *et al.*, 2010d.

similar size to those from experiment, although larger at low $E_{T,B}^{\text{jet}}$ and smaller at larger $E_{T,B}^{\text{jet}}$.

Figure 10 illustrates the need to specify the choice of algorithm when discussing jet cross sections. The quality of the theoretical description is approximately the same for the k_T (Catani *et al.*, 1993), anti- k_T (Cacciari, Salam, and Soyez, 2008), and SIScone (Salam and Soyez, 2007) algorithms, although the cross sections themselves and the necessary hadronization corrections are algorithm dependent. Figure 10 (a) shows that theory describes the data for all jet algorithms in this large- Q^2 range. In Fig. 10(b), H1 data for measurements using the k_T algorithm are shown at lower and in different regions of Q^2 ; the NLO QCD prediction also describes the data well here. In general, measurements of inclusive-jet (Adloff *et al.*, 2001b, 2002e; Chekanov *et al.*, 2002e, 2003f, 2007g, 2007h; Aktas *et al.*, 2007d; Aaron *et al.*, 2010d, 2010f, 2010g; Abramowicz *et al.*, 2010b), dijet (Adloff *et al.*, 2001b; Breitweg *et al.*, 2001a; Chekanov *et al.*, 2002b, 2007g; Aaron *et al.*, 2010f, 2010g; Abramowicz *et al.*, 2010a), and trijet (Adloff *et al.*, 2001d; Chekanov *et al.*, 2005e, 2012; Aaron *et al.*, 2010f, 2010g) production in DIS are all well described by NLO QCD, particularly at high E_T or high Q^2 and at central values of pseudorapidity. Such a description of the kinematic trends of jet production in DIS allows an extraction of the parton densities in the proton and/or the value of the strong coupling constant to be made as discussed in Sec. III.C.

Jet photoproduction has the added possibility for the photon to develop a structure and so the data can in principle be used to extract information on this. The structure, or more precisely the parton densities, of the photon are generally extracted from measurements of DIS $e\gamma$ interactions at e^+e^- colliders (Nisius, 2000). However, due to the Q^{-4} dependence of the ep cross section, measurements of photoproduction at HERA offer larger statistics than are available from e^+e^- data, as well as probing higher energy scales. Jet photoproduction is reviewed in more detail elsewhere (Butterworth and Wing, 2005), with a few of the highlights and new results included here.

Some of the first measurements at HERA established the potentially hard scattering nature of photoproduction through the observation of two jets with significant transverse energy (Ahmed *et al.*, 1992; Derrick *et al.*, 1992) in events in which no scattered electron was observed in the main detectors. The need for both direct- and resolved-photon interactions in describing photoproduction at HERA was also shown by comparing data with models of just one of the processes or the combined prediction. A variable particularly sensitive to the nature of the photon and the relative fraction of direct- and resolved-photon processes is a hadron- or detector-level estimator of x_γ , the photon's momentum fraction which takes part in the hard scatter. At LO, x_γ is identically equal to 1 for direct-photon processes and less than 1 for resolved-photon processes. Experimentally (Derrick *et al.*, 1994a) the x_γ estimator was reconstructed as

$$x_\gamma^{\text{meas}} = \frac{\sum_{\text{jets}} (E - p_z)_{\text{jets}}}{\sum_i (E - p_z)_i},$$

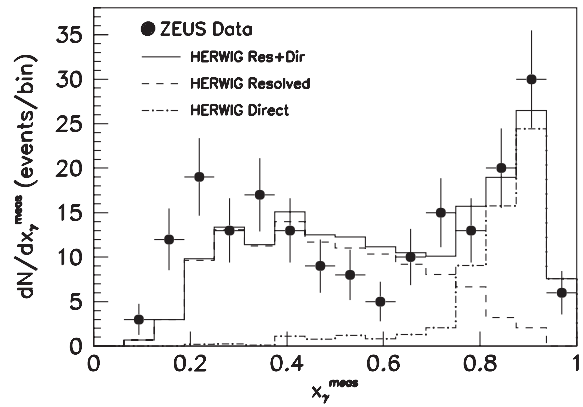


FIG. 11. Raw distribution in x_γ^{meas} for photoproduction events with two or more jets. The direct- and resolved-photon Monte Carlo predictions are fitted to the data with free normalization. From Derrick *et al.*, 1994a.

where the sums in the numerator and denominator run over all jets and all energy deposits in the calorimeter, respectively. The first measurement of a distribution in this quantity is shown in Fig. 11 and is compared with a two component fit using direct- and resolved-photon templates from the HERWIG (Marchesini *et al.*, 1992; Corcella *et al.*, 2001) Monte Carlo program. The data exhibit a two-peak structure at high and low values of x_γ^{meas} . The direct- and resolved-photon components in the Monte Carlo prediction have very different shapes. The Monte Carlo prediction gives a reasonable representation of the data when direct- and resolved-photon processes are added together. The resolved-photon component describes the low- x_γ^{meas} region reasonably well but cannot describe the data at high x_γ^{meas} . These data at high x_γ^{meas} can be described only with the inclusion of the component from direct-photon processes. Hence these data constituted the first observation of direct-photon processes in photoproduction.

After these initial findings, a multitude of results from both collaborations were published, investigating the ability of NLO QCD to describe jet photoproduction data [see the H1 (H1 Collaboration, 1992) and ZEUS (ZEUS, 1992) complete paper lists]. These studies addressed the need for an underlying event due to secondary scatters and yielded extractions of α_s and measurements of quantities sensitive to the structure of the proton and photon. The most recently published (Aktas *et al.*, 2006h; Chekanov *et al.*, 2007f; Abramowicz *et al.*, 2012a) and most precise measurements of jet photoproduction focus on high transverse energy so as to minimize the effects of any underlying event and therefore to provide a clean probe of the structure of the proton and photon.

Figure 12 shows the distribution of the mean transverse energy of the two highest E_T jets, \bar{E}_T , in two regions of x_γ^{obs} (Derrick *et al.*, 1995a), defined as

$$x_\gamma^{\text{obs}} = \frac{\sum_{\text{jet}} E_T^{\text{jet}} e^{-\eta^{\text{jet}}}}{2yE_e}, \quad (4)$$

which is closely related to x_γ^{meas} , with the high- x_γ^{obs} region enriched in direct-photon events and low- x_γ^{obs} enriched in resolved-photon events. At the high transverse energies

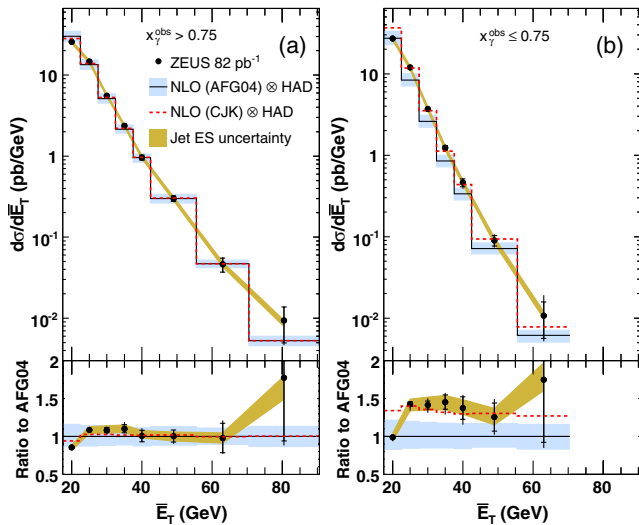


FIG. 12 (color online). Measured cross section $d\sigma/d\bar{E}_T$ for (a) $x_\gamma^{\text{obs}} > 0.75$ and (b) $x_\gamma^{\text{obs}} < 0.75$, compared with NLO QCD predictions (corrected for hadronization) using photon PDFs, AFG04 (solid line) and CJK (dashed line). From Chekanov *et al.*, 2007f.

measured here the high- x_γ^{obs} region is well described by NLO QCD, although a difference in shape is observed between data and theory. As can be seen from the predictions using two rather different photon PDFs, AFG04 (Aurenche, Fontannaz, and Guillet, 2005) and CJK (Cornet, Jankowski, and Krawczyk, 2004), the sensitivity to the structure of the photon is small at high x_γ^{obs} , as expected, although the prediction using CJK describes the data somewhat better. For $\bar{E}_T < 40$ GeV, the dominant uncertainty on the data is due to the jet energy scale (see Sec. II.E), which will not be improved in future measurements. In this region, the uncertainties on the data are also significantly smaller than those on the NLO QCD predictions.

At low x_γ^{obs} , the difference in shape between data and NLO QCD in Fig. 12(b) is more marked. For the calculations using AFG04, the data and NLO QCD prediction agree in the lowest bin whereas the prediction is significantly below the data at high \bar{E}_T . In contrast, the prediction from CJK is too high in the first bin, which dominates the cross section, but agrees well at higher \bar{E}_T . Although the prediction from CJK clearly lies above the data, it also gives the best description of the dependence on other variables such as the average pseudorapidity of the jets $\bar{\eta}$ (Chekanov *et al.*, 2007f). All other parametrizations of the photon PDFs give a qualitatively similar description of the data to that of AFG04. The fact that the gluon density in the CJK photon PDF differs from the others may hint at the origin of the improved description. These data should thus improve our knowledge of the gluon density in the photon PDFs, which is insufficiently constrained by e^+e^- data.

2. Jet substructure

The substructure of a jet gives information on the internal pattern of parton radiation, as well as details of the hadronization process. Given that gluons radiate more than quarks,

categorizing jets using measurements of their substructure offers the possibility of obtaining samples which are enriched in gluon or quark initiators. Classifying the jets in an event using this technique thus allows samples to be obtained which are dominated by particular parton-level final states, in turn giving enhanced control over the initial state. Measurements of jet substructure could thus in principle lead to improved constraints on the structure of the proton and photon, distinguishing, for example, between the $\gamma^*g \rightarrow q\bar{q}$ and $\gamma^*q \rightarrow qg$ processes in the DIS case.

Jet substructure is generally studied by measuring the jet shape (Ellis, Kunszt, and Soper, 1992) and subjet multiplicity (Catani *et al.*, 1992; Seymour, 1994, 1996; Forshaw and Seymour, 1999). The integrated jet shape $\psi(r)$, using only those particles belonging to the jet, is defined as the fraction of the jet transverse energy that lies inside a cone in the $\eta - \phi$ plane of radius r , concentric with the jet axis:

$$\psi(r) = \frac{E_T(r)}{E_T^{\text{jet}}}, \quad (5)$$

where $E_T(r)$ is the transverse energy within the given cone of radius r . The mean integrated jet shape $\langle\psi(r)\rangle$ is defined as the averaged fraction of the jet transverse energy inside the cone r :

$$\langle\psi(r)\rangle = \frac{1}{N_{\text{jets}}} \sum_{\text{jets}} \frac{E_T(r)}{E_T^{\text{jet}}}, \quad (6)$$

where N_{jets} is the total number of jets in the sample. The substructure of a jet is expected to depend primarily on the initiator of the jet and to a lesser extent on the colliding particle. This is supported in Fig. 13, where the mean integrated jet shape is shown for different processes, viz. DIS (Breitweg *et al.*, 1999c), e^+e^- collisions (Akers *et al.*, 1994), photoproduction (Breitweg *et al.*, 1998e), and $p\bar{p}$ collisions (Abe *et al.*, 1993a; Abachi *et al.*, 1995b).

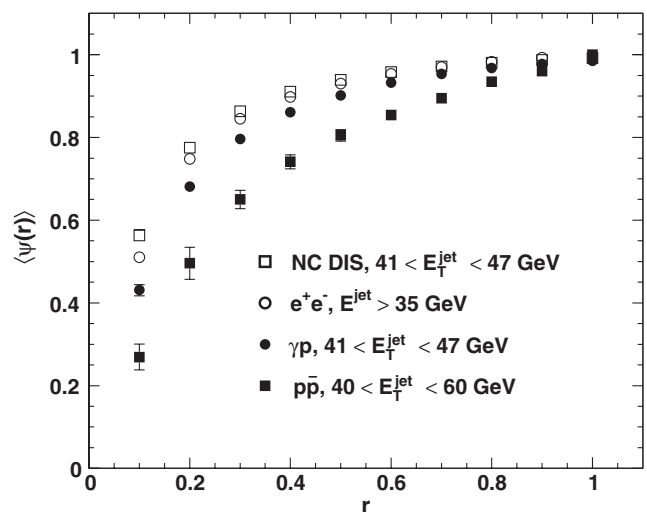


FIG. 13. Measured jet shapes in e^+e^- scattering (Akers *et al.*, 1994), from ZEUS in DIS (Breitweg *et al.*, 1999c) and photoproduction (Breitweg *et al.*, 1998e), and in $p\bar{p}$ collisions (Abe *et al.*, 1993a; Abachi *et al.*, 1995b). From Butterworth and Wing, 2005.

The results are shown for similar jet energies for all samples to remove any dependence of the particle initiator or the radiation on this quantity. In DIS and e^+e^- collisions the partonic system emerging from the hard interaction is expected to consist mainly of quarks. The similarity between the results from these processes, their relative narrowness and difference from the other samples, is consistent with this. The less-collimated and broader jets seen in $p\bar{p}$ collisions are indicative of gluon-initiated jets dominating the sample. In photoproduction at these energies, direct-photon processes are expected to dominate. However, the presence of QCD Compton and resolved-photon processes also leads to gluons in the final state. The results in photoproduction lie between those from $p\bar{p}$ scattering and those from DIS and e^+e^- collisions, compatible with the expected mixture of gluon- and quark-initiated jets.

Measurements at HERA of the internal structure of jets (Breitweg *et al.*, 1998e, 1999c; Adloff *et al.*, 1999c; Chekanov *et al.*, 2003c) have been compared with various Monte Carlo models and NLO QCD predictions and shown to be well described. This agreement has also allowed extractions of the strong coupling constant (Chekanov *et al.*, 2003c, 2004j). More recently, measurements have been made (Chekanov *et al.*, 2004j, 2009k) with the aim of distinguishing between gluon- and quark-initiated jets. By cutting on the jet shape at low r , a jet can be classified as “broad” or “narrow” (Chekanov *et al.*, 2004j) and thereby enriched in gluon and quark initiators, respectively.

An example dijet cross section is shown in Fig. 14, where both jets are tagged as either broad or narrow. A striking difference is observed between the two samples as a function of the cosine of the dijet scattering angle in the dijet center-of-mass frame, with the general trends well described by the PYTHIA Monte Carlo (Sjostrand, 1994; Sjostrand *et al.*, 2001;

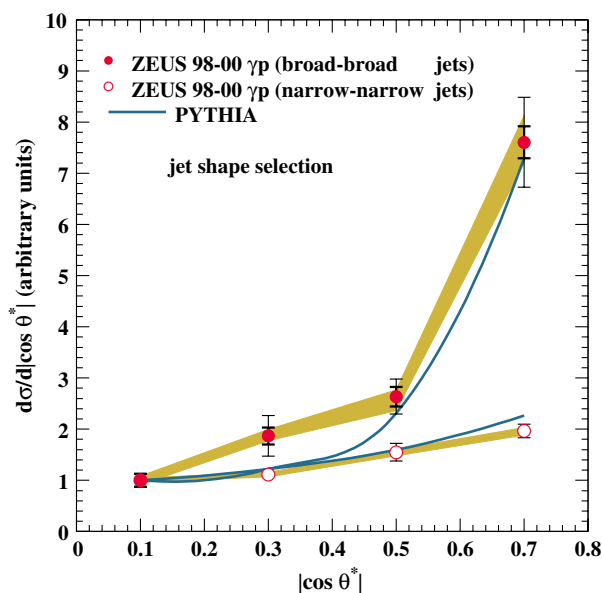


FIG. 14 (color online). Measurement of the dijet cross section differential in the cosine of the dijet scattering angle $d\sigma/d|\cos \theta^*|$ for events with two broad jets or two narrow jets. The data are compared with PYTHIA Monte Carlo predictions. From Chekanov *et al.*, 2004j.

Sjostrand, Mrenna, and Skands, 2006) predictions. The dijet scattering angle is a revealing quantity as it is sensitive to the propagator, with a spin-1/2 quark exchange giving a $(1 - |\cos \theta^*|)^{-1}$ cross-section dependence and a spin-1 gluon exchange giving a $(1 - |\cos \theta^*|)^{-2}$ cross-section dependence at leading order. The shallow rise to high $\cos \theta^*$ for the sample with two narrow jets and the steeper rise for the sample with two broad jets are indicative of such a difference in propagator. The angular distributions can be understood in terms of the dominant two-body processes: the resolved subprocess $q_\gamma g_p \rightarrow qg$, mediated by gluon exchange for the broad-broad dijet sample, and the direct subprocess $\gamma g \rightarrow q\bar{q}$, mediated by quark exchange for the narrow-narrow dijet sample. For events with two broad jets, PYTHIA predicts the parton final state to consist of 16% gg , 52% qg , and 32% qq . For events with two narrow jets, PYTHIA predicts the parton final state to consist of 71% qq , 28% qg , and 1% gg . The relatively impure sample of gluon-initiated jets is due to the dominance of the boson-gluon fusion process (with two quark-initiated jets in the final state) and the background from c and b quarks, which also yield broad jets due to the longer decay chain compared to that for light quarks.

This detailed understanding of jet substructure seeded the development of the new techniques to search for the Higgs boson (Butterworth *et al.*, 2008) or other boosted heavy particles (Abdesselam *et al.*, 2011) which are now being used at the LHC.

3. Prompt photon production

Events containing an isolated “prompt” (or “direct”) photon are a potentially powerful tool to study hard processes. Their main attractions lie in the insensitivity of photons to hadronization effects and the precise energy measurements obtainable for isolated electromagnetic objects. The number of possible processes is also smaller than for the case of jet production; to leading order in both QCD and QED, prompt photon cross sections in DIS and direct photoproduction are directly sensitive to the quark content of the proton through the Compton scattering ($\gamma q \rightarrow \gamma q$) process. Resolved-photon contributions are dominated by the $gq \rightarrow q\gamma$ process, giving sensitivity to the quark and gluon contents of both the proton and photon. These advantages have to be set against the significantly smaller event rates for prompt photon than for jet production and the experimental challenge of separating photon samples from backgrounds due to π^0 and η^0 meson decays to multiphoton states. This separation relies on many discriminating variables, such as the shape of the shower deposited in the calorimeter.

Measurements of prompt photon production have been made in both DIS (Chekanov *et al.*, 2004e, 2010e; Aaron *et al.*, 2008b; Abramowicz *et al.*, 2012b) and photoproduction (Breitweg *et al.*, 1997b, 2000b; Chekanov *et al.*, 2001b; 2007m; Aktas *et al.*, 2005e; Aaron *et al.*, 2010i; Abramowicz *et al.*, 2014). Both H1 and ZEUS have made measurements in the DIS regime using significant fractions of the available data. The data have been compared with predictions (Gehrmann-De Ridder, Kramer, and Spiesberger, 2000; Gehrmann-De Ridder, Gehrmann, and Poulsen, 2006a, 2006b) to order α^3 , which describe the shapes of the measured

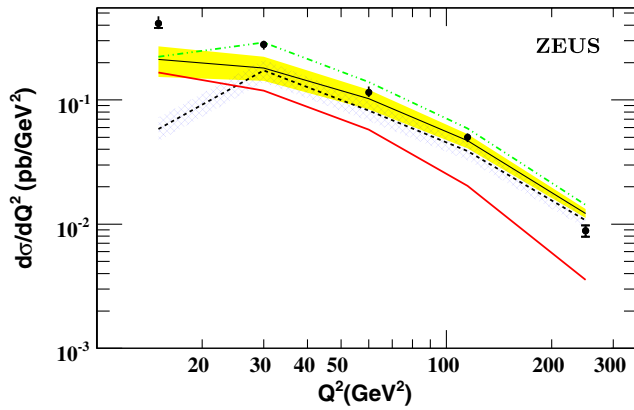


FIG. 15 (color online). Differential cross section for prompt photon production in DIS with the data compared with various theoretical predictions. An $\mathcal{O}(\alpha^3)$ calculation with radiation from the quark line (lower solid line) and additionally including radiation from the lepton line and interference between the two (shaded band around upper solid line) is shown. The photon is also treated by Martin *et al.* as a partonic constituent of the proton (hatched area surrounding dashed line) and including photon radiation, i.e., adding the prediction corresponding to the thick line, from the quark line (dot-dashed line). See text for further details of the models. From Chekanov *et al.*, 2010e.

cross sections $d\sigma/dE_T^\gamma$ and $d\sigma/d\eta^\gamma$. However, the theory is systematically below the data, with the difference concentrated at low Q^2 , as shown in Fig. 15. The alternative approach of Martin *et al.* (2005) treats photons as a partonic constituent of the proton, introduced by including QED corrections to the proton PDFs and producing high-energy photons in the final state. Predictions from this model are also shown in Fig. 15. They fall below the data over most of the measured range, but are close in the high- Q^2 region, where lepton emission is expected to be dominant. An improved description of the data is obtained by appropriately combining the two predictions, suggesting a need for further calculations to exploit the full potential of the measurements.

Cross sections for prompt photon photoproduction are shown in Fig. 16. The results use almost the full H1 data set and have a precision of about 10%. The data are compared with an NLO QCD calculation based on collinear factorization and DGLAP evolution (Fontannaz, Guillet, and Heinrich, 2001; Fontannaz and Heinrich, 2004) and with a QCD calculation based on the k_T factorization (Lipatov and Zotov, 2005) method which is expected to provide a good approximation for a significant part of the collinear higher-order QCD corrections. Both predictions are below the data with the largest differences at low E_T^γ and low η^γ . The prediction based on k_T factorization is a bit higher than that of NLO DGLAP QCD and hence is closer to the data. The same conclusions as those stated here and seen in Fig. 16 were arrived at in the latest ZEUS results (Chekanov *et al.*, 2007m). The influence of high-order QCD terms and hadronization effects are expected to be largest at low transverse energies, and further theoretical developments are needed in this region in particular.

Overall, the impact of prompt photon data on the development of QCD at HERA has been somewhat disappointing

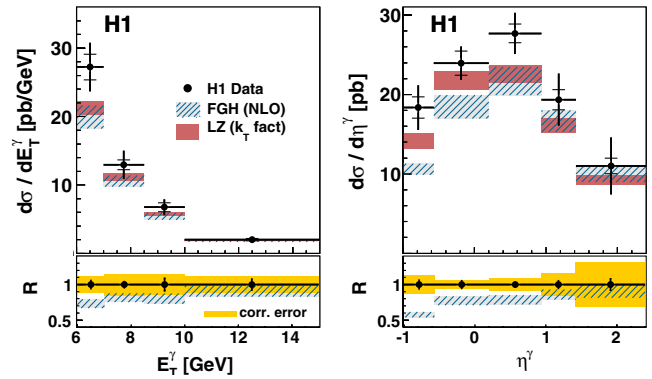


FIG. 16 (color online). Differential cross sections for prompt photons in photoproduction. The data are compared with two QCD calculations, one based on collinear factorization in NLO (hatched histogram) and the other based on k_T factorization. The lower parts show the ratio of the NLO QCD prediction to the data. From Aaron *et al.*, 2010i.

compared with the success obtained using jet observables. This is in part due to the limited statistics and experimental difficulties encountered in obtaining cross sections and partly due to the need for further improvements in the theoretical understanding to fully exploit the data.

4. Heavy quark production

Heavy quarks at HERA, as at other colliders, are tagged using many different independent techniques as summarized in Sec. II. As with inclusive-jet cross sections, the primary aim of the measurements is to test QCD [see Eq. (3)] through the sensitivity to both the perturbative prediction as discussed in this section and the proton and photon PDFs as discussed in Sec. III.C. As the masses of charm and particularly beauty quarks are so much larger than Λ_{QCD} , they can provide a hard scale for perturbative calculations that are expected to converge rapidly. Depending on the process measured, information on the fragmentation or even decays can also be extracted and searches for excited states performed (see Sec. IV.C).

The description by NLO QCD of charm production in DIS is generally good as shown in Fig. 17. The QCD calculation “HVQDIS” (Harris and Smith, 1995a, 1995b, 1998) is performed in the massive scheme, which means that it should be most reliable at low values of p_T . However, the theory describes the $p_T^{D^*}$ distribution up to 20 GeV and over 3 orders of magnitude in the cross section. Taking the correlated theoretical uncertainties into account, there is also a good description of the η^{D^*} distribution in both shape and magnitude. The good description in Fig. 17 shows that the dynamics of NLO QCD (along with the nonperturbative fragmentation inputs, given in Sec. IV.C) can describe charm production over a wide kinematic range. Importantly, it also encourages an extrapolation using this NLO QCD prediction to the full phase space in $p_T^{D^*}$ and η^{D^*} in order to give a determination of the charm contribution $F_2^{c\bar{c}}$ to the inclusive proton structure function. The validity of QCD calculations outside the measured region is unknown, but at least some confidence is given by a good description of the data within the measured region (see Sec. III.C).

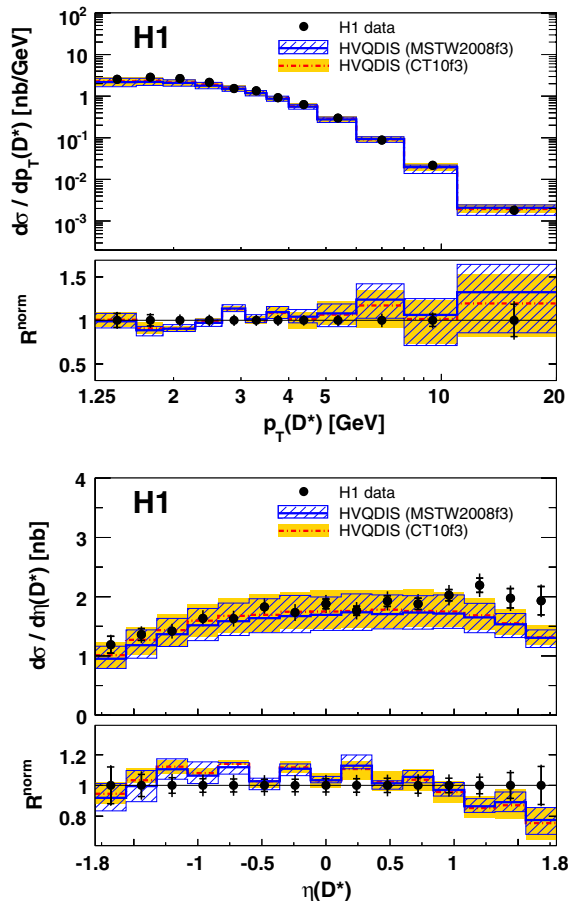


FIG. 17 (color online). Measurements of cross sections $d\sigma/dp_T^{D^*}$ and $d\sigma/d\eta^{D^*}$ for D^* production in DIS compared with NLO QCD predictions using two different proton PDFs. The lower plot for each variable shows the ratio of theory to data where each is first normalized to its corresponding total cross section. From Aaron *et al.*, 2011b.

Precise measurements of charm photoproduction have been made by reconstructing D^* mesons with no explicit jet requirements (Breitweg *et al.*, 1999b; Aktas *et al.*, 2007c). The details of the cross sections are not well reproduced by NLO QCD calculations, with notable problems at low values of $p_T^{D^*}$ and in reproducing the shape of the cross section as a function of the pseudorapidity of the D^* meson. However, at the lowest measured scales $p_T^{D^*} \sim 2$ GeV, the uncertainties from theory are large, typically 50%. More information, such as constraints on the proton and photon PDFs, could be extracted from the data with improved predictions. However, these and other such data are more commonly used to extract information on the fragmentation of heavy quarks (see Sec. IV.C).

Measurements of heavy flavor photoproduction have also been made in which the heavy quark is part of a jet. Such measurements are generally performed at high transverse energy and, as jets are reconstructed, the measurements are usually integrated over the fragmentation fraction z , with correspondingly reduced sensitivity to the details of the hadronization. Such measurements thus potentially offer a more precise comparison between data and fixed-order QCD than is the case for measurements without jet requirements.

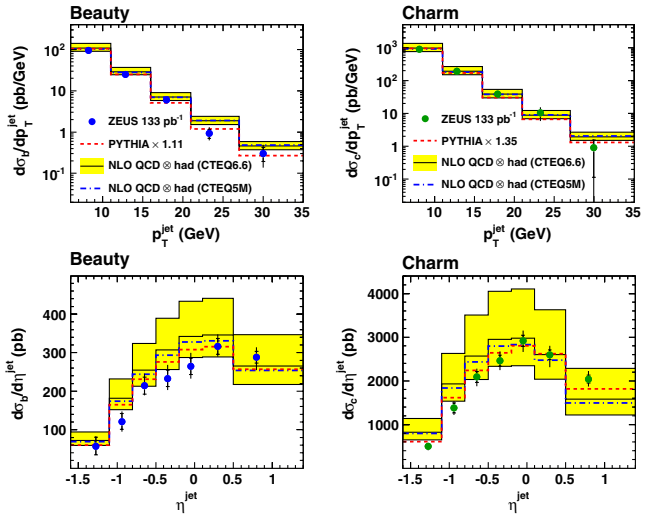


FIG. 18 (color online). Beauty (left) and charm (right) jet photoproduction cross sections $d\sigma/dp_T^{\text{jet}}$ (upper) and $d\sigma/d\eta^{\text{jet}}$ (lower) compared to PYTHIA Monte Carlo and NLO QCD predictions. From Abramowicz *et al.*, 2011b.

Example results are shown in Fig. 18. The descriptions of both the measured charm and beauty cross sections are reasonable, although the uncertainty on the theory is still large. Historically this level of agreement was not always the case for beauty production where at the turn of the millennium, data from the Tevatron (Abe *et al.*, 1993b, 1993c, 1995, 1996, Abachi *et al.*, 1995a; Abbott *et al.*, 2000a, 2000b, 2000c; Acosta *et al.*, 2002) and the first measurement from HERA (Adloff *et al.*, 1999e) were in strong disagreement with QCD. Through improved measurements, presenting results at the hadron rather than quark level and better theory (updated fragmentation functions and resummed calculations), this discrepancy was resolved and the need for new physics as was postulated at the time, rendered unnecessary. See Cacciari (2004) for a more complete discussion.

Since the first HERA results on beauty production, many channels covering a wide kinematic range have been measured in both DIS and photoproduction (Breitweg *et al.*, 2001b; Chekanov *et al.*, 2004a, 20071, 2008a, 2009d, 2009e, 2010b; Aktas *et al.*, 2005b, 2005c, 2006f; Aaron *et al.*, 2010h, 2011a, 2012b, 2012c; Abramowicz *et al.*, 2010c, 2011a). The photoproduction results are summarized in Fig. 19 and compared with predictions from NLO QCD. This figure shows that beauty production at HERA is well described with particularly the most recent and most precise data in very good agreement with theory, confirming the ability of QCD to describe heavy quark production.

C. Extracting information from the data

As explained earlier and can be seen from Eqs. (1)–(3), the measurements presented in this section are sensitive to the structure of the proton and photon and to the value of the strong coupling constant. Therefore, as well as comparing QCD predictions with the data, NLO QCD calculations can be used to extract the parton densities or α_s .

The measurement of the structure of the proton and the extraction of its parton densities are covered in detail

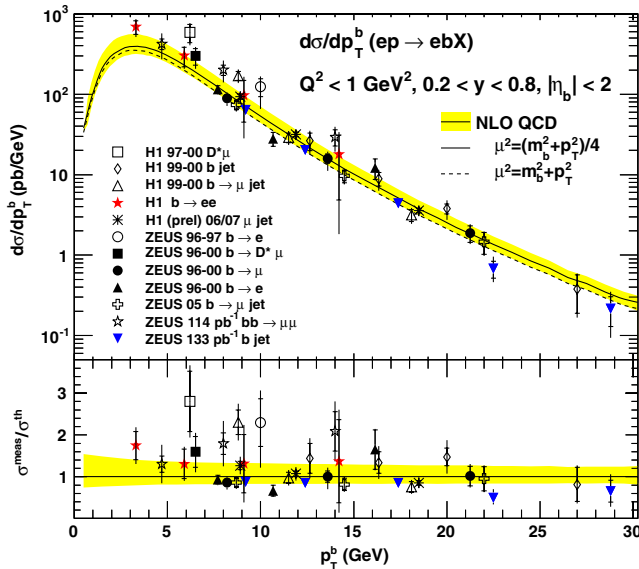


FIG. 19 (color online). Summary of beauty photoproduction measurements at HERA as a function of the transverse momentum of the b quark compared with predictions from NLO QCD. The measurements, made using different final states and in different kinematic regions, were corrected for branching ratios and extrapolated to the specified kinematic region at the quark level for this comparison.

elsewhere (Klein and Yoshida, 2008; Perez and Rizvi, 2013), with the HERA measurements of inclusive DIS having provided the strongest constraints throughout most of the kinematic range. Final-state measurements have also been used to constrain the structure of the proton as the processes involved are directly sensitive at lowest order to the gluon distribution in the proton [see Fig. 8(a)]. By using photoproduction jet data, high energy scales can also be accessed. Photoproduction jet data were included in an NLO QCD fit to ZEUS data only (Chekanov *et al.*, 2005a) and found to reduce the uncertainty on the gluon distribution by a factor of 2 at medium to high x (≥ 0.01).

The H1 and ZEUS measurements of charm production in DIS such as those in Fig. 17 have recently been combined (Abramowicz *et al.*, 2013a), accounting for correlations in the uncertainties and thereby leading to significantly increased precision. In Fig. 20, the data are presented as a reduced cross section $\sigma_{\text{red}}^{c\bar{c}}$, corresponding, at the nonextreme y values considered here, to the charm contribution to the proton structure function $F_2^{c\bar{c}}$. The data are compared with predictions based on parametrizations of the parton distribution functions in the proton at NLO and NNLO in QCD. These data provide extra constraints on the structure of the proton and the mechanism for charm production. In addition, the data are sensitive to the mass of the charm quark (Alekhin and Moch, 2011; Abramowicz *et al.*, 2013a) and could be used in the context of global fits to extract this quantity. Similar measurements from both collaborations have also been made for beauty production, but with much smaller statistics.

As can be seen in Eq. (3) and discussed in Sec. III.B.1, HERA data on jet photoproduction, in particular, are sensitive to the structure of the photon as well as the proton.

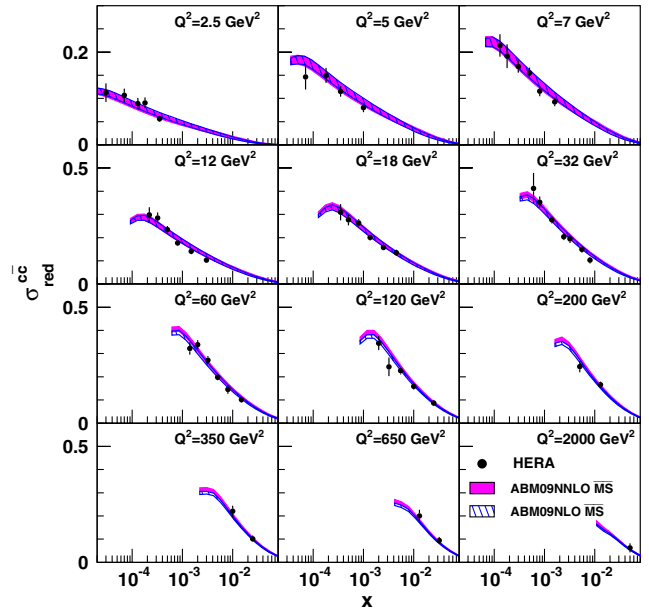


FIG. 20 (color online). Measurement of the reduced charm cross section at fixed Q^2 as a function of x , having combined all available published H1 and ZEUS data. The data are compared with a parametrization of the proton PDF from the ABM (Alekhin, Blumlein, and Moch, 2012) group at NLO and NNLO in QCD. From Abramowicz *et al.*, 2013a.

The HERA data complement the measurements of F_2^{γ} from e^+e^- colliders in that the HERA data are sensitive at LO to the gluon density in the photon, which is poorly constrained from e^+e^- data. Also, the measurements from HERA probe higher scales ($\langle \bar{E}_T^2 \rangle \sim 4000 \text{ GeV}^2$) than was accessible at LEP [$\langle Q^2 \rangle = 780 \text{ GeV}^2$ (Abbiendi *et al.*, 2002)]. There are also far more data which are sensitive to the heavy flavor structure of the photon from HERA than were obtained at LEP.

A number of challenges exist in understanding and using the HERA data in fits to the structure of the photon. To achieve as large a data sample as possible, the minimum jet transverse energy must be as small as possible. A further advantage of including the low transverse energy region is the access to correspondingly low values of x_γ , the region where the gluon density is expected to dominate the photon structure. However, typical cut values are at least 5 GeV, dictated by requirements in the trigger and the need to maintain a good correlation between the directions of the reconstructed jets and the partons which seed them. Furthermore, at these low values of transverse energy, the underlying event and hadronization uncertainties prevent a precise comparison between data and QCD predictions. For example, in a measurement of inclusive-jet photoproduction by H1 (Adloff *et al.*, 2003), the theoretical uncertainties in predicting cross sections close to the cut at 5 GeV on the jet transverse energy were too large to allow discrimination between different proton and photon PDFs. This measurement and the underlying event are discussed in detail in Sec. III.D.4. Jet cross sections can thus only be used reliably to constrain photon structure at high transverse energy, where the effects of the underlying event and hadronization are expected to be minimized, at the expense of reduced statistics and reduced sensitivity to the gluon

density at low x_γ . Figure 12 is an example of such a measurement where two jets are required with transverse energies above 20 and 15 GeV.

A combined fit of e^+e^- data and HERA dijet data has been performed in order to extract the parton densities in the photon (Slominski, Abramowicz, and Levy, 2006). The dijet data with high transverse energies, greater than 14 GeV, were not well described in the fit. Part of the problem is that the data are more sensitive to the gluon density in the proton than that in the photon. However, as seen in Fig. 12, there is a significant difference between different parametrizations of the photon PDFs, suggesting that there is some flexibility which can be explored in order to achieve a better description of the data and more stringent constraints on the photon PDFs. The data also exhibit a strong need for higher-order calculations (see also Fig. 23) and with such programs, more significant constraints on the photon could be made.

The strong coupling constant α_s has been extracted at HERA in many different processes and in a wide kinematic range, thereby providing precise results which clearly display the running with the energy scale of the process. The value of α_s has been extracted using inclusive DIS cross sections, event-shape variables (although these receive significant contributions from nonperturbative processes, see Sec. III.E), jet cross sections, and ratios of rates of different processes such as the dijet cross section normalized to the total DIS cross section or the three- to two-jet rate. The ratio of the dijet to the inclusive DIS cross section is shown versus the scale Q^2 and compared with an NLO QCD prediction in Fig. 21(a). Such a ratio reduces some systematic uncertainties which are correlated between the measurements, such as the uncertainty on the luminosity measurement. The resulting precise data are well described by the theoretical prediction. By varying α_s in the theory and fitting to the data, a value can be obtained in bins of the scale Q^2 and the running of the coupling constant with energy scale demonstrated as in Fig. 21(b). A clear variation of α_s with Q^2 is observed and the variation is well described by the two-loop solution of the renormalization group equation.

A collection of recent determinations of α_s , presented (as is conventional) at the scale of the Z boson mass, is shown in Fig. 22. The two ZEUS results were extracted at high-energy scales in order to minimize the theoretical uncertainties. When using the full power of the data and including the largest possible kinematic region, as for the H1 results, the extracted α_s values have a precision comparable to the world average (Beringer *et al.*, 2012). However, the theoretical uncertainties, arising mainly from missing higher orders in the calculations, then become large. QCD fits to inclusive DIS data yield extractions of α_s as well as parton distribution functions. Including jet cross-section information in these fits increases the sensitivity, due to the dependence on α_s at LO, and yields a precise result, as shown in Fig. 22 for the case of the HERAPDF1.6 fits. Again, the experimental precision of this result is competitive, but it suffers from large theoretical uncertainties. Development of higher-order theoretical calculations and tools is thus now the limiting factor on the precision of strong coupling determinations from ep scattering. As α_s is one of the fundamental parameters of the standard model and its extrapolation to very large scales

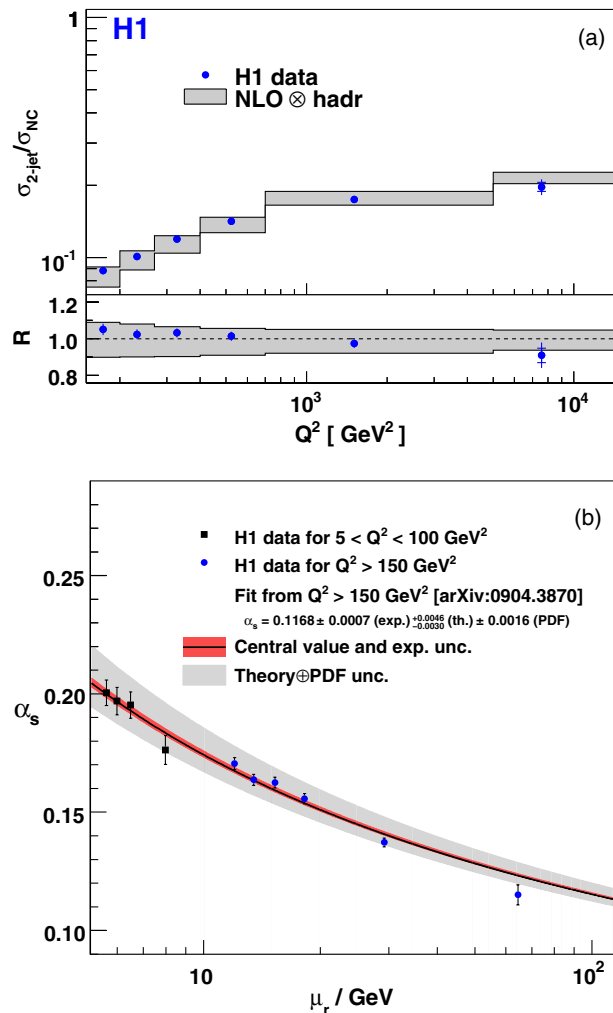


FIG. 21 (color online). (a) Measurement of the ratio of the dijet to the total cross section in DIS, compared with NLO QCD predictions (corrected for hadronization). (b) Values of α_s vs the scale of the process extracted from distributions such as that in (a). The solid line shows the two-loop solution of the renormalization group equation. (a) From Aaron *et al.*, 2010f, and (b) from Aaron *et al.*, 2010g.

provides constraints on grand unification, the case for prioritizing such calculations is strong.

D. Pushing the boundaries of applicability

Much of this section is concerned with measurements of jet production and other hard processes in a region where the data are well modeled by NLO QCD with parton evolution governed by the DGLAP equations. This is generally the case at large transverse momenta and in a reasonably central region, where large scales are present, the strong coupling α_s is relatively small and momentum fractions x are relatively large. Going beyond this region of stability requires additional theoretical tools. A successful description at smaller transverse momenta requires higher orders in the matrix elements and an improved understanding of hadronization and underlying event phenomena. More fundamentally, the kinematics of the noncentral region at HERA extend into a low- x regime

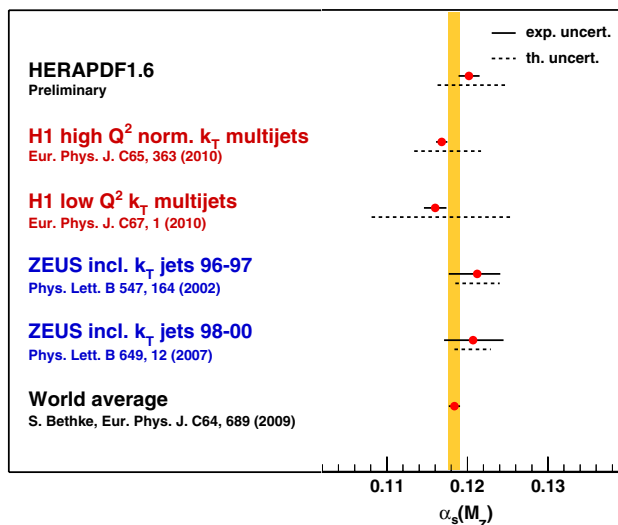


FIG. 22 (color online). Values of α_s from individual H1 and ZEUS measurements and the world average. Note the extraction in the HERAPDF1.6 fit is a preliminary result.

where dynamics beyond the DGLAP approximation are often considered likely to become apparent for the first time. These may consist of novel parton cascade arrangements in which the transverse momentum ordering of parton emissions between the photon and the proton intrinsic to DGLAP is broken and alternative, resummed, schemes, going beyond fixed-order perturbative expansions in α_s —notably the BFKL equations (Kuraev, Lipatov, and Fadin, 1977; Balitsky and Lipatov, 1978)—are appropriate. The lack of transverse momentum ordering is intimately linked to a breakdown of collinear factorization and thus to the concept of an unintegrated gluon density of the proton, with finite and variable transverse momentum, as implemented, for example, in the CCFM approach (Ciafaloni, 1988; Catani, Fiorani, and Marchesini, 1990a, 1990b). For hard scattering processes generating transverse momenta $p_T > \sqrt{Q^2}$ the lack of transverse momentum ordering has also been modeled by ascribing a partonic structure to the virtual photon (Uematsu and Walsh, 1981; Gluck, Reya, and Stratmann, 1996). At sufficiently low x , phenomena associated with very high parton densities (Gribov, 1970) including nonlinear evolution and parton “saturation” may become important. While such effects are not particularly relevant to the current discussion of hard processes in the inclusive final state, they have been considered in detail in the context of inclusive and diffractive DIS, where the smallest x values accessed at HERA are reached (see Sec. V).

In the following, photoproduction and DIS measurements extending beyond the best understood region, for example, to higher η^{jet} , lower E_T^{jet} or in higher jet-multiplicity events, are summarized. In some cases, dedicated observables have been constructed which are most likely to be sensitive to novel effects beyond NLO DGLAP QCD.

1. Higher orders

In this section, the inadequate description of the high- E_T^{jet} photoproduction data in Fig. 12(b) by NLO QCD is further

investigated. This discrepancy could be due to a need for refined photon PDFs. However, it may also indicate that NLO QCD is insufficient and higher-order calculations are needed. A variable which is particularly sensitive to higher orders is the azimuthal angle between the two jets of highest transverse energy $\Delta\phi^{jj}$. Figure 23 shows measurements of this quantity for high and low x_γ^{obs} , compared with NLO QCD predictions and expectations from the Monte Carlo models, HERWIG and PYTHIA, normalized to equal areas for a comparison of shape.

For $x_\gamma^{\text{obs}} > 0.75$, the cross section falls by about 3 orders of magnitude over the measured range in $|\Delta\phi^{jj}|$, more steeply than for $x_\gamma^{\text{obs}} \leq 0.75$. At high x_γ^{obs} , NLO QCD agrees with the data for the back-to-back configuration (i.e., at the largest $|\Delta\phi^{jj}|$), but it has a steeper falloff with increasing decorrelation between the jets. The prediction from the PYTHIA Monte Carlo program is similar to that for NLO QCD, whereas the prediction from the HERWIG program describes the data well. For low x_γ^{obs} , the NLO QCD calculation is much too steep and is significantly below the data for all values of $|\Delta\phi^{jj}|$ except the highest bin. The prediction from the PYTHIA program is less steep, but still gives a poor description. The prediction from the HERWIG program is in remarkable agreement with the data.

The results here illustrate that the parton-shower model in HERWIG gives a good simulation of high-order processes and suggest that matching it to NLO QCD [as done in the programs MC@NLO (Frixione and Webber, 2002) and POWHEG (Nason, 2004), but is not yet available for these processes in ep collisions] would give a good description of the data in both shape and normalization. Should such a calculation or other high-order prediction, such as a full NNLO QCD treatment, become available, these distributions would be ideal tests, as they are inclusive quantities of high precision.

These results and conclusions are qualitatively similar to those for the azimuthal decorrelation in high- E_T dijet

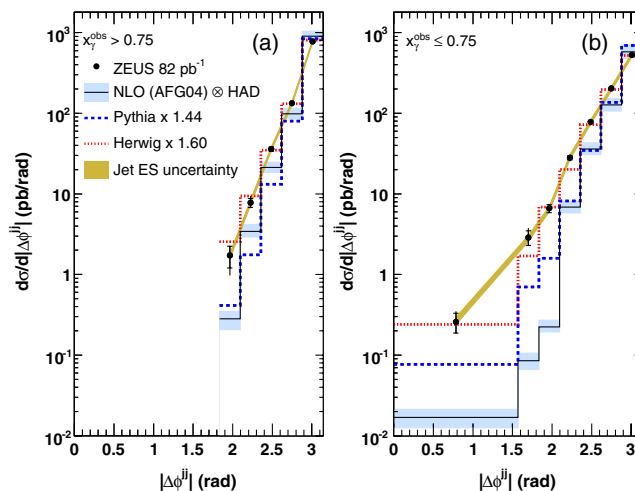


FIG. 23 (color online). Measurement of the difference in azimuth between the two highest transverse energy jets for (a) $x_\gamma^{\text{obs}} > 0.75$ and (b) $x_\gamma^{\text{obs}} \leq 0.75$ compared with NLO QCD [$\mathcal{O}(\alpha_s^2)$, corrected for hadronization] and Monte Carlo predictions. From Chekanov *et al.*, 2007f.

photoproduction in which at least one of the jets is tagged as originating from a charm quark (Chekanov *et al.*, 2005b) and in the angular distribution between a jet and a prompt photon (Aaron *et al.*, 2010i). Given that $\mathcal{O}(\alpha_s^2)$ calculations are at best LO in the $\Delta\phi$ variable, it is perhaps not surprising that the data are not always well described without NNLO, or higher order, QCD calculations.

2. New low- x phenomena

In contrast to the case shown in Fig. 10 and elsewhere, where high- Q^2 events containing jets of high transverse energy in the central part of the detector are selected, dedicated observables are required to enhance the sensitivity to low- x phenomena. An example approach is to measure forward jet production cross sections in a restricted phase space, as illustrated in Fig. 24. Events containing jets in the forward direction for which the variable $x_{\text{jet}} = E_{\text{jet}}^{\text{jet}}/E_p$ is much larger than Bjorken x (denoted x_{Bj} here) suggest a gluon cascade which is strongly ordered in fractional longitudinal momentum, as expected for BFKL-governed evolution. Further requiring that $(E_T^{\text{jet}})^2/Q^2$ is of order unity restricts evolution in transverse momentum, thus suppressing standard DGLAP evolution.

An example result using this technique is shown in Fig. 25 (Aktas *et al.*, 2006d). The events selected here are required to have low Q^2 and low x_{Bj} , specifically $5 < Q^2 < 85 \text{ GeV}^2$ and $0.0001 < x_{\text{Bj}} < 0.004$, and also to contain jets of transverse energy $E_T^{\text{jet}} > 3.5 \text{ GeV}$ in the laboratory frame in the forward part of the detector $7^\circ < \theta^{\text{jet}} < 20^\circ$. The x_{jet} variable is required to be larger than 0.035 and the scale evolution is restricted via $0.5 < (E_T^{\text{jet}})^2/Q^2 < 5$. The same data are displayed in each of the three subfigures, but they are compared with different theoretical calculations and models.

In Fig. 25(a), the data are compared with LO and NLO QCD, based on DGLAP evolution, i.e., the same calculations which described the data well in Fig. 10. The prediction from LO QCD is significantly below the data, as expected for the analysis phase space, which suppress the LO contribution.

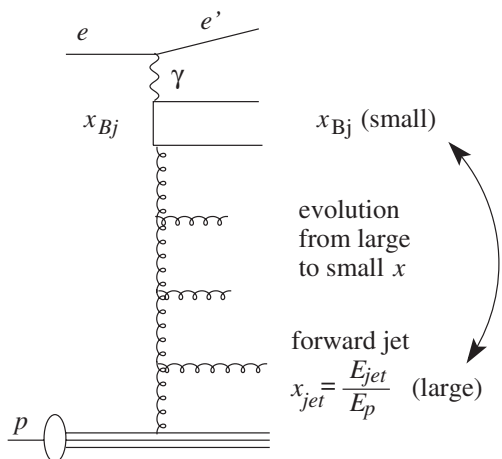


FIG. 24. Schematic illustration of ep scattering with a forward jet taking a fraction x_{jet} of the proton momentum. The evolution in the longitudinal momentum fraction x from large x_{jet} to small x_{Bj} is indicated. From Aktas *et al.*, 2006d.

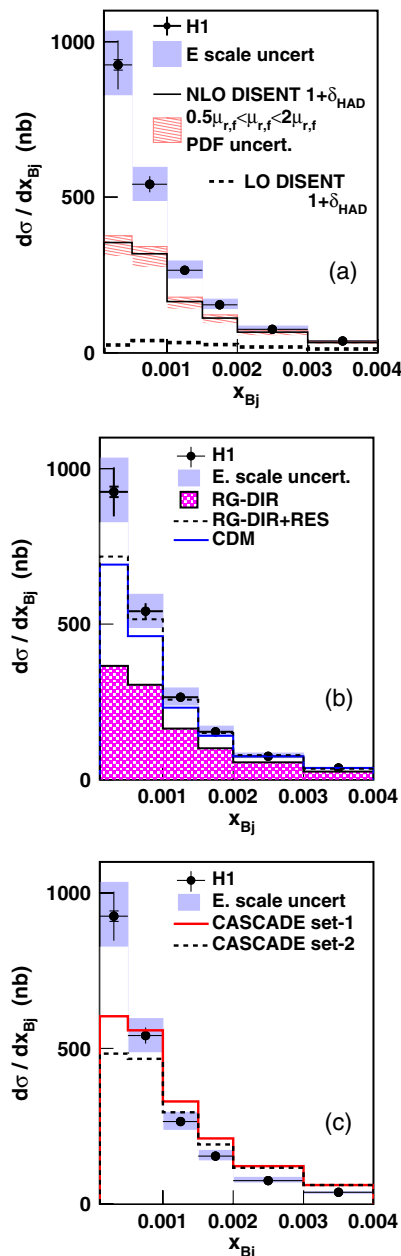


FIG. 25 (color online). Measurement of forward jet production at low x_{Bj} in DIS compared with (a) NLO DGLAP QCD (corrected for hadronization) and (b), (c) Monte Carlo models. From Aktas *et al.*, 2006d.

The NLO QCD prediction is in agreement with the data at high x_{Bj} , but increasingly deviates from the data with decreasing x_{Bj} . Notably, at low x_{Bj} the NLO QCD prediction is over a factor of 10 higher than the LO QCD prediction, suggesting that the remaining factor of 2 difference between data and NLO QCD may be resolved by the inclusion of NNLO QCD, assuming that the perturbative series is quickly convergent. The scale uncertainty band, obtained by the conventional method of varying the renormalization scale by a factor of 2, is at the 10% level. However, the order of magnitude difference between the LO and NLO QCD predictions suggests that this may not be fully representative of the uncertainties due to missing higher orders.

To ascertain whether predictions based on BFKL or otherwise-modified parton evolution provide a better description than DGLAP-based models, these results would ideally be compared with QCD calculations of next-to-leading-logarithmic (NLL) accuracy, summing terms in either $\ln(Q^2)$ or $\ln(1/x)$. Unfortunately, such calculations are not yet available and, in their absence, Monte Carlo models which incorporate appropriate LO matrix elements and leading-logarithmic parton showers are usually used. The RAPGAP model (Jung, 1995) uses LO matrix elements and parton showers based on standard DGLAP evolution. As shown in Fig. 25(b) this prediction (labeled RG-DIR) lies below the data most significantly at low x_{Bj} . The inclusion of a resolved virtual photon contribution (RG-DIR + RES, see next section) significantly improves the description of the data. The color dipole model (labeled CDM in the figure) (Andersson *et al.*, 1989; Lonnblad, 1995) uses LO matrix elements with parton emissions generated by spanning color dipoles between the partons in place of the usual leading-logarithmic transverse momentum-ordered parton showers. As the dipoles in the CDM radiate independently, there is no ordering of the emissions in transverse momentum and hence this approach shares a similar characteristic with BFKL evolution. The description of the data by this model is considerably better than that by RG-DIR. Given the large point-to-point correlated uncertainties in the data and the unquantified uncertainties in the predictions, the CDM model is in fair agreement with the data.

An alternative model which incorporates BFKL-like characteristics is CASCADE (Jung and Salam, 2001; Jung, 2002). This model in fact uses the CCFM equation (Ciafaloni, 1988; Catani, Fiorani, and Marchesini, 1990a, 1990b; Marchesini, 1995), which provides a bridge between the DGLAP and BFKL descriptions by resumming both $\ln(Q^2)$ and $\ln(1/x)$ terms, resulting in ordering by emission angle in the parton cascade. Comparisons of the CASCADE model with the data are shown in Fig. 25(c) for two different parametrizations of the unintegrated gluon density of the proton. The comparison with data is again better than that of NLO DGLAP QCD or RG-DIR at low x_{Bj} , although it still falls short of the measured cross section at the lowest value and there are also substantial discrepancies at high x_{Bj} .

Further measurements have been made of related observables to that shown in Fig. 25. A similar analysis has been performed (Aaron *et al.*, 2008d) of events which contain a jet in the central region of the detector and two jets in the forward region. The data are shown as a function of the Bjorken scaling variable x in Fig. 26 and are compared with QCD calculations to different orders in α_s . The curves labeled $\mathcal{O}(\alpha_s^2)$ and $\mathcal{O}(\alpha_s^3)$ represent LO and NLO QCD predictions for this three-jet process, respectively. Therefore, again due to kinematic restrictions, it is not surprising that the LO prediction fails to describe the data. The NLO prediction is considerably better, but still lies below the data at the lowest x , indicative of the need for higher-order calculations or dynamics beyond the DGLAP approximation.

Other related measurements include replacing the forward jets by forward π^0 mesons (Adloff *et al.*, 1999b; Aktas *et al.*, 2004b), which is complementary in that it probes lower values of x_{Bj} , but at the expense of reduced signal purity.

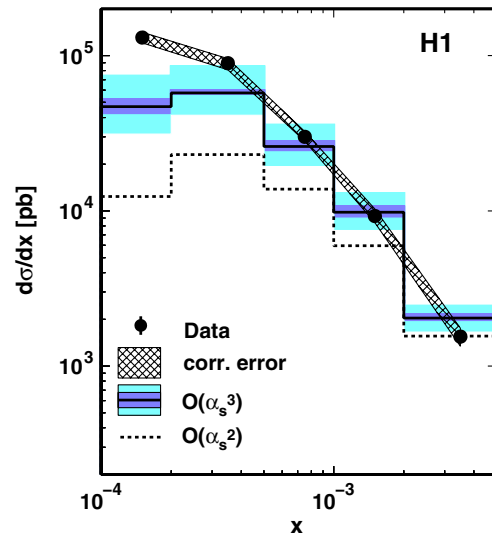


FIG. 26 (color online). Measurement of the cross section as a function of the Bjorken scaling variable x for events in which two jets are reconstructed in the forward direction and one central. The data are compared with second- and third-order QCD calculations. From Aaron *et al.*, 2008d.

Measurements of azimuthal decorrelations between jets at low x (Aktas *et al.*, 2004c) and between a forward jet and the scattered lepton (Aaron *et al.*, 2012e) have also been made. As in the examples above, common themes in these analyses include tendencies for NLO DGLAP QCD predictions to lie below the data at the lowest x and for the CDM model to provide improved descriptions.

3. Virtual photon structure

As discussed in Sec. II.F, the distinction between DIS and photoproduction is somewhat arbitrary. Although no component due to the structure of the photon is usually included in calculations of DIS processes, such a component may still be relevant where an event contains a hard process with a scale such as a jet transverse momentum which is larger than that provided by the virtuality of the photon. Under these circumstances, the photon may be considered as being the object whose structure is being probed.

A measurement which is sensitive to the need for a resolved virtual photon contribution is shown in Fig. 27. The cross section for dijet production in DIS is shown as a function of x_γ^{obs} [see Eq. (4)], here called x_γ^{jets} . The data (Aktas *et al.*, 2004e) are shown for different regions of Q^2 and jet transverse energy E_T^* in the γ^*p frame. Comparisons are made with various QCD calculations. The predictions from DISENT and NLOJET for 2 jets are both NLO QCD predictions for dijet production in DIS [i.e., $\mathcal{O}(\alpha_s^2)$]. Both of these calculations successfully describe high- Q^2 data, but for this variable at low Q^2 and low E_T^* , they lie significantly below the data at low x_γ^{jets} . The other calculation shown, JETVIP, should in principle be ideal to describe these data as it has a component due to the resolved virtual photon which may be inferred from the difference between the “full” and “dir” predictions. Although it can be seen that the addition of this component brings the NLO QCD calculations significantly closer to the data at low

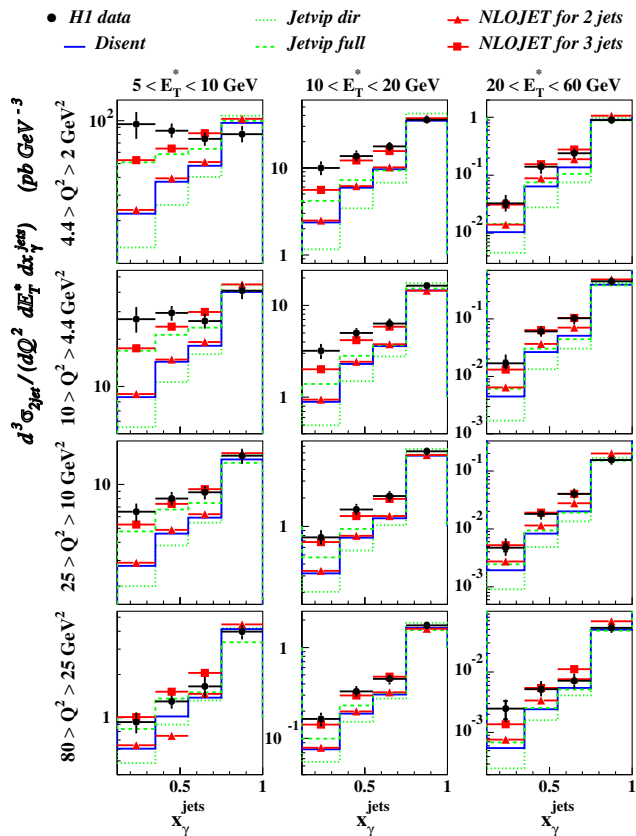


FIG. 27 (color online). Measurement of the dijet cross section in the γ^*p frame in DIS as a function of x_{γ}^{jets} in different regions of Q^2 and E_T^* . The data (Aktas *et al.*, 2004e) are compared with three NLO QCD calculations in DIS for $2 \rightarrow 2$ processes, DISENT, JETVIP dir, and NLOJET for 2 jets, with an NLO QCD calculation for $2 \rightarrow 3$ processes, NLOJET for 3 jets, and with an NLO QCD calculation in DIS for $2 \rightarrow 2$ processes, including a component of resolved virtual photon structure, JETVIP full. All of the theory predictions are corrected for hadronization effects. From Chyla *et al.*, 2005.

x_{γ}^{jets} , the “dir” component does not agree with DISENT or NLOJET at the level that they agree with each other, although all three are in principle calculations of the same contribution. Because of this, the JETVIP calculations cannot be considered to be fully reliable. It is unlikely that these calculations will be improved and hence firm conclusions on the influence of virtual photon structure on the description of observables such as this in NLO QCD cannot yet be drawn. Alternative predictions have been made (Chyla *et al.*, 2005) using the NLOJET calculation in its mode for calculating three-jet production (NLOJET for 3 jets). Although this is not a full NNLO QCD [$\mathcal{O}(\alpha_s^3)$] calculation for dijet production, as an NLO QCD calculation for $2 \rightarrow 3$ processes, it contains a number of the extra diagrams. The prediction lies significantly higher than that for 2 jets, particularly at low x_{γ}^{jets} , and the description of the data is significantly improved.

4. The underlying event

The term “underlying event” is usually used in high transverse momentum processes to refer to all hadronic final-state particles not originating from the hard partonic

scattering. While in principle this includes the influence of the proton, and possibly the photon, beam remnants, the most interesting component arises from the possibility of multiple photon-proton scatterings taking place in the same event. As with photon structure, the underlying event is therefore a concept most naturally applied to resolved photoproduction, but which in principle may still be relevant to DIS when the photon virtuality is not significantly larger than other hard scales in a process. The secondary scatters generate additional hadronic energy flow in the event, the topology, and magnitude of which are poorly understood theoretically, but which must be accounted for when measuring jet and other related cross sections. As illustrated in Fig. 28, jet measurements are most sensitive to underlying event issues at relatively low transverse momentum, where they may significantly influence the shapes as well as the normalizations of distributions.

At the center of the development of our understanding of the underlying event is the possibility of multiple hard interactions (Landshoff and Polkinghorne, 1978), in which more than one pair of partons takes part in separate processes that generate large transverse momenta (see Fig. 29). Such processes are usually modeled (Butterworth, Forshaw, and Seymour, 1996; Sjostrand *et al.*, 2001) via an integral over different impact parameters between the two hadrons, for each of which secondary partonic scattering is generated using proton PDFs at a suitably reduced momentum fraction, distributed over an appropriate spatial matter distribution. A consequence of this impact parameter-dependent physical

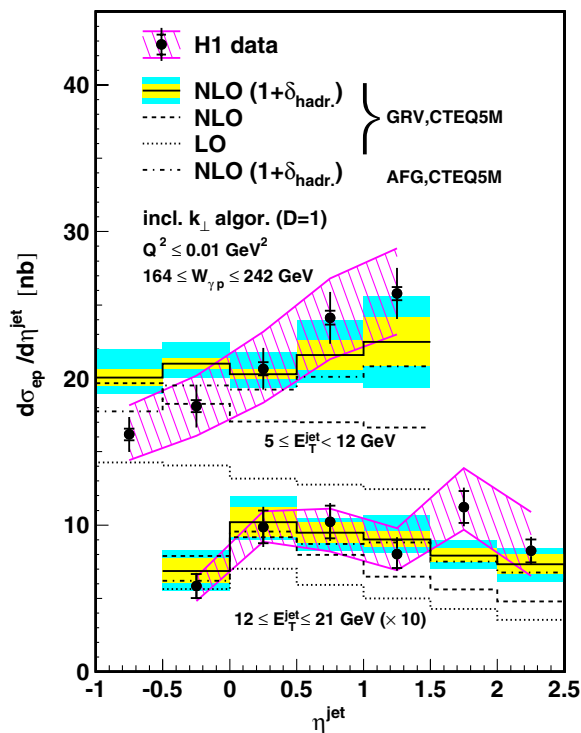


FIG. 28 (color online). Measurements of inclusive jet photo-production at the smallest jet transverse energies reached at HERA (extending to $E_T^{\text{jet}} = 5$ GeV). The data are compared with NLO QCD calculations before and after correcting for underlying event and hadronization effects, the combination of which is labeled δ_{hadr} . From Adloff *et al.*, 2003.

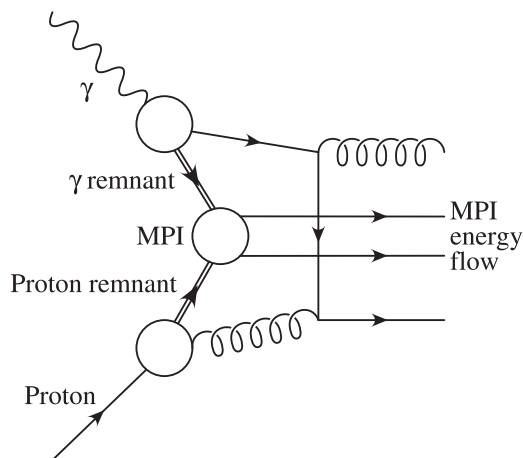


FIG. 29. A schematic representation of an event with multiparton interactions.

picture is that the hardest primary interactions are associated with the most “head-on” of collisions and are thus predicted also to exhibit high transverse momentum secondary scatterings. This predicted correlation encourages an experimental approach based on events with high jet multiplicities.

Multiparton interactions have been studied at the Tevatron (Abe *et al.*, 1993d, 1997a, 1997b; Abazov *et al.*, 2003; Acosta *et al.*, 2004), in dijet photoproduction events at HERA (Derrick *et al.*, 1995a; Aid *et al.*, 1996d; Breitweg *et al.*, 1998b; Adloff *et al.*, 2000c), and more recently at the LHC (Khachatryan *et al.*, 2010; Aad *et al.*, 2011b, 2011c, 2012c; Chatrchyan *et al.*, 2011, 2012b, 2013b). In the case of the HERA data, the inclusion of multiparton interactions in Monte Carlo models improves the description of the data at low transverse energy for regions enriched in resolved-photon events, as expected. Although this is supportive of the models including an underlying event component, it does not in itself constitute evidence for the existence of hard secondary scatters. To search for direct evidence of such processes, photoproduction events containing four jets with $E_T^{\text{jet}} > 6$ GeV have been considered. Events produced via multiparton scattering exhibiting this topology are in principle distinguishable from four-jet events produced via QCD radiation in ordinary $2 \rightarrow 2$ scattering through the lack of correlation between the angular distributions or momenta of the pairs of jets. The measured cross section for four-jet photoproduction is shown as a function of x_γ^{obs} (Chekanov *et al.*, 2008f) in Fig. 30, compared with various predictions from Monte Carlo models. As with the case of dijet production, but even more significantly, adding models of multiparton interactions to the predictions significantly improves the description of the data, with models not including this feature being clearly inadequate. However, investigation of angular correlations in these data did not reveal clear evidence of independent secondary scatters.

In summary, although some HERA data show clear evidence for some form of underlying event, the exact nature of the effect is not yet firmly established. Models which are based on multiple independent hard secondary scatters significantly improve the description of the data, but no direct evidence for this process has yet been demonstrated. In any

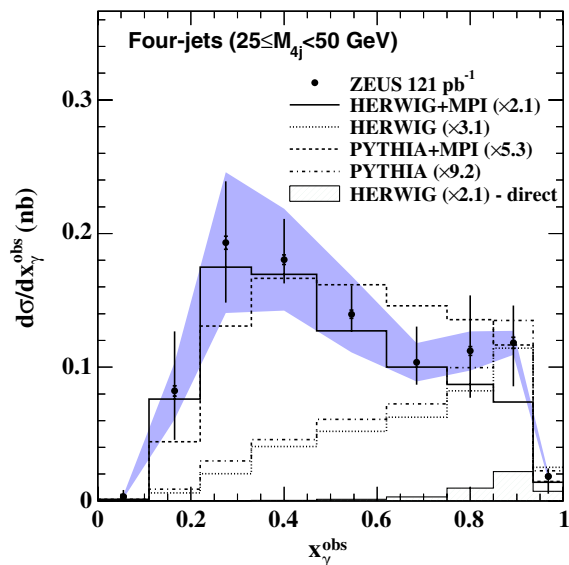


FIG. 30 (color online). Measurement of the four-jet photoproduction cross section as a function of x_γ^{obs} for low invariant masses of the four-jet system $25 < M_{4j} < 50$ GeV. The predictions from the HERWIG and PYTHIA Monte Carlo models are shown both with (Butterworth, Forshaw, and Seymour, 1996; Sjostrand *et al.*, 2001) and without multiparton interactions, as is the direct-photon component of the HERWIG prediction. Each prediction is normalized to the measured high-mass ($M_{4j} > 50$ GeV) cross section by the factors given in the legend. From Chekanov *et al.*, 2008f.

case, the HERA data will help to constrain future underlying event models and Monte Carlo tunes.

5. Discussion

The above considerations clearly indicate that an improved description of HERA hadronic final-state data could be obtained with higher-order (either NNLO QCD or NLO QCD with parton showering) calculations. Tools providing such calculations for comparisons with LHC data have generally been successful for similar observables to those considered here [e.g., Aad *et al.* (2012a)]. All further statements beyond this central conclusion are less definite. There is evidence for novel parton cascade dynamics, similar to those expected for BFKL-dominated evolution, in low- x HERA hadronic final-state data. However, the extent to which such effects can be recovered through higher-order DGLAP-based calculations is not yet clear. In the absence of such calculations, models based on virtual photon structure are often as successful in simulating the effects as those invoking alternative parton evolution schemes. The data also show considerable circumstantial evidence for multiparton interactions. However, in the absence of a direct observation of such processes, it is not yet possible to rule out the possibility that the apparent need for such effects is a consequence of missing higher-order QCD calculations.

E. Event shapes

The hadronic final states of events in DIS and e^+e^- annihilation can be characterized by a number of variables

that describe the shape of the event. These variables are sensitive to perturbative and nonperturbative QCD and given these are properties which are measurable for all events, the data samples are much larger than can be obtained, for example, by requiring high- E_T jets in DIS. Understanding the hadronization process is crucial to all measurements in this review and is often modeled phenomenologically using Monte Carlo event generators and applying the resulting corrections to fixed-order QCD calculations. An alternative approach is to use power corrections (PC), which have an $\mathcal{O}(1/Q)$ dependence, and are calculated analytically, extending perturbative methods into the nonperturbative regime. Within this framework (Dokshitzer and Webber, 1995, 1997; Dokshitzer, Marchesini, and Webber, 1996; Dokshitzer *et al.*, 1998; Dokshitzer, Marchesini, and Salam, 1999), event-shape variables depend on the strong coupling α_s and an effective coupling parameter α_0 , which is expected to be universal for all event shapes.

Event shapes have been measured in e^+e^- annihilation [for a recent review, see Okorokov (2012), and citations therein] and power corrections were found to reproduce many aspects of the hadronization process. The measurements discussed here from H1 (Aktas *et al.*, 2006g) and ZEUS (Chekanov *et al.*, 2007d) use DIS events reconstructed in the Breit frame with a minimum Q^2 of 196 and 80 GeV^2 , respectively. These most recent measurements have significantly larger data samples than previous publications (Adloff *et al.*, 1997f, 2000b; Breitweg *et al.*, 1998d; Chekanov *et al.*, 2003a) and therefore allow measurement of differential event-shape distributions rather than just the mean values. The event shapes studied are the following: the thrust, which measures the longitudinal collimation of the hadronic system relative to an appropriate axis; the broadening, which measures the complementary aspect; the jet mass; and a characteristic of the event known as the C parameter (for the exact definitions, see the H1 and ZEUS publications and their references). An example of the measurements is shown in Fig. 31, where the mean event shapes are compared with a prediction using NLO QCD to describe the perturbative production of partons and power corrections to describe the hadronization process. The figure also shows the prediction from NLO QCD alone, indicating the strong need for power corrections, which, when combined with the NLO QCD prediction, describe the data well. The differential distributions of all variables are similarly well described by the theory if the perturbative part is a combination of the NLO QCD prediction matched to a resummed prediction to NLL accuracy.

The good description of the differential distributions and their mean values allow the parameters of the theory, α_s and α_0 , to be extracted from the data. The extracted values from fits to the differential distributions are shown in Fig. 32 in the plane of the two extracted variables for all five event shapes from both collaborations. In the case of H1 [Fig. 32(a)], the values of α_s extracted for the five variables agree reasonably well with each other and with the world average. H1 also investigated the dependence of α_s on the scale Q , and observed the expected variation predicted by the renormalization group equation. Similarly, the values of α_0 are all broadly consistent with each other. Averages of α_s and α_0 were then extracted as

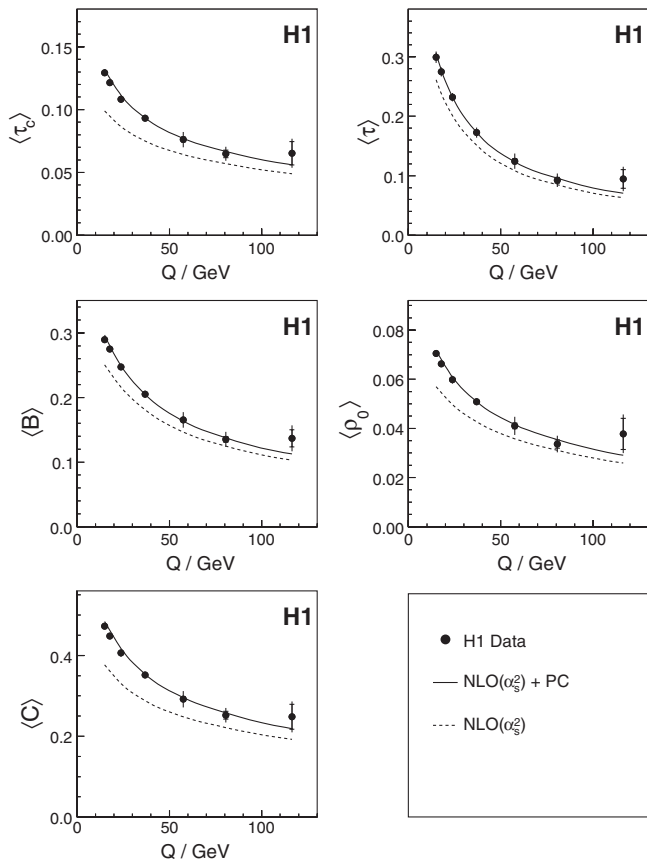


FIG. 31. Distributions of mean event shapes: the thrust variable τ , which measures the longitudinal momentum components projected onto the boson axis; the thrust variable τ_C , which maximizes the sum of the longitudinal momenta in the current hemisphere; the broadening variable B , which measures the scalar sum of transverse momenta with respect to the boson axis; the squared jet mass ρ_0 , normalized to 4 times the squared scalar momentum sum in the current hemisphere; and the C parameter. The data, as a function of the scale Q , are compared with the result of a fit based on NLO QCD with power corrections (solid lines) as well as the contribution from NLO QCD alone (dashed lines). From Aktas *et al.*, 2006g.

$\alpha_s(M_Z) = 0.1198 \pm 0.0013(\text{exp})_{-0.0043}^{+0.0056}(\text{theo})$ and $\alpha_0 = 0.476 \pm 0.008(\text{exp})_{-0.059}^{+0.018}(\text{theo})$. A similar analysis from ZEUS is shown in Fig. 32(b), where the values of α_s extracted also agree with each other and the world average. The values of α_0 are similar but show a larger spread, with the C parameter showing the largest difference from the results of H1. It should be noted that the uncertainty due to variation of the renormalization scale is significantly larger than the experimental uncertainty, the extraction of the parameters is sensitive to the kinematic range chosen for the fits, and the parameters are also sensitive to the details of the matching performed to combine the NLO and NLL QCD predictions. These issues point to a need for higher-order calculations and in the future a unified approach to fitting the data, from both DIS and e^+e^- annihilation.

In summary, the general description of the event-shape distributions and mean values at HERA is good, showing the

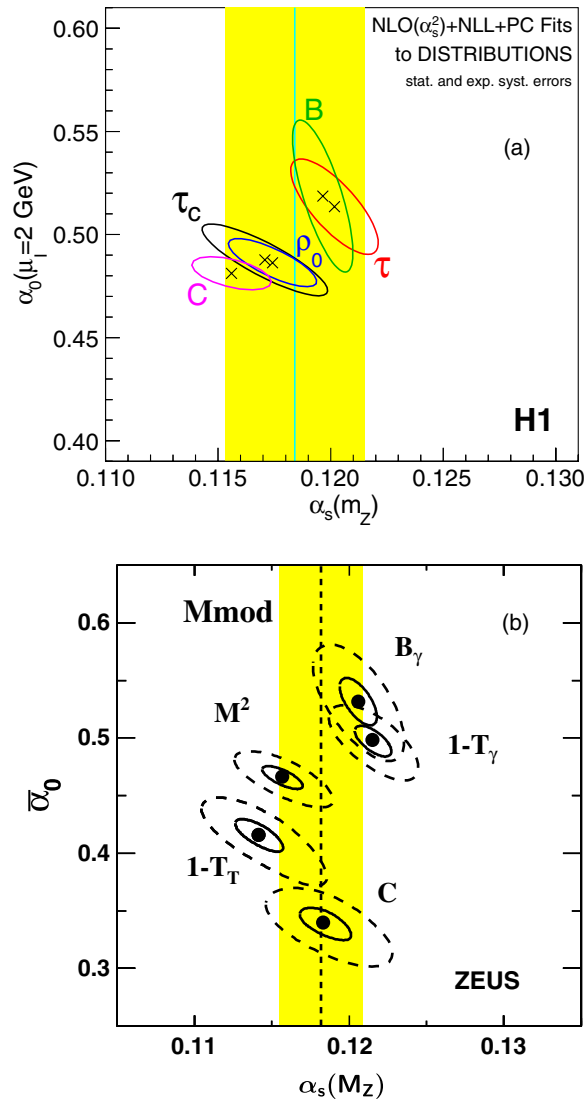


FIG. 32 (color online). Extracted values from (a) H1 and (b) ZEUS for α_0 and α_s for fits of the NLO + NLL + PC predictions to all event-shape variables. The solid lines represent the 1σ contours and for (b) the dashed line represents the 95% C.L. contour. The world-average value of α_s and its uncertainty are shown as the bands, taken from Bethke (2004). (a) From Aktas *et al.*, 2006g. (b) From Chekanov *et al.*, 2007d.

applicability of pQCD, however with indications, as in the remainder of this section, that orders beyond NLO QCD are needed. The combination of power corrections, to describe the hadronization process, with pQCD is also supported, although this can depend on the precise details of the analysis. Other aspects and models of hadronization are discussed in Sec. IV.

IV. NONPERTURBATIVE ASPECTS AND HADRONIZATION

In this section, measurements of hadron production and their interpretations in QCD, both perturbative and non-perturbative, are discussed. Charged-particle distributions and Bose-Einstein correlations are first discussed and

comparisons are made with e^+e^- and other data to test the universality of fragmentation. The parameters of charm fragmentation are then presented and again comparisons are made between different reactions. Inelastic J/ψ results follow, together with a discussion of HERA's contribution to the understanding of charmonium production mechanisms. Finally, searches for more exotic QCD objects, such as deuterons, glueballs, instantons, and pentaquarks are briefly reviewed. Inclusive energy flow measurements have also been made at HERA, most recently and precisely in Adloff *et al.* (2000d), but are not discussed further here.

A. Charged-particle distributions

Numerous measurements of charged particles have been made at HERA, investigating both the hard and soft aspects of QCD. While measurements of jet production probe higher scales and cover a wider kinematic range, the high statistics and precise reconstruction when measuring individual particles allows some more detailed tests. The basic kinematic distributions of all charged particles combined have been measured in both DIS (Abt *et al.*, 1994a; Derrick *et al.*, 1995d, 1996a; Adloff *et al.*, 1997e; Aaron *et al.*, 2007; Alexa *et al.*, 2013b) and photoproduction (Abt *et al.*, 1994b; Breitweg *et al.*, 1998a; Adloff *et al.*, 1999a) and are in general described by Monte Carlo models incorporating leading-order matrix elements and parton showers followed by hadronization. Further measurements have been made in which specific particle species are tagged, e.g., K_S^0 mesons, or different distributions or properties are investigated, such as angular correlations. The body of work is too great to cover in this short section and the interested reader is referred to the large number of relevant papers on the H1 (H1 Collaboration, 1992) and ZEUS (ZEUS, 1992) paper lists. In this section a few results are discussed, focusing on comparisons with data from other reactions and the general conclusions which can be drawn as a result, as well as comparisons with NLO QCD predictions using fragmentation functions (the probability that a parton hadronizes into a given hadron which carries a fraction z of the parton's momentum).

Charged-particle multiplicities have been measured in many experiments, at $p\bar{p}$, pp , ep , and e^+e^- colliders (Beringer *et al.*, 2012), testing models of fragmentation and the universality of the process. In ep DIS scattering, there are several combinations of scales and frames that can be used (Derrick *et al.*, 1995b; Aid *et al.*, 1996a; Adloff *et al.*, 1997c, 1998b; Breitweg *et al.*, 1999d; Chekanov *et al.*, 2001a, 2008d; Aaron *et al.* (2007)). In the results reviewed here (Chekanov *et al.*, 2008d) the final state was reconstructed in the Breit and hadronic center-of-mass frames in which, respectively, twice the energy of the current region of the Breit frame $2 \times E_B^{cr}$ and the γ^*p center-of-mass energy W were used as scales. The charged-particle multiplicities in DIS for these different frames and their respective energy scales are shown in Fig. 33 in comparison with previous DIS experiments and results from e^+e^- experiments. In general charged-particle spectra at HERA show the same trend as those from other experiments over about 2 orders of magnitude in the energy scale of the interaction. In particular, the data from the two ep frames with their respective energy scales agree well with the

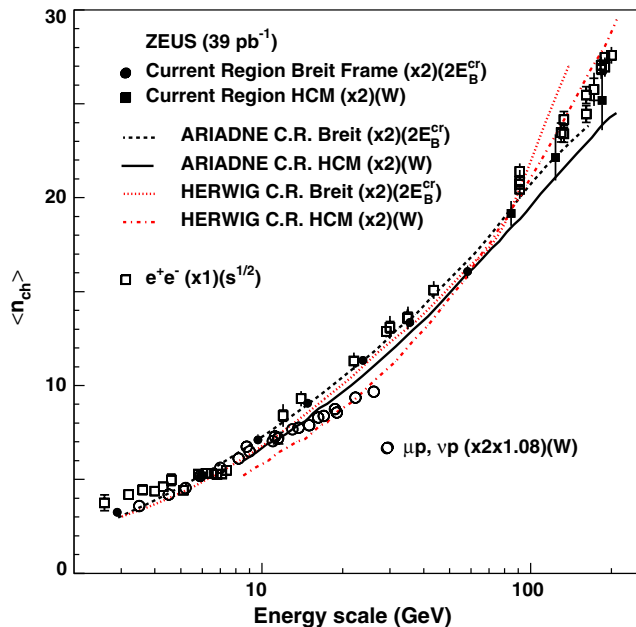


FIG. 33 (color online). Mean charged multiplicity $\langle n_{ch} \rangle$ as a function of the energy scale for ZEUS DIS measurements in the Breit and hadronic center-of-mass frames, compared with results from e^+e^- and fixed-target DIS experiments. From Chekanov *et al.*, 2008d.

results from e^+e^- experiments, in contrast to when the scale Q is used in the Breit frame (Breitweg *et al.*, 1999d). This results in a lower charged multiplicity at low values $Q < 10$ GeV than both the e^+e^- data and the DIS data when $2 \times E_B^{cr}$ is used as the scale. The fixed-target DIS data agree with the HERA and e^+e^- data at low scales, but increasingly deviate above about 15 GeV.

A related quantity considered is the number of charged particles per event per unit scaled particle momentum $x_p = 2P_B/Q$, where P_B is the momentum of a hadron in the Breit frame. This quantity, measured in DIS (Breitweg *et al.*, 1997c; Aaron *et al.*, 2007; Abramowicz *et al.*, 2010e), is shown in Fig. 34 over 2 orders of magnitude in Q in bins of x_p , compared with e^+e^- data. As Q increases, the phase space for soft gluon radiation increases, leading to a rise of the number of soft particles having small x_p , which along with the decrease with Q at high- x_p results in clear scaling violations. The comparison between HERA and e^+e^- data in Fig. 34 is good for all Q and x_p which, along with the comparison in Fig. 33, supports the concept of the universality of fragmentation. Positively and negatively charged particles have also been considered separately and the charge asymmetry measured (Aaron *et al.*, 2009e) as a function of Q and x_p . At large x_p , the observed charge asymmetry is found to increase with Q and correspondingly with the Bjorken- x value, consistent with the expectation that this observable is related to the valence quark content of the proton.

The inclusive data are compared in Fig. 35 with NLO QCD calculations which use fragmentation functions obtained from fits to e^+e^- data. The predictions from the four different groups shown are relatively similar to each other but do not describe the data well. The scaling violations are poorly

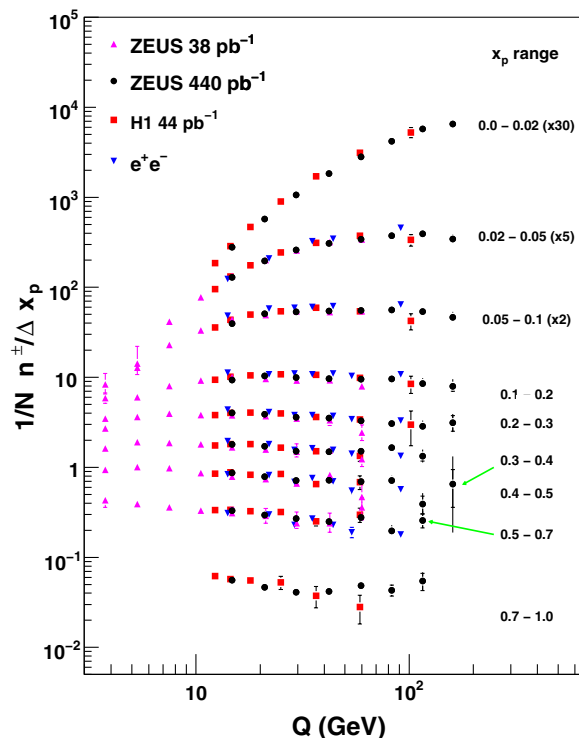


FIG. 34 (color online). The number of charged particles per event per unit x_p as a function of Q in bins of x_p . Data are shown for H1 and ZEUS and are compared with those from e^+e^- experiments (Petersen *et al.*, 1988; Braunschweig *et al.*, 1990; Li *et al.*, 1990; Abreu *et al.*, 1993). From Abramowicz *et al.*, 2010e.

described, with the theory having a shallower rise for low x_p than the data. Also, the theory predicts too many particles at low x_p , whereas too few are predicted at high x_p . The disagreements between data and theory are, in general, in

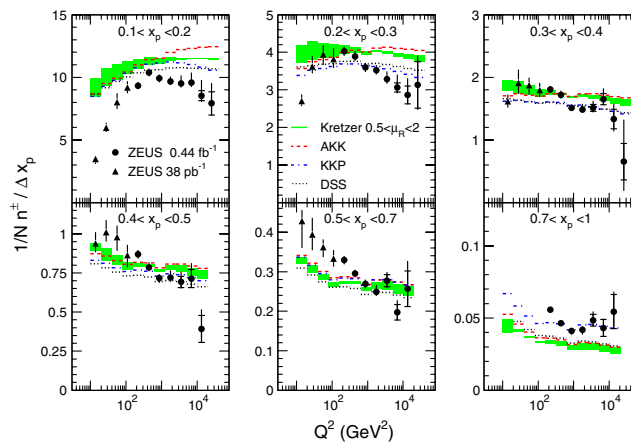


FIG. 35 (color online). The number of charged particles per event per unit x_p as a function of Q in bins of x_p . The shaded bands represent NLO QCD calculations by Kretzer (Kretzer, 2000) with their renormalization uncertainties. Additional calculations are shown: Kniehl, Kramer, and Pötter (KKP) (Kniehl, Kramer, and Potter, 2000); Albino, Kniehl, and Kramer (AKK) (Albino, Kniehl, and Kramer, 2005, 2008); and de Florian, Sassot, and Stratmann (DSS) (de Florian, Sassot, and Stratmann, 2007a, 2007b). From Abramowicz *et al.*, 2010e.

kinematic regions outside those measured in e^+e^- collisions, such as low Q^2 or high x_p . Hence the theory, which is derived from fits to the e^+e^- data, is extrapolated to regions in which it may not be applicable. Future fits should therefore use these HERA data to further constrain the fragmentation functions.

B. Bose-Einstein correlations

Goldhaber *et al.* (1959, 1960) observed the fact that pairs of like-sign pions in $p\bar{p}$ collisions had a tendency to have smaller opening angles than pairs of unlike-sign pions. This is interpreted as being due to the symmetrization of the wave functions of pairs of identical bosons and is hence known as Bose-Einstein correlations (BEC). The effect has since been studied in various hadron-hadron collisions, e^+e^- annihilation, and lepton-nucleon scattering (Alexander, 2003). The BEC in momentum space are related to the spatial dimensions of the production source, with measurements usually being characterized in terms of the effective source size r .

While measurements of r clearly reflect the size of the interacting particles in heavy-ion collisions (Aamodt *et al.*, 2011), the situation from proton-proton collisions is less clear, with dependences on the event multiplicity and transverse momentum of the bosons observed in high-energy experiments (Alexopoulos *et al.*, 1993; Aamodt *et al.*, 2010; Khachatryan *et al.*, 2011). Conclusions from BEC studies are to some extent obscured by the fact that the extracted values of r are often strongly dependent on the choice of control sample relative to which the signal is measured. Values obtained using unlike-sign control samples are up to a factor of 2 larger than those obtained relative to event-mixed control samples.

In ep scattering, the source size might be expected to reflect the size of the proton in low energy-scale processes and to evolve to smaller sizes more similar to those from e^+e^- data as the energy scale increases and the electron scatters from a single parton rather than from the proton as a whole. It is therefore interesting to study whether there is any dependence of the effective source size on the kinematic variables, in particular, Q^2 , since this reflects the effective transverse size of the exchanged virtual photon. The HERA case is therefore ideally suited to investigating whether r depends on the primary interaction or whether it is determined solely by the fragmentation stage of the process.

Measurements of BEC at HERA have been performed for various different samples and kinematic regions in DIS, spanning $0.1 < Q^2 < 8000 \text{ GeV}^2$. H1 and ZEUS have both measured the effect using an inclusive sample of hadrons (Adloff *et al.*, 1997a; Chekanov *et al.*, 2004b). H1 additionally studied a diffractive DIS event sample (Adloff *et al.*, 1997a), in order to investigate whether a difference between the production mechanisms of diffractive and nondiffractive processes could be established. Motivated by a reported dependence of r on the mass of the interfering bosons in e^+e^- annihilation [$r_{\pi\pi} > r_{KK} > r_{\Lambda\Lambda}$ (Alexander, Cohen, and Levin, 1999)], ZEUS also measured the effect for samples of charged and neutral kaons (Chekanov *et al.*, 2007a).

Selected effective source size measurements from DIS and e^+e^- collisions are collected in Table I. No dependence of the source size on the kinematic variables, including Q^2 , was

found at HERA. There is also no significant variation between the results obtained in diffractive and inclusive DIS. The results for charged and neutral kaons are consistent with one another and also with those from inclusive charged-particle production. Furthermore, the results from HERA are consistent with lower-energy DIS experiments (Arneodo *et al.*, 1986; Korotkov *et al.*, 1993). HERA and the other DIS data are also compatible with measurements from e^+e^- annihilation (Althoff *et al.*, 1986; Juricic *et al.*, 1989; Choi *et al.*, 1995; Alexander, Cohen, and Levin, 1999). From these observations, it can be concluded that, within the DIS regime, Bose-Einstein interference in ep scattering does not depend significantly on the details of the hard process. The similarity with data from e^+e^- annihilation further indicates that the presence of an incoming hadron is not important if a short distance hard interaction takes place. The effective source size is thus driven primarily by the fragmentation process in DIS.

C. Charm fragmentation

Predictions of observable heavy quark cross sections rely on a knowledge of fragmentation parameters. This is particularly true when measuring the production rate of a given, e.g., charm meson where both the fraction of charm quarks hadronizing to the given meson and the charm fragmentation function are required inputs in a QCD calculation. Because of the large charm cross section at HERA, precise measurements of charm fragmentation parameters have been performed. The parameters can be compared with results from e^+e^- data, thereby testing the universality of the charm fragmentation process. As well as the ground state charm mesons, excited charm mesons (e.g., D_1 and D_2^*) have also been reconstructed and fragmentation parameters extracted. These are not discussed further here and the reader is referred to the

TABLE I. Source sizes r extracted from hadron production in e^+e^- annihilation and in lepton-nucleon scattering. The uncertainties given for EMC and BBCNC are statistical only; the systematic uncertainties are expected to be of a similar size. All other results have the statistical and systematic uncertainties shown separately. The control samples used are the unlike-sign samples except for the LEP average and ZEUS kaon measurements. The LEP value is the average of using the unlike-sign and event-mixing samples as the control with the second error reflecting half the difference between the two and the value when using the unlike-sign sample is the higher of the two r values. For the kaon pairs, an unlike-sign sample is not usable due to the strong signal from $\phi \rightarrow K^+K^-$.

Process	Experiment	r (fm)
e^+e^-	AMY	$0.73 \pm 0.05 \pm 0.20$
	TASSO	$0.82 \pm 0.06 \pm 0.04$
	MARK II	$0.75 \pm 0.03 \pm 0.04$
	LEP	$0.78 \pm 0.01 \pm 0.16$
Previous DIS	EMC	0.84 ± 0.03
	BBCNC	0.80 ± 0.04
HERA	H1	$0.68 \pm 0.04^{+0.02}_{-0.05}$
	ZEUS	$0.666 \pm 0.009^{+0.022}_{-0.036}$
	H1 (diffractive)	$0.59 \pm 0.13^{+0.05}_{-0.05}$
HERA	ZEUS ($K^\pm K^\pm$)	$0.57 \pm 0.09^{+0.15}_{-0.08}$
	ZEUS ($K_S^0 K_S^0$)	$0.63 \pm 0.09^{+0.11}_{-0.08}$

relevant publications (Chekanov *et al.*, 2009j; Abramowicz *et al.*, 2013d).

The probability that a charm quark hadronizes into a given hadron, the fragmentation fraction, has been determined at HERA for all ground state charm hadrons, both in DIS (Aktas *et al.*, 2005a; Chekanov *et al.*, 2007k; Abramowicz *et al.*, 2010d) and in photoproduction (Chekanov *et al.*, 2005c; Abramowicz *et al.*, 2013b). The results are shown in Fig. 36 along with a combined result from e^+e^- annihilation (Gladilin, 1999; Lohrmann, 2011). The results for a given hadron are consistent between the three processes and, particularly in the photoproduction regime, the HERA results are of competitive precision to the results from e^+e^- data.

As the values of the fragmentation fractions are consistent with being independent of the process, all measurements have been combined (Lohrmann, 2011). The results of this analysis represent our best knowledge of these values and should be used in future calculations of charm production.

The so-called fragmentation function of a given hadron is the distribution in the fractional transfer z of a quark's energy to the hadron. This has been measured for the D^* meson in DIS by H1 (Aaron *et al.*, 2009f) and in photoproduction by ZEUS (Chekanov *et al.*, 2009g). Both sets of results showed a strong sensitivity to models of fragmentation with parameters in a given model varied and best-fit values extracted. The measurement from ZEUS tagged D^* mesons associated to a jet; the relatively high scale of the process $\sqrt{\hat{s}}$ given by $2 \times \langle E_T^{\text{jet}} \rangle = 23.6$ GeV, allowed a measurement of the fragmentation function which was relatively unbiased by the kinematic cuts (Chekanov *et al.*, 2009g). The ZEUS data are shown in Fig. 37 compared to results from e^+e^- collisions. The scales of the process for Belle and CLEO are similar, about 10.5 GeV, whereas for ALEPH the scale is 91.2 GeV. It can be seen that the ZEUS data, which are intermediate in scale, lie between the Belle, CLEO, and ALEPH results, which is qualitatively consistent with expectations from scaling violations in QCD in which $\langle z \rangle$ decreases with increasing energy (Cacciari, Nason, and Oleari, 2006). Similarly, the z distributions from both collaborations were

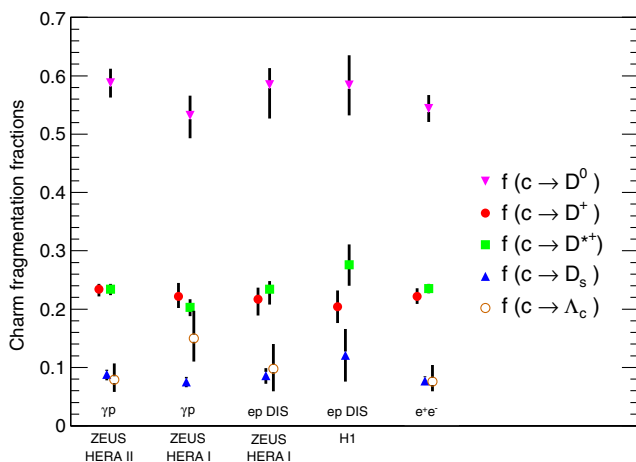


FIG. 36 (color online). Measurements of fragmentation fractions for various charm hadrons in DIS and photoproduction at HERA and also in e^+e^- annihilation at LEP. From Abramowicz *et al.*, 2013b.

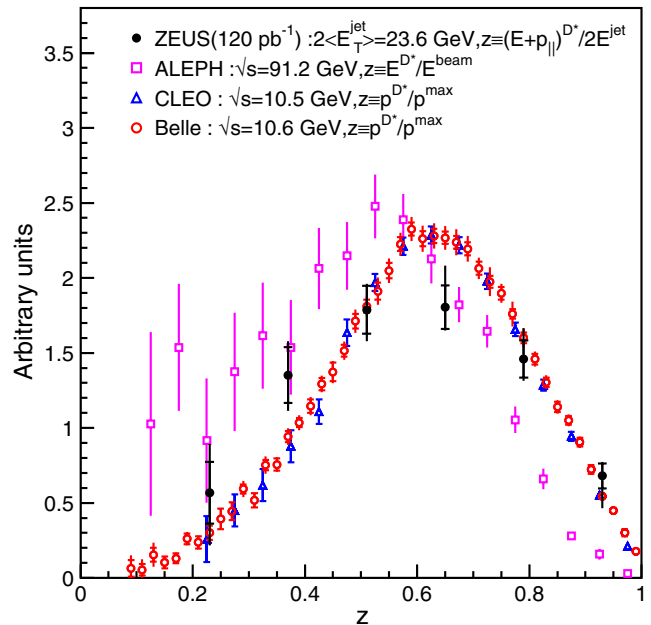


FIG. 37 (color online). D^* fragmentation function $f(z)$ for ZEUS data compared to measurements in e^+e^- collisions. To compare the shapes, the data sets were normalized to $1/(\text{bin width})$ for $z > 0.3$. From Chekanov *et al.*, 2009g.

used to extract the parameter ϵ in the Peterson fragmentation function (Peterson *et al.*, 1983) as implemented in the PYTHIA Monte Carlo model and the outcomes were found to agree with the results when fitting the e^+e^- data. These results are consistent with the hypothesis of fragmentation universality between ep and e^+e^- processes.

Both collaborations fit NLO QCD predictions to the data using the Kartvelishvili *et al.* model (Kartvelishvili, Likhoded, and Petrov, 1978) for fragmentation,

$$f(z) \propto z^\alpha (1-z), \quad (7)$$

where α is a free parameter. The result from ZEUS of $\alpha = 2.67_{-0.31}^{+0.25}$ can be compared with that from H1 for lower scales, given in Fig. 38. A higher value of α implies a high $\langle z \rangle$ and so the observation of α increasing with decreasing scale $\sqrt{\hat{s}}$ is also consistent with the expectations from scaling violations in QCD. However, it should be noted that the quality of the fit for the lowest scale, in Fig. 38(b), is poor indicating an incomplete description of the full phase space down to the production threshold. Future fits of fragmentation functions should use these HERA data as part of their input and the uncertainties in the determination of the fragmentation parameter should ideally be propagated as a systematic uncertainty in NLO QCD calculations of a given charm cross section.

D. Inelastic J/ψ production

Even though the discovery of the J/ψ meson, and hence the charm quark, was made in 1974, its hadroproduction mechanism is still uncertain [for a review, see Brambilla *et al.* (2011)]. At HERA, J/ψ production is dominated by boson-gluon fusion in which a photon emitted from the incoming electron interacts with a gluon from the proton to produce

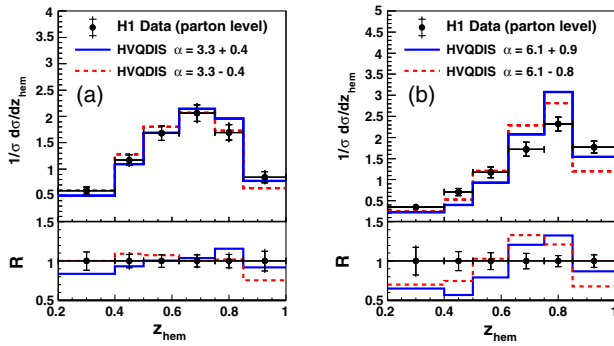


FIG. 38 (color online). Normalized D^* cross sections as a function of an estimator z_{hem} of the fragmentation function z , showing the best fits of an NLO QCD prediction using the Kartvelishvili fragmentation function with the uncertainty range on the α parameter shown. The scales of the processes are (a) $8.4 < \sqrt{s} < 18$ GeV and (b) $\sqrt{s} < 8.4$ GeV. From Aaron *et al.*, 2009f.

a $c\bar{c}$ pair which subsequently forms a J/ψ meson. In the color-singlet (CS) model (Chang, 1980; Baier and Ruckl, 1981, 1982, 1983; Berger and Jones, 1981), the $c\bar{c}$ pair produced has the same quantum numbers as the physical J/ψ bound state, achieved by radiating a hard gluon in the perturbative process. In the color-octet (CO) model (Caswell and Lepage, 1986; Thacker and Lepage, 1991; Bodwin, Braaten, and Lepage, 1995), the $c\bar{c}$ pair emerges from the hard process with quantum numbers different from those of the J/ψ and evolves into the physical J/ψ state by emitting one or more soft gluons. The probability for CO processes occurring is governed by long-distance matrix elements that can be obtained from fits to experiment. Predictions within the CS framework have also been made using the k_T factorization approach (Baranov, 1998, 2002; Lipatov and Zotov, 2003) in which the effects of nonzero incoming parton transverse momentum are taken into account. These three approaches have been compared extensively to HERA measurements.

Both H1 and ZEUS have measured inelastic J/ψ production in DIS (Adloff *et al.*, 2002c; Chekanov *et al.*, 2005d; Aaron *et al.*, 2010c) and in photoproduction (Ahmed *et al.*, 1994b; Aid *et al.*, 1996b; Breitweg *et al.*, 1997a; Adloff *et al.*, 2002d; Chekanov *et al.*, 2003e, 2009f; Aaron *et al.*, 2010c; Abramowicz *et al.*, 2013c). Inelastic J/ψ production has also been measured extensively at the Tevatron and the resulting data have been used to constrain the CS and CO contributions, usually by first applying a CS calculation and then adding a CO contribution, fitted to best describe the data. By combining the CS and fitted CO contributions in this manner, the theory is able to describe the J/ψ cross section in $p\bar{p}$ collisions (Cho and Leibovich, 1996a, 1996b). However, neither this nor the k_T factorization approach is able to describe the polarization measurements for J/ψ and $\psi(2S)$ mesons (Abulencia *et al.*, 2007, and references therein). The CO contribution fitted to the Tevatron data is expected to be applicable to ep collisions and is used to predict H1 and ZEUS data. A measurement of J/ψ photoproduction is shown in Fig. 39 in comparison to LO and NLO QCD predictions (Kramer, 1996; Artoisenet *et al.*, 2009; Butenschoen and Kniehl, 2010, 2011a, 2011b) from the CS model and the CS

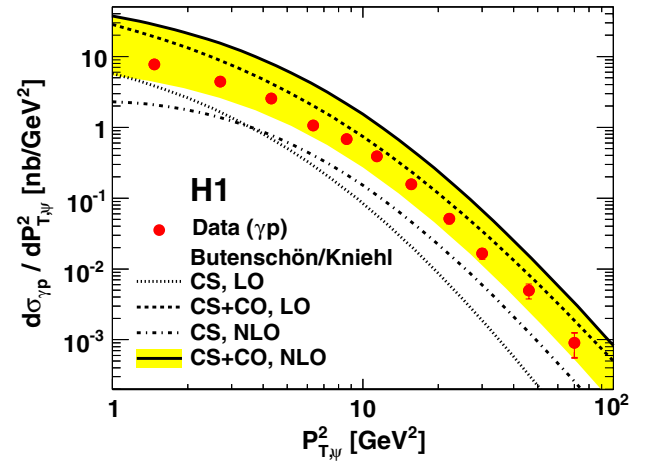


FIG. 39 (color online). Photoproduction cross section, differential in P_T^2 of the J/ψ meson, for H1 data, compared with LO and NLO QCD predictions from the CS model and the CS and CO models combined. The uncertainty on the theory (shaded band) arises from the difference between results using an LO or a higher-order color-octet contribution (Butenschoen and Kniehl, 2010). From Aaron *et al.*, 2010c.

and CO models combined. The predictions from the CS model lie below the data although the shapes of the P_T^2 and inelasticity z (not shown) distributions are well reproduced. As the uncertainties on the theoretical predictions are large, the next order in QCD may be required to describe the data. Inclusion of a CO contribution gives a higher cross section and describes the data well, although again with large uncertainties. Predictions based on k_T factorization in the CS model [using the CASCADE Monte Carlo program (Jung and Salam, 2001; Jung, 2002), not shown] also give a good description of the data.

Measurements of the polarization of the J/ψ mesons provided strong distinguishing power for the Tevatron results and comparable analyses were performed at HERA. An example is shown in Fig. 40, where the helicity parameter is plotted versus the inelasticity for the full ZEUS data sample. The theoretical and experimental uncertainties are large. None of the predictions gives a good description over the full phase space and unfortunately discrimination between different models is not possible from the HERA data alone.

Unfortunately, the production mechanism for J/ψ mesons remains largely unresolved. Although HERA has produced precise measurements of differential cross sections in DIS and photoproduction and measurements of the polarization, progress is limited by the large theoretical uncertainties. Further measurements from the Tevatron or LHC (Aad *et al.*, 2011a; Aaij *et al.*, 2011; Abelev *et al.*, 2012a, 2012b; Chatrchyan *et al.*, 2012a) extending to higher P_T along with global analyses [e.g., Butenschoen and Kniehl (2012)] including the HERA data presented here may lead to deeper insight.

E. Exotic and unusual QCD

Many of the searches for new physics at HERA have focused on the hadronic final state. The situation is perhaps well summarized by generic searches, which identify

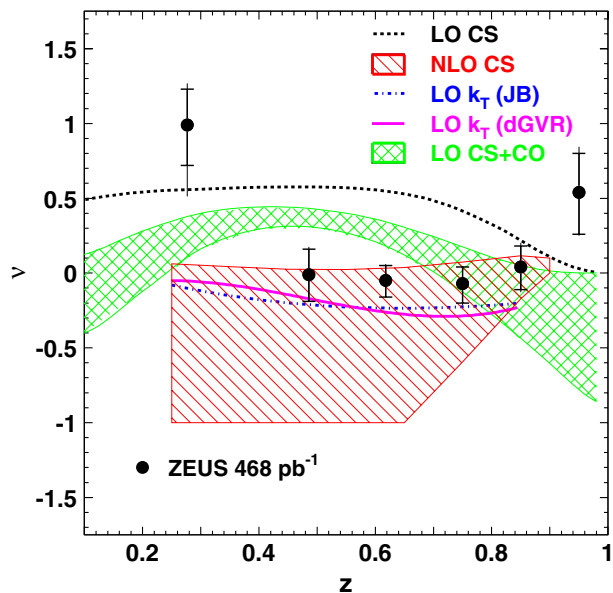


FIG. 40 (color online). Helicity parameter ν for the decay azimuthal angle in the frame where the polarization axis in the J/ψ meson rest frame is defined by the flight direction of the J/ψ meson in the γp rest frame. The value can vary between -1 and $+1$ and is shown here for different inelasticity values. From Chekanov *et al.*, 2009f.

deviations between data and predictions for arbitrary combinations of high transverse momentum objects (leptons, photons, jets, and missing energy) (Aaron *et al.*, 2009a). Both here and in dedicated studies (Adloff *et al.*, 1998c), H1 data consistently exhibited an excess of events with a single isolated lepton, a high transverse momentum jet and large missing energy, corresponding to the topology expected from a W boson produced at high p_T , recoiling against a quark or gluon. However, no comparable signal was observed by ZEUS and excitement about this channel diminished when the full H1 data became available. The final situation from HERA is summarized in a combined H1 and ZEUS result (Aaron *et al.*, 2010j). Ultimately HERA data across a wide range of signatures and channels are remarkably consistent with the standard model.

Within the standard model, a variety of previously unobserved quark and gluon bound states and other novel strong interaction phenomena are predicted. Because of its rich, complex and non-Abelian nature, the status of these states and phenomena within QCD is not always obvious. As discussed in the remainder of Sec. IV.E, in many such cases observing new effects for the first time would constitute a major discovery in its own right.

1. Pentaquark states

The possibility to have particles consisting of five quarks and antiquarks, i.e., pentaquarks, was proposed as early as the 1970s (Jaffe, 1977; Strotman, 1979; Lipkin, 1987) and is predicted within QCD (Diakonov, Petrov, and Polyakov, 1997). In the early part of the 2000s, many collaborations searched for pentaquark states, with several seemingly clear signals, but also contradictory results. The worldwide status is summarized in dedicated reviews of the subject (Dzierba,

Meyer, and Szczepaniak, 2005; Hicks, 2005a, 2005b, 2012; Danilov and Mizuk, 2008). Here we concentrate on the H1 and ZEUS contributions.

Most pentaquark searches have focused on the lightest irreducible quark combination, termed Θ^+ , which has a quark content $uudd\bar{s}$ and a mass expected to be around 1530 MeV. The ZEUS Collaboration searched (Chekanov *et al.*, 2004c) for the Θ^+ in the $K_S^0 p$ decay channel and reported a signal of around $4-4.5\sigma$ significance with a mass of 1521 ± 1.5 MeV in DIS events. Superficially this was consistent with other “observations” of the Θ^+ pentaquark. However, the comparatively low mass (Hicks, 2005b) pointed to problems. H1 subsequently performed the same analysis (Aktas *et al.*, 2006i) and saw no signal, which, along with other null results (Dzierba, Meyer, and Szczepaniak, 2005; Hicks, 2005a, 2005b, 2012; Danilov and Mizuk, 2008) and the fact that ZEUS saw this only at high Q^2 (above 20 GeV^2 , but not above 1 GeV^2) indicates that the ZEUS result had some flaw or must have been a statistical fluctuation. ZEUS have yet to confirm or refute the result even though a data sample several times larger is available.

Both collaborations searched in the $\Xi\pi$ channel (Chekanov *et al.*, 2005f; Aktas *et al.*, 2007e) for the pentaquark resonance reported by the NA49 Collaboration (Alt *et al.*, 2004). The search was performed for pentaquarks decaying to the doubly charged $\Xi^-\pi^-$ and the neutral $\Xi^-\pi^+$ final states. The HERA Collaborations observed a clean resonance for the known baryon $\Xi(1530)^0$ decaying to $\Xi^-\pi^+$, but observed no other higher-mass resonances and so set production limits in the mass range 1600–2350 MeV. These null results were in keeping with the many others for this channel [again see pentaquark review articles (Dzierba, Meyer, and Szczepaniak, 2005; Hicks, 2005a, 2005b, 2012; Danilov and Mizuk, 2008) and references therein].

Assuming the existence of a light pentaquark such as the Θ^+ , then a heavier analog with a charm quark might also be expected to exist. The H1 Collaboration searched for a D^*p resonance and found a clear signal (Aktas *et al.*, 2004a) at about 3.1 GeV, consistent with a pentaquark with quark content $uudd\bar{c}$. A similar search was performed by ZEUS with a larger statistical sample (Chekanov *et al.*, 2004h), but no signal was observed. Given the cleanliness of the H1 signal and its significance of at least $5-6\sigma$, the situation was puzzling. Further null results were published by other high-energy physics experiments (Danilov and Mizuk, 2008) and a higher-statistics analysis presented by H1 (Krueger, 2009). Although unpublished, the newer H1 measurement shows no resonance structure around 3.1 GeV, using a data sample 4 times larger than previously, suggesting that the original results arose from a statistical fluctuation.

In summary, after initial excitement and “discoveries” of new particles, the results from HERA have gone the way of the overall status for pentaquark searches in the many experiments worldwide (Amsler *et al.*, 2008; Hicks, 2012), with no convincing evidence remaining.

2. Instanton searches

In both electroweak and QCD interactions, the ground state has a rich topological structure, associated with

nonperturbative fluctuations of the gauge fields, called instantons (Belavin *et al.*, 1975; 't Hooft, 1976a, 1976b). In electroweak interactions, instantons are not expected to be observable at current colliders. In QCD, the effects of instantons are expected to be manifest at lower energies (Balitsky and Braun, 1993; Ringwald and Schrempp, 1994, 1999; Moch, Ringwald, and Schrempp, 1997), although they have yet to be seen. The rate of instanton production in DIS at HERA was expected to be sizable (Ringwald and Schrempp, 1994, 1998, 1999, 2000, 2001; Gibbs, Ringwald, and Schrempp, 1995; Moch, Ringwald, and Schrempp, 1997) and so presented the HERA experiments with an opportunity to discover the effect. The major challenge for H1 and ZEUS (Adloff *et al.*, 2002g; Chekanov *et al.*, 2004i) was that the instanton cross section was nonetheless small in comparison with the inclusive, which was hard to suppress sufficiently.

The expected characteristics of instanton events are large transverse energy, high multiplicity, and the production of different quark flavors democratically and isotropically in their center-of-mass frame (a “fireball” configuration). A search based on these criteria is presented in Fig. 41, which compares the predicted normalizations and the shapes for particular variables between data, the QCDINS instanton model (Ringwald and Schrempp, 2000) and inclusive DIS models after applying a cut based on a multivariate discriminant. The application of cuts such as this suppresses the inclusive DIS background by factors of typically 1000. Although events exhibiting instanton characteristics are observed, their isolation is hampered by the uncertainty on the remaining background, mainly due to the sometimes poor modeling of the hadronic final state by the inclusive DIS Monte Carlo simulations. It has therefore not been possible to isolate regions in which a clear signature for instanton production is expected. However, the analysis allows upper limits to be placed on instanton production cross sections which are within a factor of 3–5 of the predicted values, depending on the kinematic region. Tuning and improving the simulation of the hadronic final state using the measurements contained in this review may allow a signal for instanton production to be extracted in other experiments.

3. Search for glueball states

The existence of glueballs (bound states of two or more gluons) is predicted by QCD. The lightest state is expected to have quantum numbers $J^{PC} = 0^{++}$ and a mass in the range 1550–1750 MeV (Yao *et al.*, 2006). The state $f_0(1710)$ is frequently considered to be a glueball or tetraquark candidate (Klempt and Zaitsev, 2007; Albaladejo and Oller, 2008), since it does not fit into existing multiplet structures, but its constituent parton content is not established. As the $K_S^0 K_S^0$ system is expected to couple to glueballs, resonances in its invariant-mass spectrum have been searched for.

In an initial study from ZEUS (Chekanov *et al.*, 2004f) of the $K_S^0 K_S^0$ system in DIS, indications of two states $f_2'(1525)$ and $f_0(1710)$ were seen with statistical significances of about 3 standard deviations. A subsequent measurement (Chekanov *et al.*, 2008e) used all events and all data (0.5 fb^{-1}), dominated by photoproduction; given the gluon-rich environment, it is expected that photoproduction should be more sensitive than

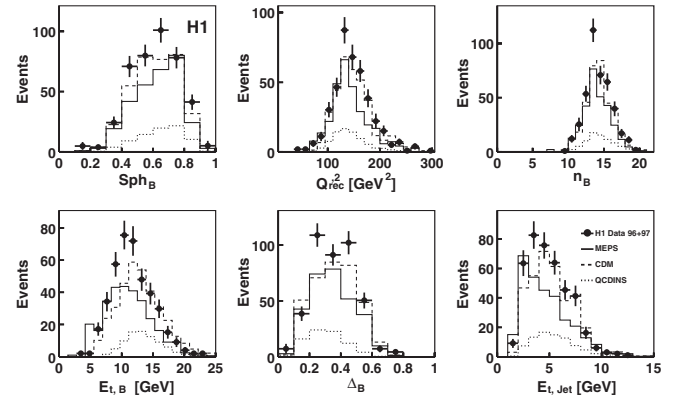


FIG. 41. Raw distributions in sphericity, Q^2 , charged-particle multiplicity, total transverse energy, isotropy, and transverse jet energy, compared with predictions for DIS events and for instanton-induced events (QCDINS), after applying a cut on a multivariate discriminant designed to enhance instantonlike signatures. From Adloff *et al.*, 2002g.

DIS to the production of glueballs. By reconstructing a secondary vertex and removing contamination from photon conversions and Λ baryons, a clean sample of K_S^0 candidates was reconstructed via their decay to $\pi^+ \pi^-$ (Chekanov *et al.*, 2008e). Using over 10^6 K_S^0 mesons, pairs were combined to give the invariant-mass spectrum shown in Fig. 42. Three peaks around 1300, 1500, and 1700 MeV are observed with no heavier state seen.

The states were fitted accounting for the interference pattern predicted by SU(3) symmetry arguments (Faiman, Lipkin, and Rubinstein, 1975). The first peak at about 1300 MeV is consistent with the combination $f_2(1270)/a_2^0(1320)$. The second and third peaks are consistent with the states $f_2'(1525)$ and $f_0(1710)$; their masses and widths are consistent with values from the Particle Data Group (Yao *et al.*, 2006) and are of similar precision. The fit yields 4058 ± 820 events for the $f_0(1710)$ resonance, constituting a statistical significance of 5 standard deviations. The $f_0(1710)$ has a mass consistent with a $J^{PC} = 0^{++}$ glueball candidate, although if it is the same state as is seen in $\gamma\gamma \rightarrow K_S^0 K_S^0$ (Althoff *et al.*, 1983; Acciarri *et al.*, 2001), it is unlikely to be a pure glueball state.

4. Deuteron and antideuteron production

The production of light stable nuclei, such as deuterons (d), in high-energy collisions is poorly understood. Antideuterons (\bar{d}) were first observed in 1965 (Dorfan *et al.*, 1965; Massam *et al.*, 1965) and subsequently in e^+e^- (Albrecht *et al.*, 1985, 1990; Akers *et al.*, 1995; Schael *et al.*, 2006; Asner *et al.*, 2007), proton-nucleus (pA) (Binon *et al.*, 1969; Antipov *et al.*, 1971; Cronin *et al.*, 1975), proton-proton (pp) (Alper *et al.*, 1973; Henning *et al.*, 1978; Abramov *et al.*, 1987), and nucleus-nucleus (Aoki *et al.*, 1992; Appelquist *et al.*, 1996; Ahle *et al.*, 1998; Bearden *et al.*, 1999, 2002; Adler *et al.*, 2001, 2005; Arsene *et al.*, 2011; Anticic *et al.*, 2012) collisions. The coalescence model (Butler and Pearson, 1963) was developed to describe the production of deuterons and antideuterons in heavy-ion collisions. This approach has also been used to

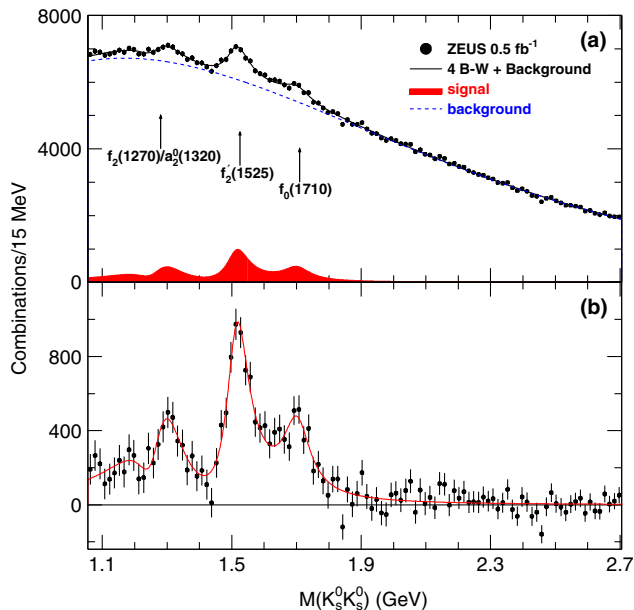


FIG. 42 (color online). (a) The measured $K_S^0 K_S^0$ invariant-mass spectrum compared with a fit including signal and background contributions. (b) The background-subtracted $K_S^0 K_S^0$ invariant-mass spectrum with the fit for the signals also shown. From Chekanov *et al.*, 2008e.

describe d or \bar{d} production in pp and e^+e^- interactions. The invariant differential cross section for deuteron production can be parametrized as

$$\frac{E_d d^3\sigma_d}{\sigma_{\text{tot}} dp_d^3} = B_2 \left(\frac{E_p d^3\sigma_p}{\sigma_{\text{tot}} dp_p^3} \right)^2, \quad (8)$$

where $E_{d(p)}$ and $\sigma_{d(p)}$ are the energy and the production cross section of the $d(p)$, $p_d(p_p)$ is the momentum of the $d(p)$, and σ_{tot} is the total cross section. The coalescence parameter B_2 is inversely proportional to the volume of the fragmentation region emitting the particle. If B_2 is the same for particles and antiparticles, then the production ratio for \bar{d}/d is expected to be equal to the square of that for \bar{p}/p .

The production of antideuterons was first measured at HERA by H1 in photoproduction (Aktas *et al.*, 2004d); ZEUS then measured both deuteron and antideuteron production in DIS (Chekanov *et al.*, 2007j). Both collaborations exploited the rate of ionization energy loss dE/dx measured in the inner tracking chambers and the distance of closest approach of the track to the event vertex. Clear signals of d and \bar{d} were seen along with small signals for tritons; no heavier nuclei or antitriton candidates were observed. After measurement of the invariant cross sections, the ratios of the different production rates were measured in order to compare with other colliders and with the coalescence model.

The ratio of production rates is shown in Fig. 43. The production rate of deuterons is 3 orders of magnitude smaller than the rate for protons. The ratios d/p and \bar{d}/\bar{p} and also the results in DIS and photoproduction in Fig. 43(a) are consistent with one another and with independence of the ratio, particle transverse momentum to mass p_T/M . These

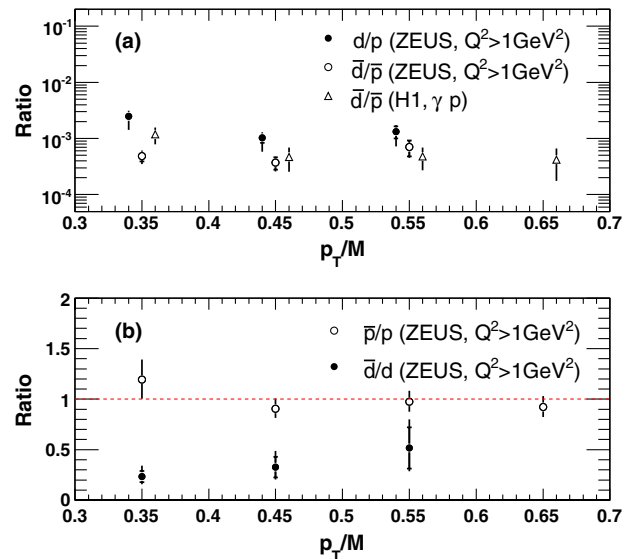


FIG. 43 (color online). (a) d/p and \bar{d}/\bar{p} production rates in DIS (ZEUS) and in photoproduction (H1) as a function of p_T/M . (b) \bar{d}/d and \bar{p}/p production rates in DIS as a function of p_T/M . From Chekanov *et al.*, 2007j.

ratios are also in agreement with those from Υ decays and pp and heavy-ion data. Similarly when analyzed within the context of the coalescence model, the value of B_2 extracted is consistent between d and \bar{d} and DIS and photoproduction. The results from HERA for B_2 agree with those from pp data, but lie above the results from e^+e^- collisions at the Z pole and from heavy-ion data. However, heavy-ion data at lower center-of-mass energy tend toward the values from HERA and pp collisions. In Fig. 43(b), the ratios \bar{d}/d and \bar{p}/p are shown versus p_T/M . The \bar{p}/p ratio is consistent with unity as expected from hadronization of quark and gluon jets. The ratio \bar{d}/d is about 0.3 ± 0.1 and is inconsistent with the coalescence model, which predicts that this ratio should be equal to that for $(\bar{p}/p)^2 \approx 1$, a relationship which is consistent with data from pp (Alper *et al.*, 1973; Henning *et al.*, 1978; Abramov *et al.*, 1987), pA (Cronin *et al.*, 1975), and heavy-ion collisions (Adler *et al.*, 2005). To summarize, the coalescence model can describe a number of features of d and \bar{d} production in high-energy collisions, but given the results here cannot provide a complete picture.

V. EXCLUSIVE AND SEMI-INCLUSIVE PROCESSES

A. Introduction

Diffraction processes in proton-(anti)proton scattering, and to a lesser extent, other projectiles scattering diffractively on proton targets, have been the subject of sustained and intense study since well before HERA. Early experimental results and their theoretical description are extensively covered in a number of review articles (Kaidalov, 1979; Alberi and Goggi, 1981; Goulianos, 1983; Zotov and Tsarev, 1988). The first results have also now started to appear from the LHC (Aad *et al.*, 2012b; Aaij *et al.*, 2013; Abelev *et al.*, 2013;

Chatrchyan *et al.*, 2013a). Although it was not widely expected prior to data taking, the study of quasielastic and diffractive processes has been one of the most successful areas of study at HERA, and certainly one of the most prolific in terms of publications. Complementary reviews can be found in Ivanov, Nikolaev, and Savin (2006) and Wolf (2010).

The kinematics of HERA, with a strong forward boost of the hadronic center of mass relative to the laboratory frame for nonextreme y values, were particularly favorable for the study of diffractive excitations of the real and virtual photon. Two separate cases are usually distinguished. In the (quasi)elastic case $\gamma^{(*)}p \rightarrow Vp$, the photon coupling to the beam lepton either remains intact [deeply virtual Compton scattering (DVCS)] or converts to a vector meson V . In the diffractive dissociation case $\gamma^{(*)}p \rightarrow Xp$ the system X produced at the proton vertex is a multiparticle state covering a continuum of invariant masses M_X .

Most of the interest has centered around the case where the proton remains intact and is scattered through a small angle, implying a small absolute value of the squared four-momentum transfer at the proton vertex $|t|$ [Figs. 45(a) and 52(a)]. Measurements of processes in which the proton dissociates to large mass systems Y , i.e., $\gamma^{(*)}p \rightarrow XY$ and $\gamma^{(*)}p \rightarrow VY$, were more limited, but have been considered, for example, in the context of the decomposition of the total photoproduction cross section into diffractive and nondiffractive channels (Aid *et al.*, 1995). The only detailed measurement of the M_X dependence in proton dissociation processes (Adloff *et al.*, 1997b) revealed a clear difference compared with the elastic-proton case, which is presumably a consequence of the subleading exchanges discussed in Sec. V.D, but has yet to be interpreted in detail.

Prior to HERA, substantial data were already available on exclusive vector meson production in both DIS and photoproduction (Bauer *et al.*, 1978; Binkley *et al.*, 1982; Shambroom *et al.*, 1982; Denby *et al.*, 1984), with fixed-target data continuing to emerge during and beyond the HERA era (Arneodo *et al.*, 1994; Adams *et al.*, 1997; Airapetian *et al.*, 2000, 2009; Alexakhin *et al.*, 2007; Adolph *et al.*, 2012). DVCS has also recently been studied in detail in fixed-target experiments at HERA (Airapetian *et al.*, 2007, 2012a, 2012b) and Jefferson Laboratory (Camacho *et al.*, 2006; Girod *et al.*, 2008; Gavalian *et al.*, 2009). In contrast, the study of the diffractive dissociation of real and virtual photons is almost entirely the preserve of HERA, with only very limited fixed-target data (Chapin *et al.*, 1985).

Before the first precise measurements emerged from HERA, a QCD-based treatment of the exclusive production of vector mesons was already fairly well advanced (Ryskin, 1993; Brodsky *et al.*, 1994; Frankfurt, Koepf, and Strikman, 1996). Cross sections were expected to be Q^2 suppressed relative to inclusive DIS and to be related to the parton densities of the proton, the lowest-order partonic exchange being a pair of gluons with compensating color charges (Low, 1975; Nussinov, 1975). There was less consensus on the appropriate QCD treatment of single diffractive photon dissociation. On the one hand, “hard” diffractive processes similar to exclusive vector meson production were predicted, in which the color-singlet exchange couples fully into the hard interaction with the photon. Such an exchange may again be perturbatively

calculable starting from knowledge of the proton structure. In contrast, in “soft” diffraction, the color-singlet exchange is a composite virtual object, similar to the Pomeron of peripheral hadronic scattering, from which a single parton participates in the hard scattering, the remainder forming a low transverse momentum remnant system, cleanly separated in rapidity from the oppositely traveling intact proton. This type of configuration (Ingelman and Schlein, 1985; Donnachie and Landshoff, 1987) produces a leading twist contribution with similar Q^2 dependence to the total cross section, limited only by kinematic constraints at large Q^2 . In the DIS regime, it can be related to a concept of diffractive parton densities. A major issue in inclusive diffraction at HERA has been determining where each of these soft and hard processes is dominant and understanding the transition between the two.

The detailed dependence on the center-of-mass energy of elastic and, via the optical theorem, total hadron-hadron cross sections has historically been remarkably well described in a large kinematic domain by Regge phenomenology (Regge, 1959, 1960). In this framework, interactions take place via the t -channel exchange of Reggeons related to mesons (Chew, Frautschi, and Mandelstam, 1962) and of the leading vacuum singularity, the Pomeron (IP) (Chew and Frautschi, 1961). The Pomeron is the mediator of diffractive scattering. Although the Pomeron is essentially a phenomenological object, associated mainly with soft processes, it can also be generated perturbatively. For example, connecting the two exchanged gluons in the lowest-order partonic process by adding further gluon “rungs” in a leading-logarithmic $1/x$ approach leads to the so-called BFKL Pomeron.

At asymptotically large energies, Pomeron exchange dominates the elastic channel, such that both elastic and total cross sections display a slow increase with center-of-mass energy. Interactions in which one or both of the hadrons dissociates to higher-mass states (Feinberg and Pomerančuk, 1956; Good and Walker, 1960) also occur naturally in this approach. Such processes are characterized by the presence of large regions of rapidity space in which no hadrons are produced and are dominated by diffractive exchange at large center-of-mass energy \sqrt{s} and small dissociation masses M_X . The inclusive dissociation mass distribution may be treated via Mueller’s generalization of the optical theorem (Mueller, 1970), such that an appropriate Regge description involves diagrams that contain three-Reggeon couplings.

Pomeron language has been adopted to a large extent at HERA, as a matter of convenience. This should not be taken to imply the existence of a universal t -channel Pomeron exchange, since the detailed properties of the exchange and its Regge trajectory clearly vary between processes and with kinematic variables at HERA, as discussed in detail below.

First evidence for diffractive dissociation processes involving sufficiently large scales for perturbative QCD to be applied came from diffractive dijet production in $p\bar{p}$ collisions at the CERN SPS collider as observed by UA8 (Brandt *et al.*, 1992). Later data from the Tevatron followed [e.g., Affolder *et al.* (2000)]. These observations lent experimental support to the idea that the Pomeron might be considered as an object with its own structure, which might be probed in DIS (Ingelman and Schlein, 1985; Donnachie and Landshoff, 1987). First ideas on the structure of the Pomeron were in place as

early as the mid-1980s (Gribov, Levin, and Ryskin, 1983; Berger *et al.*, 1987).

Alternatively to the Regge theory, an s -channel picture (Miettinen and Pumplin, 1978; Dederichs and Faessler, 1989) developed around the original Good and Walker (1960) approach in which different projectile Fock states are absorbed differently on the target. These ideas enjoyed a recent revival as part of the quest to describe diffraction at the LHC (Ryskin, Martin, and Khoze, 2011). The application of this s -channel approach to HERA data involves the elastic and quasielastic scattering of color dipoles, corresponding to $q\bar{q}$ (or higher multiplicity) fluctuations of real and virtual photons on the proton (Mueller, 1990; Nikolaev and Zakharov, 1991). An attractive feature of this approach is that the possible presence of a saturation phenomenon, whereby the low- x growth of parton densities is tamed as ultimately required to satisfy unitarity, are easily incorporated at the parametric level (Golec-Biernat and Wusthoff, 1998). While such models were originally devised to describe the total γ^*p cross section (see Fig. 44),² vector meson production and other exclusive processes are easily incorporated with no further free parameters except those that describe the t dependence [see, e.g., Kowalski and Teaney (2003) and Kowalski, Motyka, and Watt (2006) for a modern treatment]. Diffractive dissociation can also be included (Nikolaev and Zakharov, 1992), although has proved more difficult to describe, due to the need to incorporate higher terms, corresponding, for example, to a dipole formed from a $q\bar{q}$ pair and a gluon (Bartels *et al.*, 1999; Golec-Biernat and Wusthoff, 1999). The dipole approach to diffraction at HERA is discussed further in Secs. V.B.5 and V.C.8.

B. Exclusive production of 1^{--} states

1. Kinematics and experimental selection

Quasielastic vector meson production and DVCS [Fig. 45(a)] are the simplest diffractive processes that can be studied at HERA. For a fixed final state vector meson or photon, they are usually described in terms of the kinematic variables Q^2 , W , and t . Distributions in all three of these variables have been measured in analyses covering the vector meson species ρ , ω , ϕ , ρ' , J/ψ , ψ' , and Υ as well as in DVCS. No evidence has been found for the exclusive production at the photon vertex of particles with non- 1^{--} quantum numbers such as the π^0 (Adloff *et al.*, 2002f), as would be expected for the exchange of the postulated negative C -parity partner of the Pomeron, the odderon (Lukaszuk and Nicolescu, 1973).

The most precise vector meson data are obtained by reconstructing two-prong decays via charged decay products (notably $\rho^0 \rightarrow \pi^+\pi^-$, $\phi \rightarrow K^+K^-$, and $J/\psi \rightarrow e^+e^-$ or $\mu^+\mu^-$) and requiring no further activity beyond the noise levels in the detector, except that associated with the scattered beam electron. DVCS selections require a similar lack of activity in the detector beyond the final-state electron and photon, the

²The results from the inclusive cross section have been inconclusive to date, with strong evidence for saturation only at low scales $\ll 1 \text{ GeV}^2$, which preclude a partonic interpretation (Forshaw, Kerley, and Shaw, 1999).

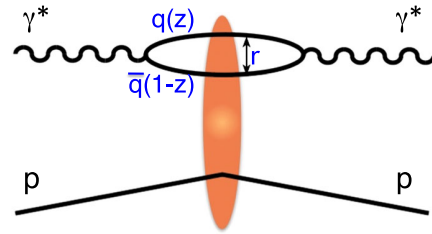


FIG. 44 (color online). Schematic illustration of the dipole model concept in which a virtual photon fluctuates to a $q\bar{q}$ pair with relative momentum fractions z and $1-z$, forming a color dipole of transverse size $r \sim 1/\sqrt{Q^2}$. The dipole then scatters elastically from the proton according to a dipole cross section. The example shown corresponds to the amplitude for the total inclusive γ^*p cross section. However, only small modifications are required to adapt this to the cases of exclusive or inclusive diffraction.

main experimental complication being separating the signal from the competing purely electromagnetic Bethe-Heitler process, which generates identical final states. In contrast to inclusive diffractive studies, the simplicity of these final states and the high precision of the tracking detectors have allowed precision t measurements without the need to tag the intact outgoing proton. This reconstruction method uses $|t - t_{\min}| = p_T^2(V)$, where the vector meson transverse momentum $p_T(V)$ is obtained from its decay products and $|t_{\min}|$, the minimum kinematically accessible value of $|t|$, is usually negligible.

2. General characteristics of vector meson production

Vector meson production has emerged as a sensitive probe of the transition from the soft diffractive dynamics which are familiar from hadronic scattering experiments to a harder regime which may be calculated perturbatively. The former regime is encountered wherever no hard scale is present, the classic example being ρ^0 photoproduction (Aid *et al.*, 1996c; Breitweg *et al.*, 1998c, 2000a). Under such circumstances, the energy dependence of the photon-proton process is in good agreement with the form predicted by Regge asymptotics:

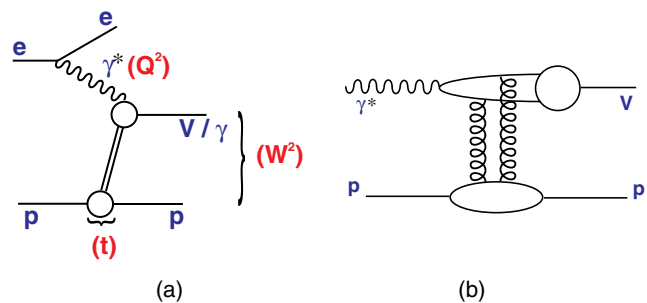


FIG. 45 (color online). (a) Generic representation of exclusive vector meson production via the quasielastic scattering of a real or virtual photon. The commonly used kinematic variables discussed in the text are indicated. (b) Lowest-order perturbative diagram for hard vector meson production, involving the exchange of a pair of gluons between the proton and the real or virtual photon.

$$\sigma^{\gamma p \rightarrow Vp} \propto (W^2)^{2\alpha_{\text{IP}}(t)-2}, \quad (9)$$

where the Pomeron trajectory $\alpha_{\text{IP}}(t) = \alpha_{\text{IP}}(0) + \alpha'_{\text{IP}}t$ is assumed to be linear and its intercept $\alpha_{\text{IP}}(0) \simeq 1.085$ (Donnachie and Landshoff, 1992; Cudell, Kang, and Kim, 1997). This has been found to work well for ρ^0 photoproduction data, although interestingly the slope of the Pomeron trajectory has been found (Breitweg *et al.*, 2000a) to be significantly smaller than the value of $\alpha'_{\text{IP}} \sim 0.25$ (Donnachie and Landshoff, 1984; Abe *et al.*, 1994) obtained from soft pp and $p\bar{p}$ scattering. A possible explanation for this may be found in process-dependent absorptive corrections, which are absent in DIS, present to some extent in photoproduction, and to a larger extent in fully hadronic scattering. Detailed models of these effects can be found, for example, in Kaidalov *et al.* (2003, 2010) and Gotsman *et al.* (2007). Further characteristics of this soft regime are (Aid *et al.*, 1996c; Breitweg *et al.*, 1998c) a skewed line shape for the ρ meson due to its interference with nonresonant $\pi^+\pi^-$ production and a large value $B \sim 10 \text{ GeV}^{-2}$ of the slope parameter describing the t dependence according to

$$\frac{d\sigma^{\gamma p \rightarrow Vp}}{dt} = \left(\frac{d\sigma^{\gamma p \rightarrow Vp}}{dt} \right)_{t=0} e^{Bt}. \quad (10)$$

Interpreted in a simple optical model as a measurement of the mean impact parameter between the incoming photon and proton, these B values suggest that the interaction takes place over a transverse distance of typically 1–1.5 fm.

Wherever hard scales are present, usually provided either by heavy quarks in the vector meson or by large Q^2 , but sometimes also by large $|t|$, the qualitative picture changes. The energy dependence becomes progressively steeper, such that the W dependence, parametrized similarly to Eq. (9), yields an increased effective value of $\alpha_{\text{IP}}(0)$. This effect is illustrated in Fig. 46, where a compilation of photoproduction data on the total cross section and different vector meson production cross sections is shown as a function of W . The steepening of the dependence on W for the heaviest vector mesons can be interpreted in terms of the scale dependence of the proton gluon density at low x , as discussed further in Sec. V.B.3.

The transition from soft hadronic to perturbative behavior is neatly mapped out in a single process in ρ^0 electroproduction data. As Q^2 increases, the t slope parameter B decreases, the W dependence becomes steeper, and the line shape skewing disappears, all in a manner which has been measured with good precision (Breitweg *et al.*, 1999a; Adloff *et al.*, 2000a; Chekanov *et al.*, 2007e; Aaron *et al.*, 2010b). An example, also including comparisons with other exclusive vector meson production processes, is shown in Fig. 47. Here the effective Pomeron intercept [Eq. (9)] is shown as a function of a scale, which is chosen to be $(Q^2 + M_V^2)/4$ (see Sec. V.B.5). As the scale increases, the effective Pomeron intercept shifts from values typical of soft hadronic scattering to values which are compatible with results for the equivalent quantity $\alpha_{\text{IP}}(0) = 1 + \lambda$ in fits of inclusive low- x HERA data to the form $F_2(x, Q^2) \propto x^{-\lambda(Q^2)}$ (Adloff *et al.*, 2001c; Chekanov *et al.*, 2008b).

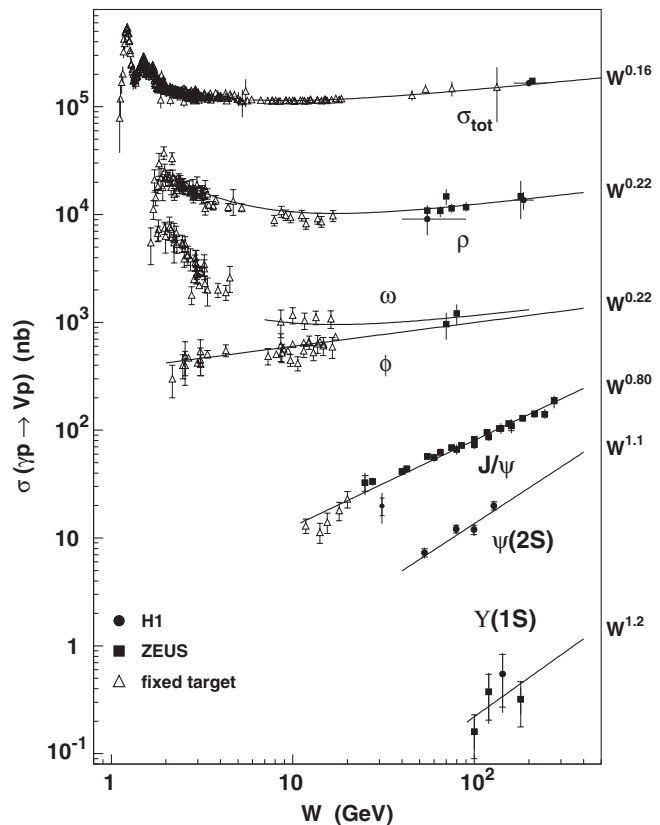


FIG. 46. Compilation of photoproduction cross-section measurements as a function of the γp center-of-mass energy W . The total cross section and various vector meson production cross sections are included, with the approximate power law dependences $\sigma \propto W^\delta$ indicated for each process.

The exponential t slopes of vector meson production processes are also found to vary systematically with scale and are approximately invariant in $Q^2 + M_V^2$. A compendium of results is shown in Fig. 48. Although the uncertainties are often large and there is some scatter, the data suggest a convergence toward an asymptotic value of $B \sim 5 \text{ GeV}^{-2}$. In optical models, this can be interpreted as the point at which the physics is entirely short distance in nature, the size of the probe becomes negligible, and the slope parameter measures the size of the proton. Quantitatively, this indicates an effective proton size of around 0.6 fm, which is interestingly smaller than the value of $\sim 0.8 \text{ fm}$ which is well measured using electromagnetic probes. Interpreting vector meson production in terms of gluon exchange, this suggests that the gluon radius of the proton may be smaller than its quark radius.

3. Vector meson production in QCD

The observed relationship between the W dependences of inclusive DIS and vector meson production in the presence of a sufficiently large scale encourages a perturbative approach. This has evolved considerably in the HERA era, to the point where most observables can be successfully predicted. Although the basic quark charge counting SU(4) prediction for the ratio of cross sections $\rho:\omega:\phi:J/\psi = 9:1:2:8$ holds approximately when viewed as a function of the scale

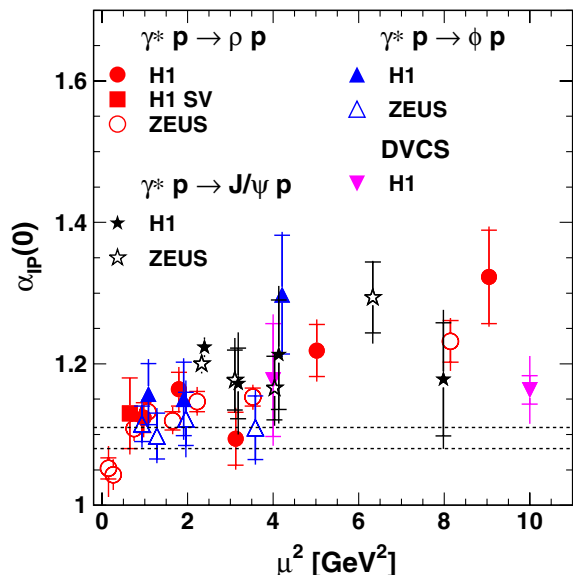


FIG. 47 (color online). Development of the effective Pomeron intercept [see Eq. (9) and surrounding text] with a characteristic scale $\mu^2 = (Q^2 + M_V^2)/4$, derived from fits to the W dependences of various vector meson production data, as well as a DVCS measurement (shown at $\mu^2 = Q^2$). The dashed lines indicate the range of values which are typical in soft diffraction. From Aaron *et al.*, 2010b.

$(Q^2 + M_V^2)/4$ (Aaron *et al.*, 2010b), vector meson wave function effects remain a significant source of uncertainty.

A QCD collinear factorization theorem (Collins, Frankfurt, and Strikman, 1997), valid for the leading power of Q^2 , where $|t| \ll \Lambda_{\text{QCD}}^2$, relates cross sections for heavy vector meson production from longitudinally polarized photons to the generalized parton densities (GPDs) of the proton (Diehl, 2003) (see Sec. V.B.4). Neglecting skewing effects, in which the two exchanged partons carry different fractions of the proton longitudinal momentum, the GPDs reduce to the square of the gluon density of the proton. The process is then driven to first approximation by the exchange of a pair of

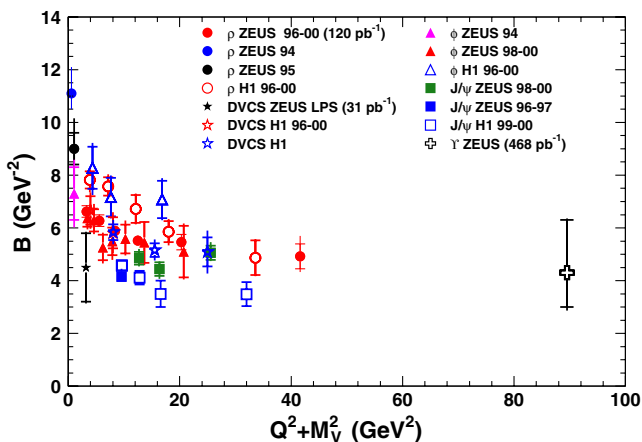


FIG. 48 (color online). Exponential t slopes for vector meson electroproduction and photoproduction as a function of the characteristic scale $Q^2 + M_V^2$. From Abramowicz *et al.*, 2012c.

gluons from the proton structure, as illustrated in Fig. 45(b). Later approaches (Martin, Ryskin, and Teubner, 1997) incorporated transversely polarized photon cross sections at sufficiently large Q^2 and light vector mesons in a similar framework, with some degree of success.

Since it is relatively uncomplicated theoretically, has a reasonably large scale, probes small- x values, and is experimentally clean, J/ψ photoproduction is an ideal testing ground for these ideas and, with sufficiently strong theoretical understanding, a potentially competitive means of extracting the gluon density of the proton. The many measurements at HERA (Chekanov *et al.*, 2002c; Aktas *et al.*, 2006c; Alexa *et al.*, 2013a) have recently been supplemented by the first measurements from ultraperipheral processes at the LHC, extending the W range to beyond 1 TeV for the forward kinematics of LHCb (Aaij *et al.*, 2013). The W dependence of the cross section for J/ψ photoproduction has been calculated using the proton gluon density by a number of groups (Martin, Ryskin, and Teubner, 2000; Frankfurt, McDermott, and Strikman, 2001; Martin *et al.*, 2008). An example comparison with data is shown in Fig. 49. From comparisons between the predictions with different gluon densities, it is clear that there is high sensitivity. However, the normalization is not well predicted and there remains considerable model dependence.

More detailed comparisons with QCD models require an understanding of the helicity structure of vector meson production. The five independent helicity amplitudes, describing transitions from either longitudinally or transversely

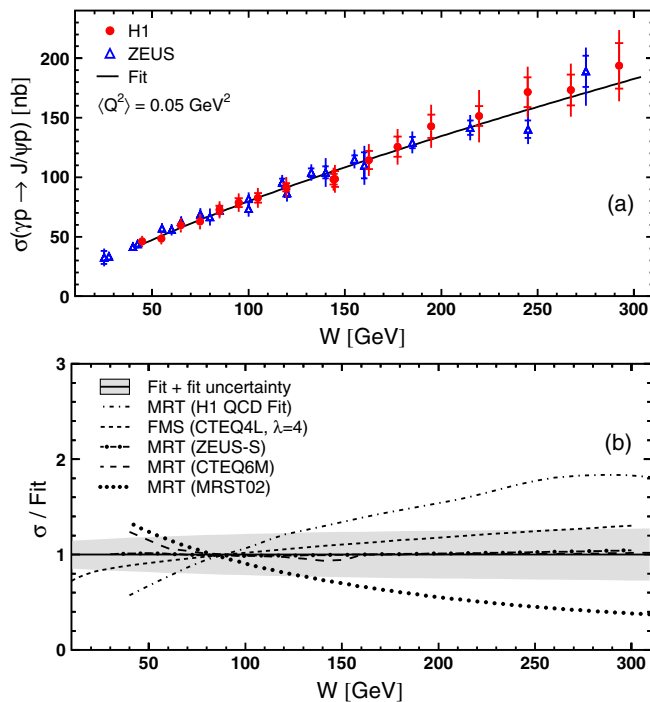


FIG. 49 (color online). J/ψ photoproduction cross section as a function of W , compared with a QCD calculation, MRT (Martin, Ryskin, and Teubner, 2000), based on four different parametrizations of the gluon density of the proton and a dipole model, FMS (Frankfurt, McDermott, and Strikman, 2001). The predictions are normalized to the data. From Aktas *et al.*, 2006c.

polarized photons to either longitudinally or transversely polarized vector mesons, can be extracted from the production and decay angular distributions via spin density matrix elements as parametrized in Schilling and Wolf (1973). While helicity amplitudes for J/ψ production at modest $|t|$ are consistent with s -channel helicity conservation (Aktas *et al.*, 2006c), significant “helicity flip” amplitudes, for which the vector meson helicity differs from that of the photon, are observed for the case of ρ production (Breitweg *et al.*, 2000c; Adloff *et al.*, 2002a; Chekanov *et al.*, 2007e; Aaron *et al.*, 2010b) and for J/ψ production at large $|t|$ (Aktas *et al.*, 2003; Chekanov *et al.*, 2010f). This reflects the often unequal sharing of the longitudinal momentum between the two quarks, corresponding to values of z close to 0 or 1 in Fig. 44, particularly for the transverse polarization case with ρ mesons. This allows the helicity to flip at sufficiently large t , an effect which can be reasonably well predicted in QCD-based models.

Probably the most important feature of angular distribution analyses is that they allow an unfolding of the cross sections σ_L and σ_T , corresponding to vector meson production from longitudinally and transversely polarized vector mesons, respectively. The Q^2 dependences of σ_L and σ_T are separately predicted by QCD models. The basic leading-order dependences at $t = 0$ of $\sigma_L \propto 1/Q^6$ and $\sigma_T \propto 1/Q^8$ (Brodsky *et al.*, 1994) are expected to be strongly violated, in particular, due to the Q^2 dependence of the proton gluon density, but also due to the quark virtuality and the running of α_s (Frankfurt, Koepf, and Strikman, 1996). The HERA data for all vector meson species exhibit approximate scaling with power law dependences of approximately $\sigma_L \propto (Q^2 + M_V^2)^{-1}$ and $\sigma_T \propto (Q^2 + M_V^2)^{-2}$, which are reasonably well reproduced by both collinear factorization and dipole-based models (Martin, Ryskin, and Teubner, 1997; Kowalski, Motyka, and Watt, 2006).

As discussed in Sec. V.B.2 the variation of the slope parameter B with center-of-mass energy W is usually parametrized in terms of the slope of the Pomeron trajectory α'_{IP} . Values close to zero are measured with small uncertainties in some hard exclusive processes, notably J/ψ production at large $|t|$ (Chekanov *et al.*, 2002c, 2004d; Aktas *et al.*, 2006c). This is consistent with expectations in the BFKL approach (Nikolaev, Zakharov, and Zoller, 1996; Brodsky *et al.*, 1999), where α'_{IP} is related to the average transverse momentum of partons along the gluon ladder. However, it is hard to draw quantitative conclusions in light of the smaller-than-expected α'_{IP} values for soft processes such as ρ^0 photoproduction (see Sec. V.B.2).

4. Deeply virtual Compton scattering and generalized parton densities

Because of the underlying exchange of a pair of gluons, which in general differ in both longitudinal and transverse momentum, hard exclusive DIS processes have emerged in recent years as being sensitive to correlations between partons in the proton and thus the transverse spatial, momentum, and spin distributions of partons. This information is encoded in GPDs (Diehl, 2003), which were introduced in Sec. V.B.3. HERA data offer unique sensitivity to GPDs at low x . This

topic is most commonly associated with the DVCS process, although it is also relevant to vector meson production.

The dominant underlying parton-level process for DVCS at low x is similar to that shown in Fig. 45(b), although there is also a “handbag” contribution in which the incoming (virtual) and outgoing (real) photons couple directly to quarks from the GPDs. DVCS has the advantage of avoiding the complication of the vector meson wave function, but cross sections are suppressed due to the final-state photon coupling. Because of the smaller cross sections compared with their vector meson counterparts, DVCS studies emerged relatively late in the lifetime of HERA. For the HERA kinematic region, integrated over azimuthal degrees of freedom, interference between DVCS and the competing Bethe-Heitler process is small and DVCS cross sections can be extracted by statistically subtracting the Bethe-Heitler component using Monte Carlo models tuned in regions in which the DVCS contribution can be neglected.

By the time HERA ceased operating, Q^2 , W , and t distributions had all been measured with good precision (Aaron *et al.*, 2008a, 2009c; Chekanov *et al.*, 2009a). As shown in Figs. 47 and 48, the exponential t slope is $B \approx 5 \text{ GeV}^{-2}$ and parametrizations of the cross section in the usual W^δ form yield $\delta \approx 0.5\text{--}0.6$. Example Q^2 dependence data are shown in Fig. 50. The DVCS cross section falls more slowly [roughly as $(Q^2)^{-1.5}$] with photon virtuality than is the case for vector meson production. This observation is in line with theoretical predictions (Frankfurt, Freund, and Strikman, 1998) and is partially explained by the presence of the quark-driven handbag contribution, which is not relevant to vector meson production. Together, these observations indicate that DVCS can be considered as a hard process, even at relatively small Q^2 .

Asymmetries in the azimuthal degree of freedom between the lepton and the (virtual-to-real) photon scattering planes in DVCS give access to the real part of the amplitude and are most sensitive to the nondiagonal GPDs. The first H1 data have appeared on the DVCS beam charge asymmetry (Aaron *et al.*, 2009c). It is clearly nonzero and its azimuthal dependence has been used to confirm that the DVCS

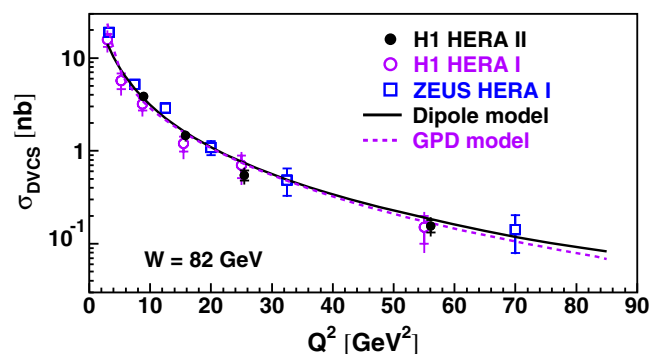


FIG. 50 (color online). Dependence of HERA DVCS cross-section measurements on Q^2 . The data are compared with a GPD-based model (Kumericki and Mueller, 2010) and also with a dipole-based model (Marquet, Peschanski, and Soyez, 2007). See Sec. V.B.3 for an explanation of the latter. From Aaron *et al.*, 2009c.

amplitude is dominantly imaginary for HERA kinematics. It has not yet been possible to determine beam polarization asymmetries in the manner successfully pursued in the fixed-target configuration by HERMES (Airapetian *et al.*, 2012a, 2012b). Nonetheless, the H1 and ZEUS data will provide essential low- x ingredients in models of GPDs for a long time to come (Kumericki and Mueller, 2010), the principal sensitivity being to the GPD, H .

5. Exclusive processes in dipole models and low- x saturation

Viewed in the proton rest frame, vector meson production naturally factorizes into three separate processes, occurring on distinct time scales [cf. Figs. 44 and 45(b)]. The incoming real or virtual photon first fluctuates into a $q\bar{q}$ pair, which creates a color dipole of transverse size $r_\perp \sim 1/\sqrt{Q^2}$ (Wusthoff, 1997). The dipole then scatters elastically from the proton, a process which is generically described in terms of a dipole cross section. Finally, the outgoing color dipole combines back to a photon in the DVCS case, or else hadronizes to a final-state vector meson in a manner which depends on the nonperturbative vector meson wave function. The scale choice of $(Q^2 + M_V^2)/4$, already used in the previous sections, corresponds to the inverse of the scanning radius of the dipole-proton interaction, for the case where the incoming photon longitudinal momentum is shared equally between the quark and antiquark forming the dipole (Frankfurt, Koepf, and Strikman, 1996; Ivanov, Nikolaev, and Savin, 2006). It is appropriate for heavy vector mesons and for light vector mesons produced by longitudinally polarized photons.

At small enough r_\perp , the dipole cross section can be described perturbatively in the manner discussed in Sec. V.B.3. At larger r_\perp , the dipole cross section is not known *a priori*, but is sensitive to any low- x saturation of the proton parton densities. There are various parametrizations of the dipole cross section which include saturation phenomena, some of which are based on particular approximations to QCD with nonlinear evolution such as the color glass condensate (Iancu, Itakura, and Munier, 2004) and some of which are purely phenomenological (Golec-Biernat and Wusthoff, 1998, 1999; Forshaw, Kerley, and Shaw, 1999; Forshaw, Sandapen, and Shaw, 2004).

In the most sophisticated dipole models of vector meson production, the target matter density, and hence any saturation effects, depend on the distance from the center of the proton, such that the dipole cross section varies with impact parameter (Kowalski and Teaney, 2003; Kowalski, Motyka, and Watt, 2006; Rezaeian *et al.*, 2013), which in turn is closely related to $1/t$ [see also Marquet, Peschanski, and Soyez (2007) for a complementary approach]. When viewed differentially in t , the influence of the saturation effects thus becomes stronger as t increases (Kowalski, Motyka, and Watt, 2006; Abelleira Fernandez *et al.*, 2012). Such models adequately describe almost all aspects of vector meson production and DVCS at HERA. An example comparison with the inclusive J/ψ photoproduction cross section as a function of W , also illustrating the predicted size of the saturation effects, is shown in Fig. 51.

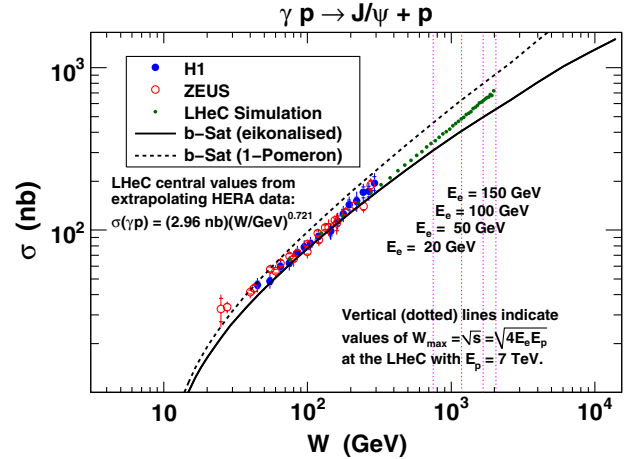


FIG. 51 (color online). Exclusive J/ψ photoproduction data compared with versions of the b-Sat dipole model (Kowalski, Motyka, and Watt, 2006) both with (eikonalized) and without (1-Pomeron) saturation effects included. An extrapolation into the kinematic regime of a possible future ep collider is also included. From Abelleira Fernandez *et al.*, 2012.

C. Inclusive diffractive dissociation

1. Kinematics and experimental selection of diffraction

The kinematic variables describing the inclusive diffractive DIS (DDIS) process $ep \rightarrow eXp$ are illustrated in Fig. 52(a). In addition to x , Q^2 , and t (< 0), there is one further non-trivial invariant, corresponding to the mass M_X of the diffractive final state. In practice, the variable M_X is usually expressed in terms of

$$\beta = \frac{Q^2}{Q^2 + M_X^2 - t}. \quad (11)$$

Small values of β thus refer to events with diffractive masses much bigger than the photon virtuality, while exclusive processes have values of β close to unity. In models based on a factorizable Pomeron (see Sec. V.C.3), β may be interpreted as the fraction of the Pomeron longitudinal momentum which is carried by the struck parton. The longitudinal momentum fraction of the colorless exchange with respect to the incoming proton is denoted as x_{IP} , such that $\beta x_{\text{IP}} = x$.

Experimentally, diffractive ep scattering is characterized by the presence of a leading proton in the final state, retaining most of the initial state proton energy, and by a lack of any other hadronic activity in the forward (outgoing proton) direction, such that the system X is cleanly separated and M_X may be measured in the central detector components. These signatures have been widely exploited at HERA to select diffractive events by tagging the outgoing proton in the H1 forward proton spectrometer or the ZEUS leading proton spectrometer (proton-tagging method, see Fig. 7) or by requiring the presence of a large gap in the rapidity distribution of hadronic final-state particles in the forward region (large rapidity gap or LRG method). In a third approach [M_X method (Breitweg *et al.*, 1999e; Chekanov *et al.*,

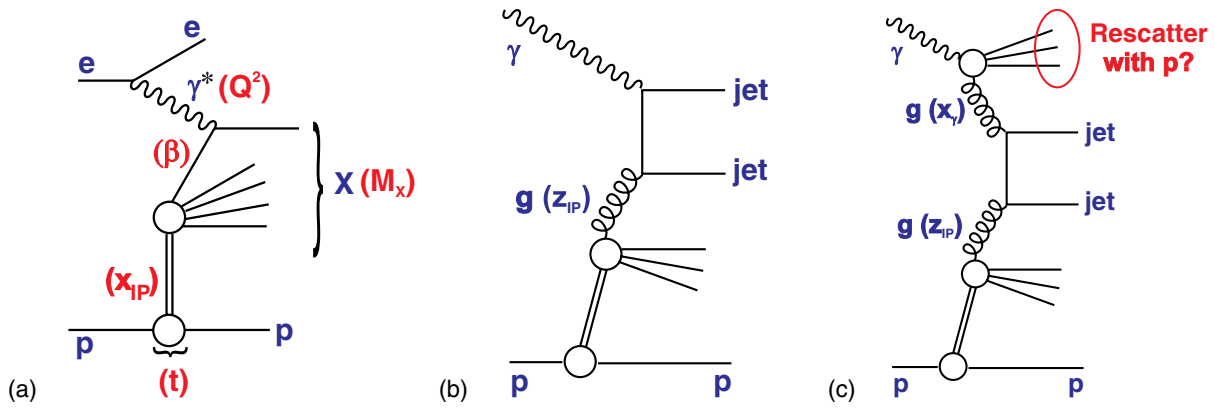


FIG. 52 (color online). Sketches of diffractive ep processes. (a) Inclusive DDIS at the level of the quark-parton model, illustrating the kinematic variables discussed in the text. (b) Dominant leading-order QCD diagram for hard scattering in DDIS or direct photoproduction, in which a parton of momentum fraction z_{IP} from the DPDFs enters the hard scattering. (c) A leading-order process in resolved photoproduction involving a parton of momentum fraction x_γ relative to the photon.

2005g, 2008b)], the inclusive DIS sample is decomposed into diffractive and nondiffractive contributions based on their characteristic dependences on M_X . While the LRG and M_X -based techniques yield better statistics than the LPS method, they suffer from systematic uncertainties associated with an admixture of proton dissociation to baryon states with small masses, typically $M_Y \lesssim 1.6$ GeV, which is irreducible due to the limited forward detector acceptance. Detailed comparisons between cross sections obtained by the LRG and proton tagging methods can be found in Chekanov *et al.* (2009b) and Aaron *et al.* (2011c). Neither collaboration observes any evidence for deviations from a constant ratio of cross sections measured by the two methods, indicating that the ratio of probabilities for the proton to scatter elastically and to undergo a low mass excitation is independent of the inclusive kinematic quantities.

2. Inclusive diffraction data

Observations of diffractive dissociation in DIS (Derrick *et al.*, 1993; Ahmed *et al.*, 1994a) and jet production in diffractive photoproduction (Ahmed *et al.*, 1995b; Derrick *et al.*, 1995c) and DIS (Derrick *et al.*, 1994b) were among the earliest HERA publications, based on rapidity gaps which were much larger than could conceivably occur at significant rates in standard fragmentation models (Andersson *et al.*, 1983). As increasingly larger data sets became available, the precision on the inclusive diffraction cross sections improved correspondingly, until the final measurements covered three-fold differential cross sections with a precision of a few percent (Chekanov *et al.*, 2009b; Aaron *et al.*, 2012a) over large phase-space regions.

In analyses of data with protons tagged in the LPS and FPS, the t dependence of DDIS has been measured and, as in the case of exclusive vector meson production, found to be compatible with an exponential parametrization of the form of Eq. (10). Example H1 data on the slope parameter B are shown in Fig. 53 (Aaron *et al.*, 2011c). Similar results, with globally slightly larger B values, are obtained by ZEUS (Chekanov *et al.*, 2009b). Beyond the low- M_X resonance region, B is typically around 6–7 GeV⁻², independently of β

and Q^2 , but with some dependence on x_{IP} , which is further discussed in Sec. V.C.4. This is indicative of an approximate factorization of the proton vertex from the virtual photon vertex in DDIS (see Sec. V.C.3).

The semi-inclusive DDIS cross section is usually presented in the form of a diffractive reduced cross section $\sigma_r^{D(3)}$, related to the experimentally measured differential cross section by

$$\frac{d^3 \sigma^{ep \rightarrow eXp}}{dx_{IP} dx dQ^2} = \frac{2\pi\alpha^2}{xQ^4} Y_+ \sigma_r^{D(3)}(x_{IP}, x, Q^2), \quad (12)$$

where $Y_+ = 1 + (1 - y)^2$ and y is the usual Bjorken variable. The reduced cross section depends at moderate scales Q^2 on two diffractive structure functions $F_2^{D(3)}$ and $F_L^{D(3)}$ according to

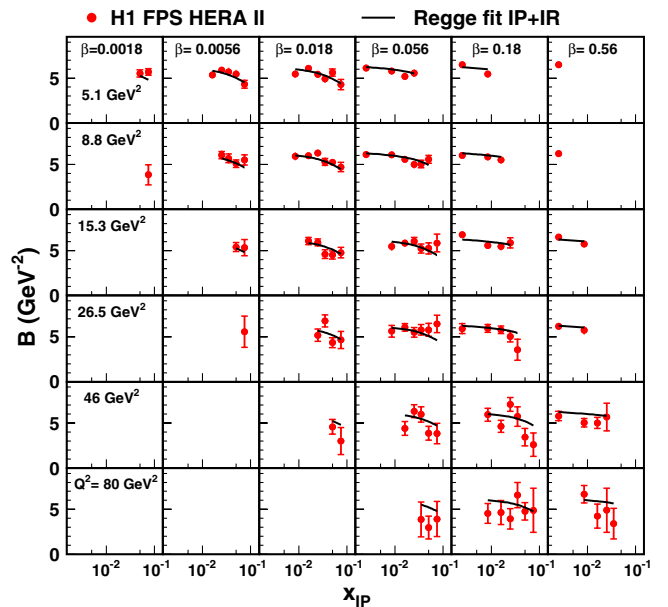


FIG. 53 (color online). Example data on the dynamics of the slope parameter B describing the t dependence of DDIS, as measured using the H1 FPS. From Aaron *et al.*, 2011c.

$$\sigma_r^{D(3)} = F_2^{D(3)} - \frac{y^2}{Y_+} F_L^{D(3)}. \quad (13)$$

For y not too close to unity, $\sigma_r^{D(3)} = F_2^{D(3)}$ holds to very good approximation. Measurements have also been made of the full four-dimensional reduced cross section, dependent also on t (Chekanov *et al.*, 2009b; Aaron *et al.*, 2011c). However, since the t dependence factorizes to good approximation, this degree of freedom is usually integrated out. A more detailed exposition of the formalism of diffractive DIS can be found, for example, in Aktas *et al.* (2006e).

With the most recent σ_r^D data, close agreement has developed between the H1 and ZEUS measurements. A first combination of data from the two experiments, using the proton-tagging method, was recently published (Aaron *et al.*, 2012g). The cross calibration of the systematic uncertainties between the two experiments implicit in the averaging procedure leads to an improvement in precision well beyond that expected from statistical considerations alone. Full combinations of data from the two collaborations for the LRG method have yet to be performed, mainly due to some nontrivial discrepancies, usually at the edges of the accessible phase space. An investigation of the residual differences and crude combination can be found in Newman and Ruspa (2009). The comparison of final data in the most precise region is illustrated in Fig. 54. While there is good agreement in the bulk of the phase space, residual disagreements are apparent at small β and small x_{IP} . These discrepancies have thus far prevented a combination of the H1 and ZEUS data, although they have only a small influence on the interpretation of the data discussed in the following.

Various models have been used to interpret DDIS data. Since it has become standard, Secs. V.C.3–V.C.7 focus mainly on the “proton vertex factorization” approach, in which the diffractive exchange (“Pomeron”) has a resolved structure. The relevance of DDIS to dipole models is discussed separately in Sec. V.C.8. It is worth noting that a third approach, in which rapidity gaps are randomly produced from final-state color interactions in otherwise standard DIS

events, has been at least partially successful. This model is attractive in its simplicity. Indeed an early incarnation (Buchmuller and Hebecker, 1995) in which diffractive final states simply emerge randomly due to color rotations in one-ninth of all low- x DIS events works remarkably well for inclusive data. Closely related ideas are encoded in the “semiclassical model” (Buchmuller, McDermott, and Hebecker, 1997; Buchmuller, Gehrman, and Hebecker, 1999). The “soft color interaction” model (Edin, Ingelman, and Rathsman, 1996) offers a rather different, but again related, approach, which later developed into the “generalized area law” (Rathsman, 1999) model. All of these approaches have enjoyed success, particularly in comparisons with F_2^D and σ_r^D data, but none provides a comprehensive description, breaking down, for example, when confronted with more exclusive processes such as diffractive dijet production (Adloff *et al.*, 2001a).

3. Factorization studies

Cleanly interpreting a three- (or even four)fold differential cross section is far from easy. It is simplified considerably if the dependences on the relevant kinematic variables can be factorized. QCD hard scattering collinear factorization, when applied to diffractive DIS (Collins, 1998), implies that the cross section for the process $ep \rightarrow eXY$ can be written in terms of convolutions of partonic cross sections $\hat{\sigma}^{ei}(x, Q^2)$ with diffractive parton density functions (DPDFs) f_i^D as

$$d\sigma^{ep \rightarrow eXY}(x, Q^2, x_{\text{IP}}, t) = \sum_i f_i^D(x, Q^2, x_{\text{IP}}, t) \otimes d\hat{\sigma}^{ei}(x, Q^2), \quad (14)$$

with additional implicit dependences on μ_F , μ_R , and α_S as in Eq. (1). The partonic cross sections are the same as those for inclusive DIS. This factorization formula is valid for sufficiently large Q^2 and fixed x_{IP} and t .

The experimental data over most of the accessible phase space are compatible with the deeper proton vertex factorization (Ingelman and Schlein, 1985), in which the DPDFs

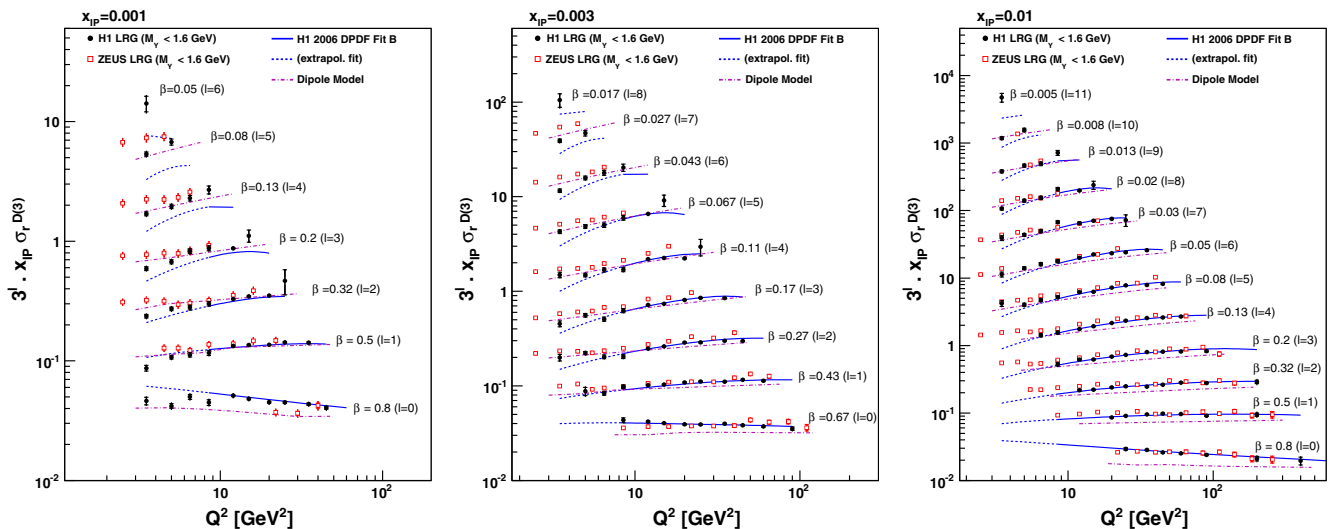


FIG. 54 (color online). Comparisons between H1 and ZEUS DDIS data measured using the LRG method at $x_{\text{IP}} = 0.001$, $x_{\text{IP}} = 0.003$, and $x_{\text{IP}} = 0.01$. From Aaron *et al.*, 2012a.

may be factorized into a term containing only variables associated with the virtual photon vertex (β , Q^2) and a term containing variables associated with the proton vertex (x_{IP} , t):

$$f_i^D(x, Q^2, x_{\text{IP}}, t) = f_{\text{IP}/p}(x_{\text{IP}}, t) f_i(\beta = x/x_{\text{IP}}, Q^2). \quad (15)$$

This is equivalent to considering the diffractive exchange as a Pomeron with a partonic structure given by the parton distributions $f_i(\beta, Q^2)$, the variable β corresponding to the fraction of the Pomeron longitudinal momentum carried by the struck quark. The ‘‘Pomeron flux factor’’ $f_{\text{IP}/p}(x_{\text{IP}}, t)$ represents the probability that a Pomeron with particular values of x_{IP} and t couples to the proton. While this approach cannot be valid to ultimate precision (e.g., it is clearly violated in the high- β region where higher twist processes such as exclusive vector meson production play an important role), it is justified theoretically for the leading twist case (Blumlein and Robaschik, 2001).

As first shown by Adloff *et al.* (1997d), a good description of the data at relatively large x_{IP} cannot be obtained by considering Pomeron exchange alone. As in the case of total hadronic cross sections (Donnachie and Landshoff, 1992), subleading exchanges become important away from the asymptotic ($x_{\text{IP}} \rightarrow 0$ in this case) limit. An additional subleading exchange (IR) is therefore usually considered in addition, contributing at low x_{IP} and β and exhibiting a similar factorization to the Pomeron term, such that Eq. (15) is modified to

$$f_i^D(x, Q^2, x_{\text{IP}}, t) = f_{\text{IP}/p}(x_{\text{IP}}, t) f_i(\beta, Q^2) + n_{\text{IP}} f_{\text{IP}/p}(x_{\text{IP}}, t) f_i^{\text{IP}}(\beta, Q^2), \quad (16)$$

where n_{IP} sets the relative normalization of the subleading term. Further investigations of the subleading trajectory contribution can be found in Sec. V.D.

With the above ansatz, a rather complete description is obtained of all HERA inclusive diffractive data. The energy dependence of DDIS is encoded in the Pomeron flux factor, which is parametrized based on Regge phenomenology, as discussed further in Sec. V.C.4. The DPDFs are treated in a similar way to the case of inclusive DIS, as described in Sec. V.C.5. Full details of the standard fitting scheme adopted for the most recent data by both collaborations can be found in Aktas *et al.* (2006a, 2006e). An improved heavy flavor treatment is described by Chekanov *et al.* (2010a).

4. Energy dependences and soft phenomenology

In the fits to DDIS data described in Sec. V.C.3, the x_{IP} and t dependences are parametrized using a flux factor motivated by Regge theory,

$$f_{\text{IP}/p}(x_{\text{IP}}, t) = A_{\text{IP}} \frac{e^{B_{\text{IP}} t}}{x_{\text{IP}}^{2\alpha_{\text{IP}}(t)-1}}. \quad (17)$$

The parameters B_{IP} and α'_{IP} and their uncertainties are obtained from fits to FPS or LPS data (Aktas *et al.*, 2006a), which also take subleading contributions into account. The x_{IP} dependence of the data principally determines the effective Pomeron intercept $\alpha_{\text{IP}}(0)$, appropriate to the DDIS data. The most precise determinations are obtained from LRG data, with remarkable consistency between statistically

independent data sets (Aktas *et al.*, 2006e; Chekanov *et al.*, 2009b; Aaron *et al.*, 2012b):

$$\alpha_{\text{IP}}(0) = 1.118 \pm 0.008 \text{ (exp)}_{-0.010}^{+0.029} \text{ (model)} \\ \text{(Aktas et al., 2006e),}$$

$$\alpha_{\text{IP}}(0) = 1.117 \pm 0.006 \text{ (exp)}_{-0.007}^{+0.022} \text{ (model)} \\ \text{(Chekanov et al., 2009b),}$$

$$\alpha_{\text{IP}}(0) = 1.113 \pm 0.002 \text{ (exp)}_{-0.015}^{+0.029} \text{ (model)} \\ \text{(Aaron et al., 2012b),}$$

the model dependence uncertainties being highly correlated between the different data sets.

These $\alpha_{\text{IP}}(0)$ values are only slightly larger than their counterparts obtained from fits to total (Donnachie and Landshoff, 1992; Cudell, Kang, and Kim, 1997) and diffractive (Goulianos, 1983; Aad *et al.*, 2012b) cross sections in pp and $p\bar{p}$ scattering and are compatible with results from soft photoproduction at HERA (Adloff *et al.*, 1997b; Breitweg *et al.*, 1997d). They are significantly smaller than the results obtained from the energy dependences of hard exclusive processes at HERA (see Sec. V.B.2) and are much smaller than values predicted based on leading-logarithmic BFKL (Kuraev, Lipatov, and Fadin, 1976, 1977; Balitsky and Lipatov, 1978) or other ‘‘hard Pomeron’’ (Donnachie and Landshoff, 1998) approaches. This supports the picture of the dominating process in DDIS being the application of a hard virtual photon probe to an approximately factorizable exchange object, closely related to the Pomeron of soft hadronic scattering.

The slope of the effective DDIS Pomeron trajectory can be determined from the x_{IP} dependence of the slope parameter B , as obtained using the LPS and FPS detectors. In this case, the best values obtained to date are (Chekanov *et al.*, 2009b; Aaron *et al.*, 2011c)

$$\alpha'_{\text{IP}} = -0.01 \pm 0.06 \text{ (stat)}_{-0.08}^{+0.04} \text{ (syst)} \pm 0.04 \text{ (model)} \\ \text{(Chekanov et al., 2009b),}$$

$$\alpha'_{\text{IP}} = 0.04 \pm 0.02 \text{ (exp)}_{-0.06}^{+0.08} \text{ (model)} \\ \text{(Aaron et al., 2011c).}$$

While the precision on these results is limited, the trajectory slope is clearly smaller than the canonical value from soft pp and $p\bar{p}$ scattering of $\alpha'_{\text{IP}} \sim 0.25$ (Donnachie and Landshoff, 1984; Abe *et al.*, 1994). As discussed in Sec. V.B.2, soft vector meson photoproduction data also show lower α'_{IP} values than those usually taken from pp and $p\bar{p}$ scattering (Breitweg *et al.*, 2000a), suggesting that this is a heavily process-dependent parameter, which is highly sensitive to absorptive corrections.

The validity of the factorization assumption implicit in the fits to inclusive diffractive data is tested by adding further free parameters, which allow the Pomeron intercept and the slope parameter B to vary freely between different Q^2 or β bins. A summary of ZEUS results on possible variations of $\alpha_{\text{IP}}(0)$ with Q^2 is shown in Fig. 55. Both here and in corresponding H1 studies (Aaron *et al.*, 2012a), there is no evidence for any variation of the effective Pomeron intercept with Q^2 or β when

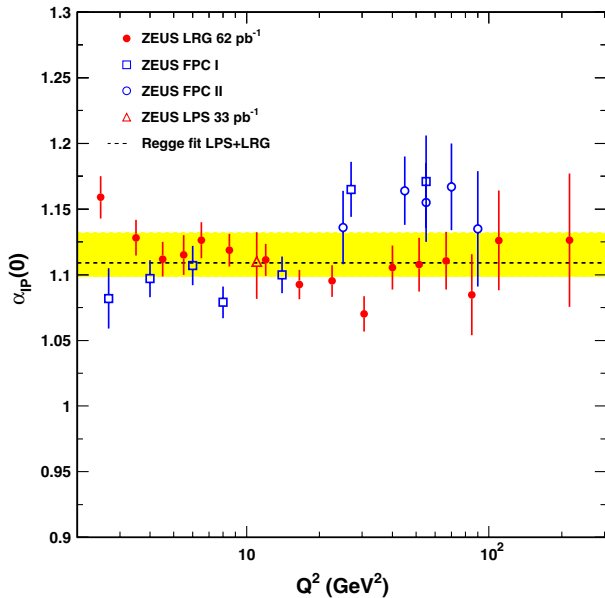


FIG. 55 (color online). Summary of ZEUS data on tests of proton vertex factorization in the form of possible Q^2 variations of the Pomeron intercept in fits to LRG and LPS data, as well as FPC (forward plug calorimeter) data obtained by the M_X decomposition method. From Chekanov *et al.*, 2009b.

considering data taken using the LRG or proton-tagging methods. Similar searches for a Q^2 or β dependence of α'_{IP} or B have also yielded null results (Aaron *et al.*, 2011c), albeit with lesser precision than for the $\alpha_{IP}(0)$ case.

It is informative to compare the photon-proton center-of-mass energy (W or equivalently $1/x$ at fixed Q^2) dependences of the diffractive and the inclusive cross sections. Basic Regge pole phenomenology predicts that the growth with center-of-mass energy of the diffractive cross section [$\sim(W^2)^{2\alpha_{IP}(t)-2}$ at fixed Q^2 and β , with $\langle t \rangle \sim 1/B \sim 0.2 \text{ GeV}^2$] should be faster than that of the total cross section [$\sim(W^2)^{\alpha_{IP}(0)-1}$]. However, in numerous studies of HERA data, the ratio of diffractive to inclusive cross sections has been found to be relatively flat as a function of W . The first example (Breitweg *et al.*, 1999e) is shown in Fig. 56; see also Aktas *et al.* (2006e) and Aaron *et al.* (2012a) for more recent results. This flatness represents a clear breakdown of the simple Regge approach, showing conclusively that there is no universal Pomeron in virtual photon-proton scattering, as also discussed in Sec. V.B.2. The flatness of the ratio has been interpreted (Golec-Biernat and Wusthoff, 1998, 1999) as evidence for saturation of low- x parton densities, which is expected to be visible in diffraction at higher x than in the inclusive case, due to the exchange of two, rather than one, gluon in the simplest interpretation. Any saturation effects thus tend to reduce the diffractive cross section relative to the inclusive in a manner which becomes more important as x falls or W grows. While this is a highly suggestive observation, it has also been explained without invoking saturation, for example, in models which explain rapidity gap formation as a random process, due to soft color rearrangements (Edin, Ingelman, and Rathsman, 1996; Buchmuller, Gehrmann, and Hebecker, 1999).

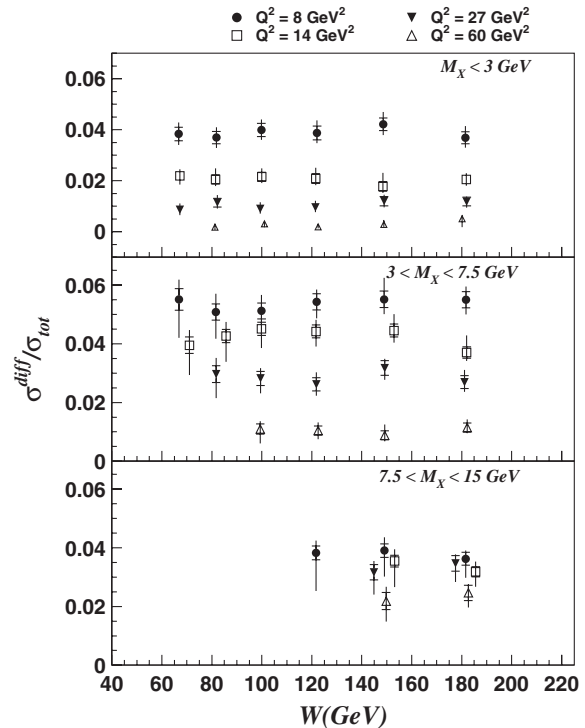


FIG. 56. The ratio of diffractive to inclusive cross sections as a function of W , integrated over different M_X regions at fixed Q^2 . Obtained using ZEUS 1994 data. From Breitweg *et al.*, 1999e.

5. QCD phenomenology and diffractive parton densities

A cursory glance at Fig. 54 immediately leads to the conclusion that the scaling violations in diffraction remain of positive sign ($\partial\sigma_r^D/\partial Q^2 > 0$) up to large values of $\beta \sim 0.5$, which may be compared with $x \sim 0.1$ for the inclusive cross section.³ This is indicative of a large role of gluons in the diffractive exchange (Ahmed *et al.*, 1995a). This qualitative conclusion is formalized through the extraction of DPDFs, as described in more detail in this section.

The DPDFs in Eq. (14) represent probability distributions for partons i in the proton under the constraint that the proton is scattered to a particular system Y with a specified four-momentum. They are essentially equivalent to the fracture functions developed in an earlier approach (Trentadue and Veneziano, 1994). They are not known from first principles, but can be determined from fits to the data using the DGLAP evolution equations (Blumlein and Robaschik, 2001). Because of kinematic constraints, it is not possible to access the full range of β and Q^2 using data from only one value of x_{IP} at HERA. The parametrizations of the x_{IP} dependence of the DPDFs described in Sec. V.C.4, together with the proton vertex factorization assumption introduced in Sec. V.C.3, is therefore adopted, such that data from multiple x_{IP} values can be used simultaneously in extracting DPDFs which then depend on β and Q^2 only.

³See Aktas *et al.* (2006e) for an alternative comparison between scaling violations in diffractive and inclusive DIS considered at the same x values in each case.

DPDFs have been extracted using standard NLO QCD procedures, similar to those employed to extract inclusive proton PDFs, but with smaller numbers of free parameters for the momentum fraction dependence of the parton densities at the starting scale for evolution. This momentum fraction is usually denoted z or z_{IP} (it is equal to β when used to describe the quark coupling to the exchange boson). In the fits made to date, only two distinct parton densities are considered: a gluon density and a singlet quark density, which is assumed to be flavor symmetric between up, down, and strange quarks and their antiquarks. This latter assumption, particularly on the size of the strange quark density, is rather *ad hoc* and remains to be tested in detail.

The most recent results obtained when fitting inclusive σ_r^D data alone can be found in Aktas *et al.* (2006e) and Chekanov *et al.* (2010a); see Fig. 57. Since σ_r^D measures essentially the charge-squared-weighted sum of quarks, these fits result in tight constraints (to around 5%) on the singlet quark density. From the scaling violations, the gluon distribution is also rather well constrained at moderate z values (to around 10%–15%). However, the sensitivity to the gluon density with $z \gtrsim 0.5$ is poor, due to the inevitable dominance of the evolution by the $q \rightarrow qg$ splitting as $z \rightarrow 1$. If diffractive jet production (see Sec. V.C.6) is used as an additional constraint, the high- z gluon precision is improved considerably, at the expense of additional theoretical assumptions on the large β dynamics. Results of fits of this type can be found in Aktas *et al.* (2007b) and Chekanov *et al.* (2010a); see Fig. 58.

In all fits performed, the DPDFs are dominated by the gluon density, which extends to large values of z and accounts

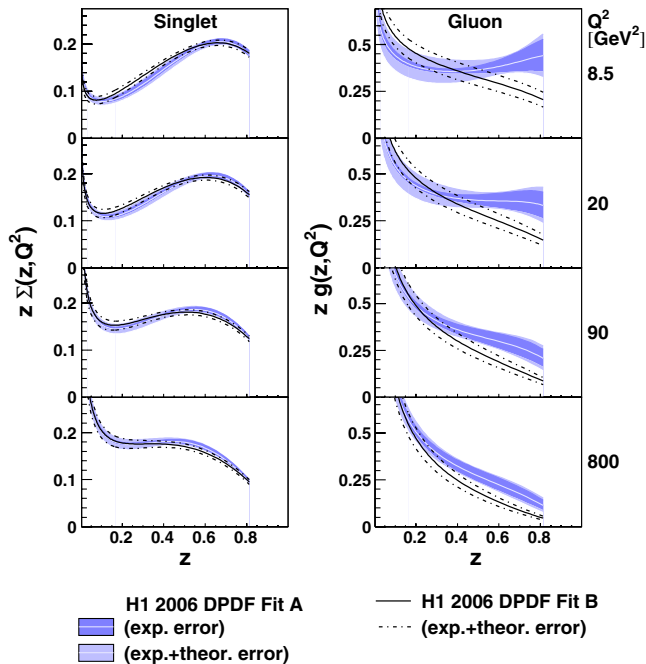


FIG. 57 (color online). DPDFs extracted from an H1 fit to inclusive LRG data only. The two different sets of DPDFs shown (Fit A and Fit B) have very similar fit qualities, illustrating the lack of sensitivity to the gluon density at large momentum fractions. From Aktas *et al.*, 2006e.

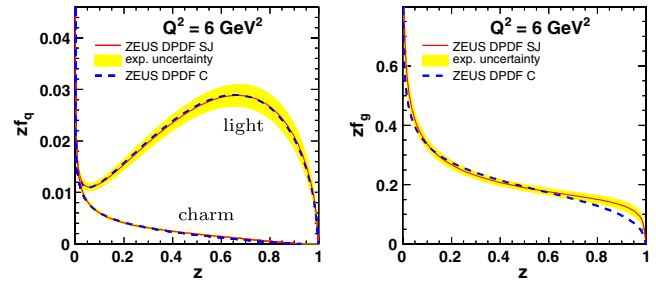


FIG. 58 (color online). Diffractive quark (left) and gluon (right) distributions extracted from a ZEUS fit to inclusive LRG and LPS data, with diffractive dijet data also included. From Chekanov *et al.*, 2010a.

for typically 60% [ZEUS (Chekanov *et al.*, 2010a)] to 70% [H1 (Aktas *et al.*, 2006e)] of the total longitudinal momentum of the diffractive exchange.

It is interesting to note that the DPDFs, particularly the quark distribution, resemble the parton densities of the photon (Nisius, 2000). The hadronic structure of the photon is generated from an initial $\gamma \rightarrow q\bar{q}$ splitting, with lower x structure emerging from further splittings and evolution. This superficial similarity is as might be expected if diffraction emerges from a single gluon exchange, dressed in a manner which neutralizes the color. The structure then develops from $g \rightarrow q\bar{q}$ similarly to the photon case, but with an admixture of $g \rightarrow gg$ initial splittings.

More sophisticated approaches to DPDFs exist, notably in which a direct, hard, Pomeron contribution is also included (Martin, Ryskin, and Watt, 2007) or which include a higher twist contribution at large β (see Sec. V.C.8) (Royon *et al.*, 2001; Golec-Biernat and Luszczak, 2007). While these contributions arise naturally in QCD and must be present at some level, the evidence from both these fits and hadronic final-state comparisons (see Sec. V.C.6) is that they are numerically small, compared with the standard resolved structure contribution. The DPDF approach does, however, appear to undergo an infrared breakdown at larger Q^2 scales than is the case in inclusive QCD fits (Aktas *et al.*, 2006e; Chekanov *et al.*, 2010a). While this may provide further evidence for saturation effects in DDIS (Frankfurt, Guzey *et al.*, 2001), it may also be a consequence of enhanced higher twist contributions or a less quickly convergent QCD order expansion in the diffractive than the inclusive case.

6. Applications of diffractive parton densities

The DPDFs described in Sec. V.C.5 and their predecessors have been used to predict a wide variety of observables in DIS and photoproduction at HERA, as well as at the Tevatron and the LHC. At one level, this is done through implementations [usually of the H1 fit B DPDFs (Aktas *et al.*, 2006e)] in Monte Carlo generators (Jung, 1995; Cox and Forshaw, 2002; Navin, 2010). In particular, the RAPGAP model has been used extensively as an experimental tool for modeling both inclusive and hadronic final-state diffractive data at HERA. The DPDFs have also been interfaced to various NLO QCD calculations in order to compare their predictions with measurements.

There is a wealth of literature on this topic, which is summarized with a few examples below. These tests are very similar in design and scope to those discussed in Sec. III. However, the level of precision is poorer in the diffractive case, due to smaller data samples, added experimental complications, and kinematic restrictions placed, for example, on jet transverse momenta.⁴

Early measurements of inclusive final-state observables in DDIS were sufficient to rule out a diffractive exchange with a quark-dominated structure by showing that the basic event topology is consistent with the boson-gluon fusion process $\gamma^*g \rightarrow q\bar{q}$ [Fig. 52(b)], yielding copious high- p_T particle production and leaving behind a color-octet remnant of the diffractive exchange. The full list of inclusive final-state observables measured in DDIS now comprises charged-particle spectra, multiplicities and their rapidity correlations (Adloff *et al.*, 1998a, 1998b; Chekanov *et al.*, 2002f), energy flows (Adloff *et al.*, 1998a; Chekanov *et al.*, 2002f), and event shapes (thrust and sphericity) (Adloff *et al.*, 1998d; Breitweg *et al.*, 1998d; Chekanov *et al.*, 2002f). These measurements are universally in agreement with predictions based on DPDFs extracted from σ^D data, reinforcing the picture of a diffractive exchange dominated by gluons extending to large momentum fractions.

The most precise tests of DPDFs in diffractive DIS have been obtained from exclusive final-state observables formed from relatively high transverse momentum jet production, the rate for which is closely related to the diffractive gluon density. Dijet measurements have been made as a function of many different variables (Aktas *et al.*, 2007b, 2007f; Chekanov *et al.*, 2007c; Aaron *et al.*, 2012d) and have been extensively used in comparisons with DPDF-based NLO predictions (Aktas *et al.*, 2007b; Chekanov *et al.*, 2010a). An example is shown in Fig. 59. This sort of comparison has again been universally successful. In fact, the factorizable (resolved Pomeron) model in diffractive DIS works in a wider range of contexts than might be expected. For example, DPDF-based predictions also describe 3-jet diffractive final states fairly well (Adloff *et al.*, 2001a; Chekanov *et al.*, 2001c), despite being at the LO, rather than the NLO, level in the 3-jet case. A further intriguing example is the case where one of the reconstructed jets is close in rapidity to the edge of the rapidity gap (Aaron *et al.*, 2012d), a topology which can be measured by exploiting the proton-tagging method. This latter case rules out a dominant contribution from hard (Pomeron remnant-free) diffractive production of the type discussed by Hebecker and Teubner (2001) and Martin, Ryskin, and Watt (2007), which ought not to be describable using the DPDF approach. The strong experimental evidence for proton vertex factorization and the applicability of DPDFs to diffractive dijets in DIS, together with the relatively high precision with which the momentum fraction z can be reconstructed from the kinematics of the diffractive final state and the jet pair, have led to the argument more recently being reversed, with jet data being used as an input to DPDF

⁴The total available invariant mass M_X for final-state particle production in diffraction is typically a factor of 10 smaller than the analogous variable W in the inclusive case.

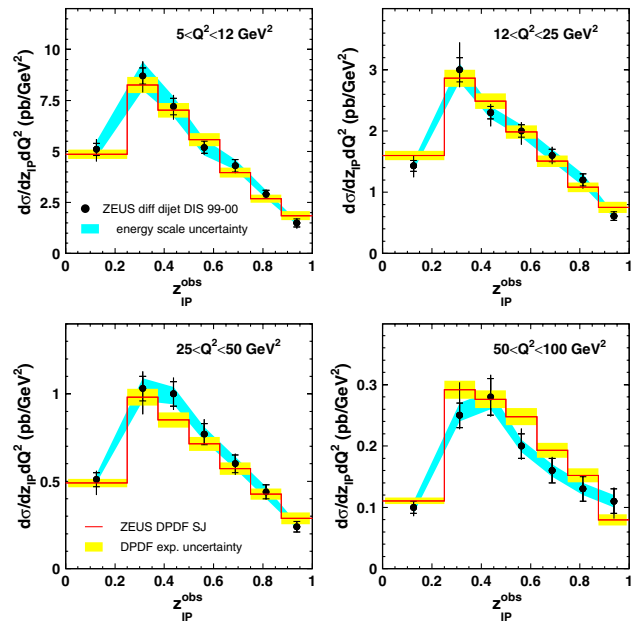


FIG. 59 (color online). Comparison of diffractive DIS dijet cross sections, measured double differentially in z_{IP} and Q^2 , with NLO QCD predictions based on DPDFs. In this case, the data shown were used together with inclusive diffraction measurements in the fit, to improve the high- β sensitivity. From Chekanov *et al.*, 2010a.

extractions (Aktas *et al.*, 2007b; Chekanov *et al.*, 2010a), as discussed in Sec. V.C.5.

Diffractive open charm production in DIS (Chekanov *et al.*, 2003d; Aktas *et al.*, 2007a) provides a further exclusive final state with high sensitivity to the diffractive gluon density via the lowest-order contributing process $\gamma^*g \rightarrow c\bar{c}$. In all measurements made to date, the charm quarks are tagged through the reconstruction of a D^* meson using the usual $D^* - D^0$ mass difference technique (see Sec. II.D). Because of larger backgrounds and smaller statistics, charm observables have not yielded the precision tests of diffractive factorization and DPDFs that have been achieved with jets. In principle, due to the weaker kinematic constraints on M_X , it should be possible to probe smaller z values by using charm as a tag. However, the problems of forward-going track reconstruction experienced by both collaborations has limited progress in this direction. Nonetheless, as can be seen from the example comparisons in Fig. 60, open charm production is well described by DPDF-based models, providing complementary support for this approach and a constraint on the heavy flavor treatment in diffractive QCD fits.

A final class of DPDF tests in DIS may be performed using only inclusive diffractive cross sections. While these tests require measurements at the extremes of the accessible kinematic range, resulting in only limited precision, they are complementary to hadronic final-state constraints. An H1 measurement of the diffractive charged current cross section is shown to be consistent with DPDF-based predictions by Aktas *et al.* (2006e). This is the only comparison to date which is sensitive to the light quark flavor decomposition of the diffractive quark density. The rather *ad hoc* flavor-democratic assumptions made in the standard

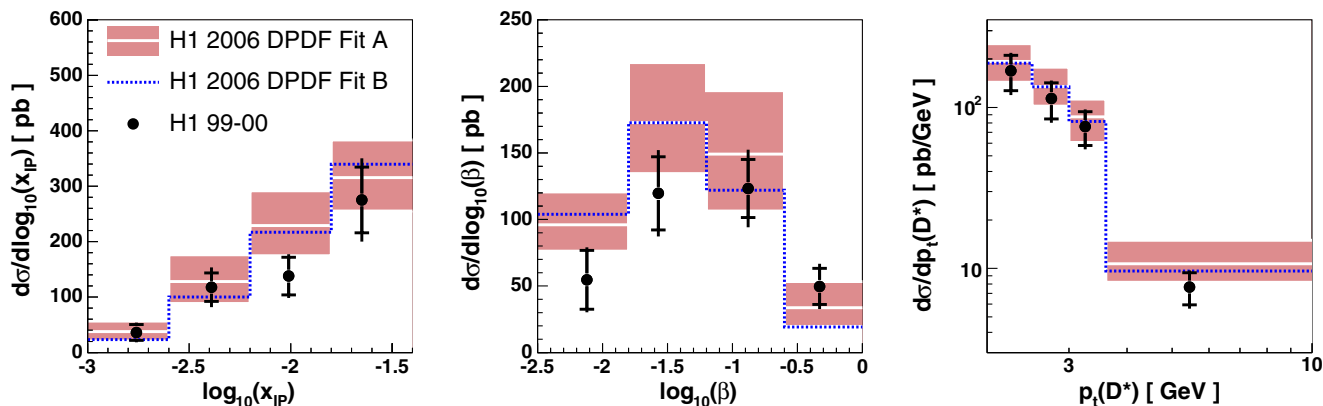


FIG. 60 (color online). Comparisons between diffractive open charm (D^*) production measurements and NLO QCD predictions based on DPDFs. From Aktas *et al.*, 2007a.

QCD fitting procedures (see Sec. V.C.5) are consistent with the data within the large statistical uncertainties.

The diffractive longitudinal structure function F_L^D (Newman, 2005) is a further independent observable with sensitivity to both the quark and the gluon densities in novel ways. In particular, it provides a unique test of the low- x gluon. F_L^D can in principle be measured from variations in the DDIS cross section with the azimuthal angle between the lepton and jet scattering planes, although attempts to observe this effect using the FPS and LPS detectors have yielded results consistent with zero (Chekanov *et al.*, 2009b). Significantly nonzero results have, however, been obtained (Aaron *et al.*, 2012f) using the Rosenbluth technique, comparing diffractive reduced cross-section data at fixed x_{IP} , β , and Q^2 , but different ep center-of-mass energy, exploiting the data taken at $\sqrt{s} = 460$ and 525 GeV at the very end of the HERA running. The sensitivity to F_L^D requires highly challenging measurements at large y (small scattered electron energy). Nonetheless, this structure function has been measured over a fairly large kinematic region. As summarized in Fig. 61, the data are again supportive of the DPDF approach.

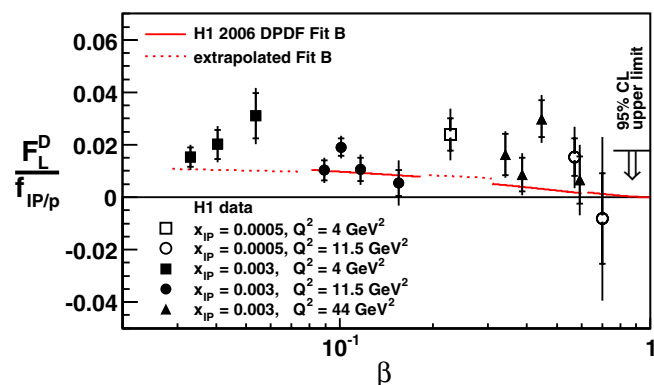


FIG. 61 (color online). Summary of H1 measurements of the diffractive longitudinal structure function F_L^D , exploiting data taken with variations in the proton beam energy. To allow comparisons between measurements at different x_{IP} values, the data are normalized by a diffractive flux factor $f_{IP/p}$ (see Sec. V.C.4). The data are compared with an NLO QCD prediction based on DPDFs. From Aaron *et al.*, 2012f.

7. Limitations of diffractive parton densities

While models based on proton vertex factorization and DPDFs work well to describe all diffractive processes beyond the lowest M_X resonance region in DIS, they fail spectacularly when DPDFs extracted from HERA σ_r^D data are applied to diffractive $p\bar{p}$ scattering at the Tevatron. For example, predictions for diffractive dijet production at the Tevatron exceed the data by a factor of around 10 (Affolder *et al.*, 2000; Klasen and Kramer, 2009). This limitation is predicted as part of the QCD hard scattering factorization theorem for diffraction (Collins, 1998) and is usually interpreted in terms of multiple scattering, or “absorptive” effects, which occur in the presence of beam remnants. These effects can be parametrized in terms of a “rapidity gap survival probability” (Dokshitzer, Khoze, and Sjostrand, 1992; Bjorken, 1993). Similar effects are emerging at the LHC (Chatrchyan *et al.*, 2013a).

Measurements of diffractive dijet photoproduction have been pursued as a control experiment for gap destruction models. In a lowest-order interpretation, direct-photon processes ought to be unaffected by such effects, whereas they should be present in resolved-photon processes, where the photon interacts through its hadronic structure [Fig. 52(c)]. For example, a theoretical model which successfully describes the Tevatron result predicted a suppression of the resolved contribution by a factor of 0.34 (Kaidalov *et al.*, 2003). Multiple measurements of diffractive dijet photoproduction have been made by H1 and ZEUS and have been compared with NLO calculations based on DPDFs extracted in DDIS. While the experimental data are just about compatible between the two collaborations, the conclusions from H1 and ZEUS differ slightly in this area. Notably, neither collaboration sees any evidence for the expected x_γ dependence of the survival probability. H1 data (Aktas *et al.*, 2007f; Aaron *et al.*, 2010a) suggest a suppression of the data by a factor of around 0.6 relative to NLO QCD predictions, independently of x_γ . ZEUS results, which correspond to larger jet transverse energies (Chekanov *et al.*, 2008c, 2010a), suggest a smaller suppression and are, in fact, consistent with no suppression whatsoever. Selected data from both collaborations are shown in Fig. 62. These apparent problems are at least partially resolved by a recent model in which a more careful treatment of pointlike, as distinct from

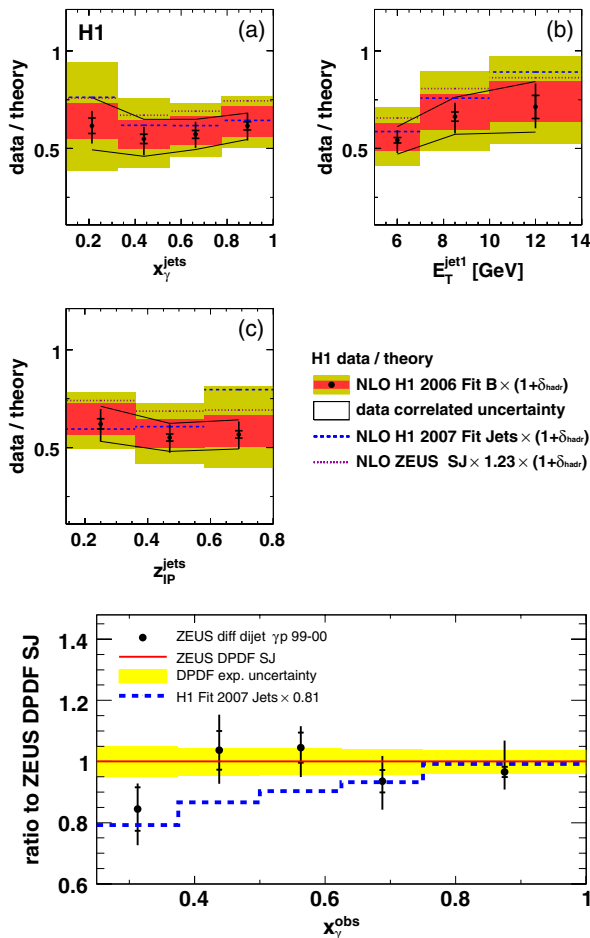


FIG. 62 (color online). Diffractive dijet photoproduction data shown as ratios of measured cross sections to DPDF-based NLO predictions (i.e., as measurements of the rapidity gap survival probability). (a)–(c) H1 data. From Aaron *et al.*, 2010a. Bottom panel: ZEUS data. From Chekanov *et al.*, 2010a.

fully resolved, photon structure is introduced (Kaidalov *et al.*, 2010), leading to a much larger, and E_T dependent, survival probability for $0.1 \lesssim x_\gamma < 1$.

Diffractive charm production has also been studied in photoproduction (Aktas *et al.*, 2007a; Chekanov *et al.*, 2007b). The measurements are kinematically restricted to the large x_γ direct-photon region and are described, within large experimental and theoretical (scale) uncertainties, by DPDF-based predictions without recourse to gap destruction effects.

Rapidity gap survival probabilities and their kinematic dependences remain an area which is not yet fully resolved. This is unfortunate, since in addition to the interest this topic generates in its own right, it is an essential ingredient in predicting hard diffractive cross sections at the LHC.

8. Diffractive DIS in dipole models

The application of the dipole picture to inclusive DDIS has proved to be problematic, mainly due to the need for higher multiplicity fluctuations ($q\bar{q}g$ and perhaps others) in order to describe the large- M_X , small- β region. This need was first

shown in a quantified manner through the BEKW (Bartels-Ellis-Kowalski-Wüsthoff) fits to F_2^D data in Bartels *et al.* (1999). In this parametrization, the data at low and moderate β are described in terms of $q\bar{q}$ and $q\bar{q}g$ dipole fluctuations of transversely polarized photons, while the high- β region contains a Q^2 -suppressed nonleading twist contribution from $q\bar{q}$ fluctuations of longitudinally polarized photons. This approach was further developed for comparisons with inclusive DDIS data, for example, in the saturation model (Golec-Biernat and Wüsthoff, 1999; Golec-Biernat and Luszczak, 2007). An example decomposition of the β dependence of DDIS data is shown in Fig. 63. Predictions have also been made for hadronic final-state observables, based on a two-gluon exchange model of exclusive $q\bar{q}$ (Bartels, Lotter, and Wüsthoff, 1996; Lotter, 1997) and $q\bar{q}g$ (Bartels, Jung, and Wüsthoff, 1999; Bartels, Jung, and Kyrieleis, 2002) production. However, progress has been limited by significant theoretical uncertainties associated with the low- β $q\bar{q}g$ contribution and a lack of direct evidence for the high- β higher twist $q\bar{q}$ term.

D. Leading protons and neutrons beyond the Pomeron region

Both H1 and ZEUS had proton spectrometers (see Fig. 7) with acceptance in the range $0.1 \lesssim x_{\text{IP}} \lesssim 0.3$, well beyond the classic diffractive region where Pomeron exchange is expected to dominate. In this region, the $ep \rightarrow eXp$ cross section may be understood in terms of the exchange of subleading exchanges of neutral meson states (Adloff *et al.*, 1999d; Chekanov *et al.*, 2009c). In the case of ZEUS, the scattered proton sensitivity extended as far as $x_{\text{IP}} \sim 0.7$. The acceptance of the zero degree forward neutron calorimeters in both experiments extended over a wide range in neutron energies, from low values, where neutron production is describable by standard proton fragmentation, to large values,

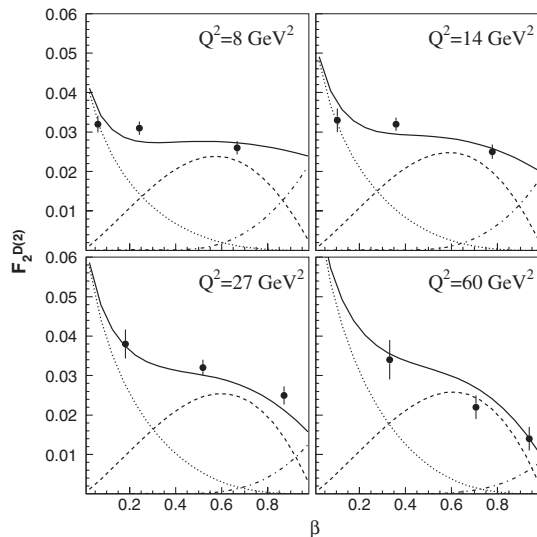


FIG. 63. An example decomposition of the β dependence of ZEUS DDIS data (Breitweg *et al.*, 1999e) into different dipole terms, according to the parametrization in Golec-Biernat and Wüsthoff (1999). The dashed, dotted and dot-dashed curves correspond to leading twist transverse $q\bar{q}$, leading twist transverse $q\bar{q}g$, and higher twist longitudinal $q\bar{q}$ contributions, respectively. The solid curves represent the sum of the three.

where charged color-singlet exchange $ep \rightarrow eXn$ becomes dominant. Interpreted in terms of meson trajectory exchanges, this latter reaction proceeds only via isospin-1 exchanges, for which the relative rates of leading neutron and leading proton production are simply related via a Clebsch-Gordan coefficient of 2. Studying the leading proton and leading neutron data together in a Regge pole model [e.g., [Szczyrek, Nikolaev, and Speth \(1998\)](#)] leads to the tentative conclusion that the subleading trajectory with $\alpha_{\text{IR}}(0) \sim 0.5$ in Eq. (16), which becomes important for $x_{\text{IP}} \approx 0.05$, may be that associated with the f_2 meson.

At larger x_{IP} values, leading proton and neutron production can be described simultaneously only if the exchanged trajectory is dominantly the pion, with $\alpha_{\pi}(0) \approx 0$ ([Bishari, 1972](#)), although other contributions also appear to be present ([Kaidalov et al., 2006](#); [Khoze, Martin, and Ryskin, 2006](#)). The study of leading neutron data at relatively large neutron energies therefore raises the interesting, but not uncontroversial ([Frankfurt, Koepf, and Strikman, 1997](#)), opportunity of measuring the partonic structure of the pion using a similar factorization between pion flux and structure function to that described for the Pomeron in Sec. V.C.3.

For $x_{\text{IP}} \lesssim 0.3$, reconstructed using the neutron energy E_n and assuming exclusive production at the proton vertex via $x_{\text{IP}} \equiv 1 - E_n/E_p$, inclusive leading neutron data in DIS ([Chekanov et al., 2005h, 2007i](#); [Aaron et al., 2010e](#)) are broadly consistent with the pion exchange hypothesis. An example analysis is shown in Fig. 64. Leading neutron data at $x_{\text{IP}} = 0.27$ are shown after dividing by a parametrization of the pion flux. Up to residual contributions from standard fragmentation processes and possibly other isovector exchanges, the data then correspond to the pion structure function $F_2^{\pi}(\beta, Q^2)$. Existing pion structure function parametrizations are broadly in-line with the data, but clearly overshoot when considered in detail. A simple model based on valence quark counting, such that $F_2^{\pi} = 2F_2/3$, is slightly closer to the data. Considering the large uncertainties in the pion flux factor and the lack of previous data sensitive to the measured range, which extends to $\beta < 10^{-3}$, the level of agreement is reasonable. An analysis in which HERA leading neutron data are used as an input to a pion parton density extraction is, however, yet to be performed.

In addition to the inclusive neutron production process, measurements have also been made of dijet ([Aktas et al., 2005d](#); [Chekanov et al., 2010c](#)) and charm quark ([Chekanov et al., 2004g](#)) photoproduction in association with leading neutrons. Considered together with the inclusive leading neutron data, these final-state measurements show evidence for considerable absorptive corrections. This complication, together with the uncertainties inherent in factoring out the pion flux, have limited the information finally extracted on the pion structure function.

E. Very hard diffraction and the BFKL Pomeron

For the diffractive processes discussed in Secs. V.B–V.D, $|t|$ is generally smaller than typical hadronic mass scales. However, diffractive processes have also been studied at HERA at $|t|$ values which are large enough to provide a hard scale in their own right. Under such circumstances, the

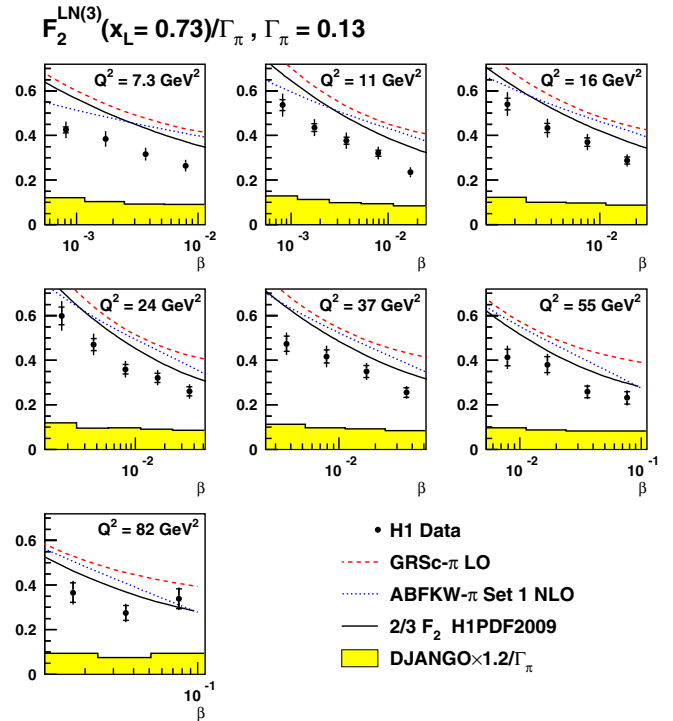


FIG. 64 (color online). Leading neutron structure function data (integrated over neutron transverse momenta up to 200 MeV), divided by a parametrization ([Holtmann et al., 1994](#)) of the pion flux Γ_{π} at $x_L \equiv 1 - x_{\text{IP}} = 0.73$. The estimated contribution from standard fragmentation processes is shown as a shaded band. After accounting for this, the data are compared with two parametrizations of the pion structure function ([Aurenche et al., 1989](#); [Gluck, Reya, and Schienbein, 1999](#)) and with a parametrization of the proton structure function ([Aaron et al., 2009b](#)) multiplied by $2/3$. From [Aaron et al., 2010e](#).

t -channel Pomeron exchange ought to be genuinely hard in the sense that it couples as a whole to individual partons. Cases where the hard subprocess satisfies $\hat{s} \gg -\hat{t} \gg \Lambda_{\text{QCD}}$ correspond to a perturbatively calculable limit of Regge theory. Where there is no particular ordering in transverse momentum within the color-singlet exchange, the dynamics may be driven primarily by BFKL evolution (see Sec. III.D). Diffractive processes at large $|t|$ therefore represent a promising area in which to search for low- x parton dynamics driven by the BFKL Pomeron.

One striking signature for perturbative color-singlet exchange is the photoproduction of pairs of jets separated by a large rapidity gap. For such “gap between jets” configurations, $|t| \approx p_{T,\text{jet}}^2$ is very large, typically $|t| > 25 \text{ GeV}^2$ in HERA studies, and calculations using the leading-logarithmic BFKL approximation ([Mueller and Tang, 1992](#)) with appropriate modifications ([Forshaw and Sutton, 1998](#); [Enberg, Ingelman, and Motyka, 2002](#)) can be applied to the scattering between a parton from the proton and a parton from the resolved structure of the photon. However, the situation is complicated by the possibility of secondary scattering and a rapidity gap survival probability significantly smaller than unity, similar to that discussed for the diffractive dijet photoproduction process in Sec. V.C.7. The HERA data ([Derrick et al., 1996b](#); [Adloff et al., 2002b](#); [Chekanov et al.,](#)

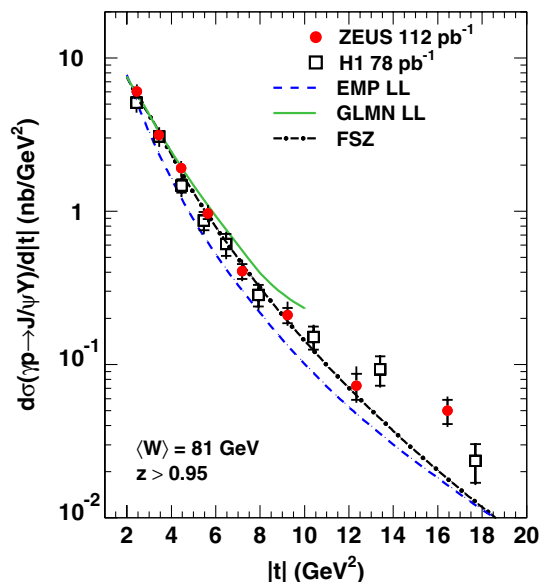


FIG. 65 (color online). Dependence on $|t|$ of proton dissociative J/ψ production integrated over proton dissociation masses satisfying $M_V^2/W^2 < 0.05$. The data are compared with a prediction [GLMN LL (Gotsman *et al.*, 2002)] which is based on DGLAP evolution and is expected to be valid for $|t| < m_V^2$. They are also compared with a BFKL-based prediction [EMP LL (Enberg, Motyka, and Poludniowski, 2002)] and a more phenomenological approach [FSZ (Frankfurt, Strikman, and Zhavoronkov, 2008)]. From Chekanov *et al.*, 2010f.

2007n) have shown clear evidence for events with little energy flow between jets, which occur more frequently than expected from hadronization fluctuations in standard Monte Carlo models of jet photoproduction. The order of magnitude of the signal is also in agreement with that expected from the BFKL calculations. While this is highly suggestive, and is in fact perhaps the best evidence for BFKL dynamics at HERA, more quantitative conclusions have been precluded by the uncertainties in the perturbative calculations, the gap survival probability, and the residual nondiffractive contributions.

Another candidate process in which to observe perturbative color-singlet exchange is quasielastic vector meson production at large $|t|$. Although $|t|$ values are smaller here than in the gaps-between-jets case and the proton essentially always dissociates, the exclusive production mechanism at the photon vertex [Fig. 45(b)] implies significantly reduced complications from gap destruction effects, even in photoproduction. The possibility of perturbative color-singlet exchange has long been considered for this process (Ginzburg, Panfil, and Serbo, 1987) and detailed calculations have been performed in the leading-logarithmic BFKL framework (Forshaw and Ryskin, 1995; Bartels *et al.*, 1996; Enberg *et al.*, 2003; Forshaw and Poludniowski, 2003; Poludniowski *et al.*, 2003). BFKL evolution is expected to be relevant for $|t| > m_V^2$, where m_V is the vector meson mass. For the case of heavy vector meson production, there is an interim region where $|t| < m_V^2$, yet $|t|$ remains large enough to apply perturbative techniques. Here the transverse momenta along the gluon ladder remain ordered and DGLAP dynamics are expected to apply (Gotsman *et al.*, 2002; Blok, Frankfurt, and Strikman, 2010). Studies have

been made at HERA for light vector mesons (Chekanov *et al.*, 2003b; Aktas *et al.*, 2006b) and J/ψ (Aktas *et al.*, 2003; Chekanov *et al.*, 2010f) mesons, as well as of exclusively produced photons (Aaron *et al.*, 2009d). Since it offers adequate statistics as well as a relatively clean theoretical interpretation, the J/ψ channel has yielded the most precise tests. An example analysis is shown in Fig. 65. The t dependences generally follow the expected approximate power law behavior at large $|t|$ and the effective trajectory slope α'_{ip} is much smaller than that describing soft diffraction, as expected in a BFKL treatment. However, the overall description by specific BFKL predictions is not yet sufficiently good for strong claims to be made.

VI. SUMMARY AND OUTLOOK

Condensing a total of about 200 publications from H1 and ZEUS on the hadronic final state has been a challenge. Further reducing this to a one-page summary is a task fraught with omissions and generalizations. With this caveat, the following represents an attempt to summarize the essential highlights of studies of the HERA hadronic final state as briefly as possible.

- Measurements of jet production among the most precise in the world, which have led to significant constraints on the parton density functions in the proton and precise determinations of α_s .
- Similarly, data on heavy quark production which have led to important constraints on the charm contribution to the proton structure functions, unique to HERA, and on the heavy quark masses.
- A demonstration of the power of QCD and, in particular, the applicability of the DGLAP equations for a multitude of processes covering a wide kinematic range. Despite considerable attempts to isolate evidence for BFKL or other parton evolution schemes and a handful of measurements which have yet to be satisfactorily described, no unequivocal evidence has been found for the need for non-DGLAP dynamics.
- Many measurements of light- and heavy quark fragmentation processes and charged-particle spectra which show similar behavior to that observed in e^+e^- or other collisions. Despite some anomalies, the data are broadly consistent with the concept of universal fragmentation.
- A wide variety of searches for evidence of exotic QCD processes, such as pentaquarks and instantons. Of all searches performed, a glueball candidate decaying to a $K_S^0 K_S^0$ pair with a mass consistent with the $f_0(1710)$ state was the only clear signal.
- A detailed exploration of the quasielastic exclusive production of vector mesons ($\gamma^{(*)}p \rightarrow Vp$) and photons ($\gamma^{(*)}p \rightarrow \gamma p$) over a wide range in scale, an appropriate choice for which is often $(Q^2 + M_V^2)/4$. The data illustrate and explore the transition with scale from a regime familiar from soft hadronic elastic and diffractive scattering to a region governed by hard diffractive exchanges which can be interpreted in terms of partons.
- Precise measurements of hard exclusive diffractive processes, for example, J/ψ photoproduction, and the development of successful methods for calculating

related observables starting from a knowledge of the parton densities of the proton.

- The precise measurement and interpretation of inclusive diffraction over a vast, usually three-dimensional, kinematic range, which has shown the process to be well modeled as the deep inelastic scattering of the electron from a factorizable soft object, not dissimilar from the Pomeron of soft hadronic physics.
- The extraction of the partonic structure of the soft-Pomeron-like exchange and its successful application in predicting diffractive final-state observables using standard NLO DGLAP-based tools.

Although these essential points are now unlikely to change, the H1 and ZEUS collaborations are still regularly publishing new results, and in several important areas the most precise measurements are still yet to come. Examples which have been discussed here include inclusive jet production in DIS and dijet photoproduction, for both of which only around 10% of the available data has been used in published measurements. Extending to the full data set and, where possible, combining H1 and ZEUS data will improve the precision and accessible kinematic range at high E_T (equivalently large x). The precision on heavy flavor cross sections, particularly those in the beauty sector, is also often statistically limited at present, with substantial power to improve if the full HERA data are exploited. In many areas, the understanding of the existing data can be improved considerably by the application of theoretical or phenomenological techniques which in principle already exist. Most prominently, the development for ep scattering of a Monte Carlo model which matches NLO QCD calculations to parton showers would represent a major breakthrough in our ability to model and interpret jet and other final-state data. A major impact could also be achieved by feeding into HERA analyses the improved understanding of the underlying event and of hadronization which is currently developing through model-tuning exercises at the LHC. The impact of these phenomenology improvements would be greatest in allowing low- E_T data to be exploited more fully, leading to better constraints on photon and low- x proton structure. New parametrizations of photon structure which include a wider range of HERA photoproduction data would also be a significant step forward. Many of the above improvements would extend the list of HERA observables which could reliably be included in fits to extract information on the proton structure. Combining the final inclusive DIS HERA and fixed-target data with carefully chosen HERA hadronic final-state measurements has the potential to produce constraints on the proton PDFs, α_s , and heavy quark masses which are unlikely to be surpassed for many years. Indeed, it may not be too ambitious to attempt a simultaneous extraction of proton and photon structure from HERA and other data, a program of work which may gain new impetus should a high-energy e^+e^- linear collider be constructed.

While there is still considerable room for improvement for the topics discussed above, there are also areas of the HERA physics program which are essentially complete. Given the current experimental precision and the limitations in our theoretical understanding, further substantial progress in areas such as the search for novel low- x dynamics, the measurement of charged-particle spectra, and the unraveling

of soft and hard contributions to diffractive DIS appears unlikely. Particularly for unresolved issues in low- x physics such as parton saturation, we may have to wait for data from a future higher energy lepton-hadron collider before drawing firm conclusions.

The impact of HERA hadronic final-state data and the new techniques developed for its analysis have been strongly felt at the LHC. Apart from the obvious need for precise knowledge of the proton structure as obtained from the well-matched HERA range of sensitivity, H1 and ZEUS input has contributed significantly in deciding how to make well-defined measurements of, for example, jet, heavy quark, and diffractive processes. There are also less obvious fields which have benefited, for example, the modeling of high-energy cosmic ray air showers and of the hadronic final states produced when neutrinos interact with hadronic matter in neutrino experiments. Whenever and wherever the next facility for high-energy lepton-hadron scattering is built, the HERA results will give strong steers as to how and where to make precise measurements of familiar physics and to look for new phenomena, such as low- x parton saturation.

In conclusion, the hadronic final state in electron-proton collisions at HERA has provided a rich source of data and deepened our understanding of strong interactions.

ACKNOWLEDGMENTS

P. R. N. and M. W. are fortunate to have been members of the H1 and ZEUS Collaborations, respectively, for around two decades. There are far too many colleagues with whom we have worked closely to name in person, but we want to record our thanks for many pleasant working relationships and much intellectual stimulation. We also thank J. Butterworth for providing input in the initial planning stages of this review.

REFERENCES

- Aad, G., *et al.* (ATLAS Collaboration), 2011a, *Nucl. Phys.* **B850**, 387.
- Aad, G., *et al.* (ATLAS Collaboration), 2011b, *Phys. Rev. D* **83**, 112001.
- Aad, G., *et al.* (ATLAS Collaboration), 2011c, *Eur. Phys. J. C* **71**, 1636.
- Aad, G., *et al.* (ATLAS Collaboration), 2012a, *Phys. Rev. D* **86**, 014022.
- Aad, G., *et al.* (ATLAS Collaboration), 2012b, *Eur. Phys. J. C* **72**, 1926.
- Aad, G., *et al.* (ATLAS Collaboration), 2012c, *Phys. Rev. D* **86**, 072004.
- Aaij, R., *et al.* (LHCb Collaboration), 2011, *Eur. Phys. J. C* **71**, 1645.
- Aaij, R., *et al.* (LHCb Collaboration), 2013, *J. Phys. G* **40**, 045001.
- Aamodt, K., *et al.* (ALICE Collaboration), 2010, *Phys. Rev. D* **82**, 052001.
- Aamodt, K., *et al.* (ALICE Collaboration), 2011, *Phys. Lett. B* **696**, 328.
- Aaron, F. D., *et al.* (H1 Collaboration), 2007, *Phys. Lett. B* **654**, 148.
- Aaron, F. D., *et al.* (H1 Collaboration), 2008a, *Phys. Lett. B* **659**, 796.
- Aaron, F. D., *et al.* (H1 Collaboration), 2008b, *Eur. Phys. J. C* **54**, 371.
- Aaron, F. D., *et al.* (H1 Collaboration), 2008c, *Phys. Lett. B* **665**, 139.

- Aaron, F. D., *et al.* (H1 Collaboration), 2008d, *Eur. Phys. J. C* **54**, 389.
- Aaron, F. D., *et al.* (H1 Collaboration), 2009a, *Phys. Lett. B* **674**, 257.
- Aaron, F. D., *et al.* (H1 Collaboration), 2009b, *Eur. Phys. J. C* **64**, 561.
- Aaron, F. D., *et al.* (H1 Collaboration), 2009c, *Phys. Lett. B* **681**, 391.
- Aaron, F. D., *et al.* (H1 Collaboration), 2009d, *Phys. Lett. B* **672**, 219.
- Aaron, F. D., *et al.* (H1 Collaboration), 2009e, *Phys. Lett. B* **681**, 125.
- Aaron, F. D., *et al.* (H1 Collaboration), 2009f, *Eur. Phys. J. C* **59**, 589.
- Aaron, F. D., *et al.* (H1 and ZEUS Collaborations), 2009g, *J. High Energy Phys.* **10**, 013.
- Aaron, F. D., *et al.* (H1 Collaboration), 2010a, *Eur. Phys. J. C* **70**, 15.
- Aaron, F. D., *et al.* (H1 Collaboration), 2010b, *J. High Energy Phys.* **05**, 032.
- Aaron, F. D., *et al.* (H1 Collaboration), 2010c, *Eur. Phys. J. C* **68**, 401.
- Aaron, F. D., *et al.* (H1 Collaboration), 2010d, *Eur. Phys. J. C* **67**, 1.
- Aaron, F. D., *et al.* (H1 Collaboration), 2010e, *Eur. Phys. J. C* **68**, 381.
- Aaron, F. D., *et al.* (H1 Collaboration), 2010f, *Eur. Phys. J. C* **65**, 363.
- Aaron, F. D., *et al.* (H1 Collaboration), 2010g, *Eur. Phys. J. C* **67**, 1.
- Aaron, F. D., *et al.* (H1 Collaboration), 2010h, *Eur. Phys. J. C* **65**, 89.
- Aaron, F. D., *et al.* (H1 Collaboration), 2010i, *Eur. Phys. J. C* **66**, 17.
- Aaron, F. D., *et al.* (H1 and ZEUS Collaborations), 2010j, *J. High Energy Phys.* **03**, 035.
- Aaron, F. D., *et al.* (H1 Collaboration), 2011a, *Eur. Phys. J. C* **71**, 1509.
- Aaron, F. D., *et al.* (H1 Collaboration), 2011b, *Eur. Phys. J. C* **71**, 1769; **72**, 2252(E) (2012).
- Aaron, F. D., *et al.* (H1 Collaboration), 2011c, *Eur. Phys. J. C* **71**, 1578.
- Aaron, F. D., *et al.* (H1 Collaboration), 2012a, *Eur. Phys. J. C* **72**, 2074.
- Aaron, F. D., *et al.* (H1 Collaboration), 2012b, *Eur. Phys. J. C* **72**, 2047.
- Aaron, F. D., *et al.* (H1 Collaboration), 2012c, *Eur. Phys. J. C* **72**, 2148.
- Aaron, F. D., *et al.* (H1 Collaboration), 2012d, *Eur. Phys. J. C* **72**, 1970.
- Aaron, F. D., *et al.* (H1 Collaboration), 2012e, *Eur. Phys. J. C* **72**, 1910.
- Aaron, F. D., *et al.* (H1 Collaboration), 2012f, *Eur. Phys. J. C* **72**, 1836.
- Aaron, F. D., *et al.* (H1 and ZEUS Collaborations), 2012g, *Eur. Phys. J. C* **72**, 2175.
- Abachi, S., *et al.* (D0 Collaboration), 1995a, *Phys. Rev. Lett.* **74**, 3548.
- Abachi, S., *et al.* (D0 Collaboration), 1995b, *Phys. Lett. B* **357**, 500.
- Abazov, V. M., *et al.* (D0 Collaboration), 2003, *Phys. Rev. D* **67**, 052001.
- Abbiendi, G., *et al.*, 1993, *Nucl. Instrum. Methods Phys. Res., Sect. A* **333**, 342.
- Abbiendi, G., *et al.* (OPAL Collaboration), 2002, *Phys. Lett. B* **533**, 207.
- Abbott, B., *et al.* (D0 Collaboration), 2000a, *Phys. Rev. Lett.* **85**, 5068.
- Abbott, B., *et al.* (D0 Collaboration), 2000b, *Phys. Rev. Lett.* **84**, 5478.
- Abbott, B., *et al.* (D0 Collaboration), 2000c, *Phys. Lett. B* **487**, 264.
- Abdesselam, A., *et al.*, 2011, *Eur. Phys. J. C* **71**, 1661.
- Abe, F., *et al.* (CDF Collaboration), 1993a, *Phys. Rev. Lett.* **70**, 713.
- Abe, F., *et al.* (CDF Collaboration), 1993b, *Phys. Rev. Lett.* **71**, 2396.
- Abe, F., *et al.* (CDF Collaboration), 1993c, *Phys. Rev. Lett.* **71**, 500.
- Abe, F., *et al.* (CDF Collaboration), 1993d, *Phys. Rev. D* **47**, 4857.
- Abe, F., *et al.* (CDF Collaboration), 1994, *Phys. Rev. D* **50**, 5518.
- Abe, F., *et al.* (CDF Collaboration), 1995, *Phys. Rev. Lett.* **75**, 1451.
- Abe, F., *et al.* (CDF Collaboration), 1996, *Phys. Rev. D* **53**, 1051.
- Abe, F., *et al.* (CDF Collaboration), 1997a, *Phys. Rev. D* **56**, 3811.
- Abe, F., *et al.* (CDF Collaboration), 1997b, *Phys. Rev. Lett.* **79**, 584.
- Abelev, B., *et al.* (ALICE Collaboration), 2012a, *Phys. Rev. Lett.* **108**, 082001.
- Abelev, B., *et al.* (ALICE Collaboration), 2012b, *J. High Energy Phys.* **11**, 065.
- Abelev, B., *et al.* (ALICE Collaboration), 2013, *Eur. Phys. J. C* **73**, 2456.
- Abelleira Fernandez, J., *et al.* (LHeC Study Group), 2012, *J. Phys. G* **39**, 075001.
- Abramov, V., *et al.*, 1987, *Sov. J. Nucl. Phys.* **45**, 845 [<http://inspirehep.net/search?p=find+j+Sov.J.Nucl.Phys.,45.845>].
- Abramowicz, H., A. Caldwell, and R. Sinkus, 1995, *Nucl. Instrum. Methods Phys. Res., Sect. A* **365**, 508.
- Abramowicz, H., *et al.* (ZEUS Collaboration), 2010a, *Eur. Phys. J. C* **70**, 965.
- Abramowicz, H., *et al.* (ZEUS Collaboration), 2010b, *Phys. Lett. B* **691**, 127.
- Abramowicz, H., *et al.* (ZEUS Collaboration), 2010c, *Eur. Phys. J. C* **69**, 347.
- Abramowicz, H., *et al.* (ZEUS Collaboration), 2010d, *J. High Energy Phys.* **11**, 009.
- Abramowicz, H., *et al.* (ZEUS Collaboration), 2010e, *J. High Energy Phys.* **06**, 009.
- Abramowicz, H., *et al.* (ZEUS Collaboration), 2011a, *Eur. Phys. J. C* **71**, 1573.
- Abramowicz, H., *et al.* (ZEUS Collaboration), 2011b, *Eur. Phys. J. C* **71**, 1659.
- Abramowicz, H., *et al.* (ZEUS Collaboration), 2012a, *Nucl. Phys.* **B864**, 1.
- Abramowicz, H., *et al.* (ZEUS Collaboration), 2012b, *Phys. Lett. B* **715**, 88.
- Abramowicz, H., *et al.* (ZEUS Collaboration), 2012c, *Phys. Lett. B* **708**, 14.
- Abramowicz, H., *et al.* (H1 and ZEUS Collaborations), 2013a, *Eur. Phys. J. C* **73**, 2311.
- Abramowicz, H., *et al.* (ZEUS Collaboration), 2013b, *J. High Energy Phys.* **09**, 058.
- Abramowicz, H., *et al.* (ZEUS Collaboration), 2013c, *J. High Energy Phys.* **02**, 071.
- Abramowicz, H., *et al.* (ZEUS Collaboration), 2013d, *Nucl. Phys.* **B866**, 229.
- Abramowicz, H., *et al.* (ZEUS Collaboration), 2014, *Phys. Lett. B* **730**, 293.
- Abreu, P., *et al.* (DELPHI Collaboration), 1993, *Phys. Lett. B* **311**, 408.
- Abt, I., *et al.* (H1 Collaboration), 1994a, *Z. Phys. C* **63**, 377.
- Abt, I., *et al.* (H1 Collaboration), 1994b, *Phys. Lett. B* **328**, 176.
- Abt, I., *et al.* (H1 Collaboration), 1997a, *Nucl. Instrum. Methods Phys. Res., Sect. A* **386**, 310.
- Abt, I., *et al.* (H1 Collaboration), 1997b, *Nucl. Instrum. Methods Phys. Res., Sect. A* **386**, 348.
- Abulencia, A., *et al.* (CDF Collaboration), 2007, *Phys. Rev. Lett.* **99**, 132001.
- Acciarri, M., *et al.* (L3 Collaboration), 2001, *Phys. Lett. B* **501**, 173.
- Acosta, D., *et al.* (CDF Collaboration), 2002, *Phys. Rev. D* **65**, 052005.

- Acosta, D., *et al.* (CDF Collaboration), 2004, *Phys. Rev. D* **70**, 072002.
- Adams, M., *et al.* (E665 Collaboration), 1997, *Z. Phys. C* **74**, 237.
- Adler, C., *et al.* (STAR Collaboration), 2001, *Phys. Rev. Lett.* **87**, 262301.
- Adler, S., *et al.* (PHENIX Collaboration), 2005, *Phys. Rev. Lett.* **94**, 122302.
- Adloff, C., *et al.* (H1 Collaboration), 1997a, *Z. Phys. C* **75**, 437.
- Adloff, C., *et al.* (H1 Collaboration), 1997b, *Z. Phys. C* **74**, 221.
- Adloff, C., *et al.* (H1 Collaboration), 1997c, *Nucl. Phys.* **B504**, 3.
- Adloff, C., *et al.* (H1 Collaboration), 1997d, *Z. Phys. C* **76**, 613.
- Adloff, C., *et al.* (H1 Collaboration), 1997e, *Nucl. Phys.* **B485**, 3.
- Adloff, C., *et al.* (H1 Collaboration), 1997f, *Phys. Lett. B* **406**, 256.
- Adloff, C., *et al.* (H1 Collaboration), 1998a, *Phys. Lett. B* **428**, 206.
- Adloff, C., *et al.* (H1 Collaboration), 1998b, *Eur. Phys. J. C* **5**, 439.
- Adloff, C., *et al.* (H1 Collaboration), 1998c, *Eur. Phys. J. C* **5**, 575.
- Adloff, C., *et al.* (H1 Collaboration), 1998d, *Eur. Phys. J. C* **1**, 495.
- Adloff, C., *et al.* (H1 Collaboration), 1999a, *Eur. Phys. J. C* **10**, 363.
- Adloff, C., *et al.* (H1 Collaboration), 1999b, *Phys. Lett. B* **462**, 440.
- Adloff, C., *et al.* (H1 Collaboration), 1999c, *Nucl. Phys.* **B545**, 3.
- Adloff, C., *et al.* (H1 Collaboration), 1999d, *Eur. Phys. J. C* **6**, 587.
- Adloff, C., *et al.* (H1 Collaboration), 1999e, *Phys. Lett. B* **467**, 156; **518**, 331(E) (2001).
- Adloff, C., *et al.* (H1 Collaboration), 2000a, *Eur. Phys. J. C* **13**, 371.
- Adloff, C., *et al.* (H1 Collaboration), 2000b, *Eur. Phys. J. C* **14**, 255.
- Adloff, C., *et al.* (H1 Collaboration), 2000c, *Phys. Lett. B* **483**, 36.
- Adloff, C., *et al.* (H1 Collaboration), 2000d, *Eur. Phys. J. C* **12**, 595.
- Adloff, C., *et al.* (H1 Collaboration), 2001a, *Eur. Phys. J. C* **20**, 29.
- Adloff, C., *et al.* (H1 Collaboration), 2001b, *Eur. Phys. J. C* **19**, 289.
- Adloff, C., *et al.* (H1 Collaboration), 2001c, *Phys. Lett. B* **520**, 183.
- Adloff, C., *et al.* (H1 Collaboration), 2001d, *Phys. Lett. B* **515**, 17.
- Adloff, C., *et al.* (H1 Collaboration), 2002a, *Phys. Lett. B* **539**, 25.
- Adloff, C., *et al.* (H1 Collaboration), 2002b, *Eur. Phys. J. C* **24**, 517.
- Adloff, C., *et al.* (H1 Collaboration), 2002c, *Eur. Phys. J. C* **25**, 41.
- Adloff, C., *et al.* (H1 Collaboration), 2002d, *Eur. Phys. J. C* **25**, 25.
- Adloff, C., *et al.* (H1 Collaboration), 2002e, *Phys. Lett. B* **542**, 193.
- Adloff, C., *et al.* (H1 Collaboration), 2002f, *Phys. Lett. B* **544**, 35.
- Adloff, C., *et al.* (H1 Collaboration), 2002g, *Eur. Phys. J. C* **25**, 495.
- Adloff, C., *et al.* (H1 Collaboration), 2003, *Eur. Phys. J. C* **29**, 497.
- Adolph, C., *et al.* (COMPASS Collaboration), 2012, *Nucl. Phys.* **B865**, 1.
- Affolder, T., *et al.* (CDF Collaboration), 2000, *Phys. Rev. Lett.* **84**, 5043.
- Ahle, L., *et al.* (E802 Collaboration), 1998, *Phys. Rev. C* **57**, 1416.
- Ahmed, T., *et al.* (H1 Collaboration), 1992, *Phys. Lett. B* **297**, 205.
- Ahmed, T., *et al.* (H1 Collaboration), 1994a, *Nucl. Phys.* **B429**, 477.
- Ahmed, T., *et al.* (H1 Collaboration), 1994b, *Phys. Lett. B* **338**, 507.
- Ahmed, T., *et al.* (H1 Collaboration), 1995a, *Phys. Lett. B* **348**, 681.
- Ahmed, T., *et al.* (H1 Collaboration), 1995b, *Nucl. Phys.* **B435**, 3.
- Aid, S., *et al.* (H1 Collaboration), 1995, *Z. Phys. C* **69**, 27.
- Aid, S., *et al.* (H1 Collaboration), 1996a, *Z. Phys. C* **72**, 573.
- Aid, S., *et al.* (H1 Collaboration), 1996b, *Nucl. Phys.* **B472**, 3.
- Aid, S., *et al.* (H1 Collaboration), 1996c, *Nucl. Phys.* **B463**, 3.
- Aid, S., *et al.* (H1 Collaboration), 1996d, *Z. Phys. C* **70**, 17.
- Airapetian, A., *et al.* (HERMES Collaboration), 2000, *Eur. Phys. J. C* **17**, 389.
- Airapetian, A., *et al.* (HERMES Collaboration), 2007, *Phys. Rev. D* **75**, 011103.
- Airapetian, A., *et al.* (HERMES Collaboration), 2009, *Phys. Lett. B* **679**, 100.
- Airapetian, A., *et al.* (HERMES Collaboration), 2012a, *J. High Energy Phys.* **07**, 032.
- Airapetian, A., *et al.* (HERMES Collaboration), 2012b, *J. High Energy Phys.* **10**, 042.
- Akers, R., *et al.* (OPAL Collaboration), 1994, *Z. Phys. C* **63**, 197.
- Akers, R., *et al.* (OPAL Collaboration), 1995, *Z. Phys. C* **67**, 203.
- Aktas, A., *et al.* (H1 Collaboration), 2003, *Phys. Lett. B* **568**, 205.
- Aktas, A., *et al.* (H1 Collaboration), 2004a, *Phys. Lett. B* **588**, 17.
- Aktas, A., *et al.* (H1 Collaboration), 2004b, *Eur. Phys. J. C* **36**, 441.
- Aktas, A., *et al.* (H1 Collaboration), 2004c, *Eur. Phys. J. C* **33**, 477.
- Aktas, A., *et al.* (H1 Collaboration), 2004d, *Eur. Phys. J. C* **36**, 413.
- Aktas, A., *et al.* (H1 Collaboration), 2004e, *Eur. Phys. J. C* **37**, 141.
- Aktas, A., *et al.* (H1 Collaboration), 2005a, *Eur. Phys. J. C* **38**, 447.
- Aktas, A., *et al.* (H1 Collaboration), 2005b, *Eur. Phys. J. C* **41**, 453.
- Aktas, A., *et al.* (H1 Collaboration), 2005c, *Phys. Lett. B* **621**, 56.
- Aktas, A., *et al.* (H1 Collaboration), 2005d, *Eur. Phys. J. C* **41**, 273.
- Aktas, A., *et al.* (H1 Collaboration), 2005e, *Eur. Phys. J. C* **38**, 437.
- Aktas, A., *et al.* (H1 Collaboration), 2006a, *Eur. Phys. J. C* **48**, 749.
- Aktas, A., *et al.* (H1 Collaboration), 2006b, *Phys. Lett. B* **638**, 422.
- Aktas, A., *et al.* (H1 Collaboration), 2006c, *Eur. Phys. J. C* **46**, 585.
- Aktas, A., *et al.* (H1 Collaboration), 2006d, *Eur. Phys. J. C* **46**, 27.
- Aktas, A., *et al.* (H1 Collaboration), 2006e, *Eur. Phys. J. C* **48**, 715.
- Aktas, A., *et al.* (H1 Collaboration), 2006f, *Eur. Phys. J. C* **47**, 597.
- Aktas, A., *et al.* (H1 Collaboration), 2006g, *Eur. Phys. J. C* **46**, 343.
- Aktas, A., *et al.* (H1 Collaboration), 2006h, *Phys. Lett. B* **639**, 21.
- Aktas, A., *et al.* (H1 Collaboration), 2006i, *Phys. Lett. B* **639**, 202.
- Aktas, A., *et al.* (H1 Collaboration), 2007a, *Eur. Phys. J. C* **50**, 1.
- Aktas, A., *et al.* (H1 Collaboration), 2007b, *J. High Energy Phys.* **10**, 042.
- Aktas, A., *et al.* (H1 Collaboration), 2007c, *Eur. Phys. J. C* **50**, 251.
- Aktas, A., *et al.* (H1 Collaboration), 2007d, *Phys. Lett. B* **653**, 134.
- Aktas, A., *et al.* (H1 Collaboration), 2007e, *Eur. Phys. J. C* **52**, 507.
- Aktas, A., *et al.* (H1 Collaboration), 2007f, *Eur. Phys. J. C* **51**, 549.
- Albaladejo, M., and J. Oller, 2008, *Phys. Rev. Lett.* **101**, 252002.
- Alberi, G., and G. Goggi, 1981, *Phys. Rep.* **74**, 1.
- Albino, S., B. A. Kniehl, and G. Kramer, 2005, *Nucl. Phys.* **B725**, 181.
- Albino, S., B. A. Kniehl, and G. Kramer, 2008, *Nucl. Phys.* **B803**, 42.
- Albrecht, H., *et al.* (ARGUS Collaboration), 1985, *Phys. Lett.* **157B**, 326.
- Albrecht, H., *et al.* (ARGUS Collaboration), 1990, *Phys. Lett. B* **236**, 102.
- Alekhin, S., J. Blumlein, S. Klein, and S. Moch, 2010, *Phys. Rev. D* **81**, 014032.
- Alekhin, S., J. Blumlein, and S. Moch, 2012, *Phys. Rev. D* **86**, 054009.
- Alekhin, S., and S. Moch, 2011, *Phys. Lett. B* **699**, 345.
- Alexa, C., *et al.* (H1 Collaboration), 2013a, *Eur. Phys. J. C* **73**, 2466.
- Alexa, C., *et al.* (H1 Collaboration), 2013b, *Eur. Phys. J. C* **73**, 2406.
- Alexakhin, V. Y., *et al.* (COMPASS Collaboration), 2007, *Eur. Phys. J. C* **52**, 255.
- Alexander, G., 2003, *Rep. Prog. Phys.* **66**, 481.
- Alexander, G., I. Cohen, and E. Levin, 1999, *Phys. Lett. B* **452**, 159.
- Alexopoulos, T., *et al.* (E735 Collaboration), 1993, *Phys. Rev. D* **48**, 1931.
- Allfrey, P. D., *et al.*, 2007, *Nucl. Instrum. Methods Phys. Res., Sect. A* **580**, 1257.
- Alper, B., *et al.*, 1973, *Phys. Lett.* **46B**, 265.
- Alt, C., *et al.* (NA49 Collaboration), 2004, *Phys. Rev. Lett.* **92**, 042003.
- Altarelli, G., and G. Parisi, 1977, *Nucl. Phys.* **B126**, 298.
- Althoff, M., *et al.* (TASSO Collaboration), 1983, *Phys. Lett.* **121B**, 216.
- Althoff, M., *et al.* (TASSO Collaboration), 1986, *Z. Phys. C* **30**, 355.
- Amsler, C., *et al.* (Particle Data Group), 2008, *Phys. Lett. B* **667**, 1.

- Andersson, B., G. Gustafson, G. Ingelman, and T. Sjostrand, 1983, *Phys. Rep.* **97**, 31.
- Andersson, B., G. Gustafson, L. Lonnblad, and U. Pettersson, 1989, *Z. Phys. C* **43**, 625.
- Andresen, A., *et al.* (ZEUS Calorimeter Group), 1991, *Nucl. Instrum. Methods Phys. Res., Sect. A* **309**, 101.
- Andrieu, B., *et al.* (H1 Calorimeter Group), 1993, *Nucl. Instrum. Methods Phys. Res., Sect. A* **336**, 460.
- Anticic, T., *et al.* (NA49 Collaboration), 2012, *Phys. Rev. C* **85**, 044913.
- Antipov, Y., *et al.*, 1971, *Phys. Lett.* **34B**, 164.
- Aoki, M., *et al.*, 1992, *Phys. Rev. Lett.* **69**, 2345.
- Appelquist, G., *et al.* (NA52 (NEWMASS) Collaboration), 1996, *Phys. Lett. B* **376**, 245.
- Appuhn, R. D., *et al.* (H1 SPACAL Group), 1997, *Nucl. Instrum. Methods Phys. Res., Sect. A* **386**, 397.
- Arneodo, M., *et al.* (EMC Collaboration), 1986, *Z. Phys. C* **32**, 1.
- Arneodo, M., *et al.* (NMC Collaboration), 1994, *Nucl. Phys.* **B429**, 503.
- Arsene, I., *et al.* (BRAHMS Collaboration), 2011, *Phys. Rev. C* **83**, 044906.
- Artoisenet, P., J. M. Campbell, F. Maltoni, and F. Tramontano, 2009, *Phys. Rev. Lett.* **102**, 142001.
- Asner, D., *et al.* (CLEO Collaboration), 2007, *Phys. Rev. D* **75**, 012009.
- Aurenche, P., R. Baier, M. Fontannaz, M. Kienzle-Focacci, and M. Werlen, 1989, *Phys. Lett. B* **233**, 517.
- Aurenche, P., L. Bourhis, M. Fontannaz, and J. P. Guillet, 2000, *Eur. Phys. J. C* **17**, 413.
- Aurenche, P., M. Fontannaz, and J. P. Guillet, 2005, *Eur. Phys. J. C* **44**, 395.
- Baier, R., and R. Ruckl, 1981, *Phys. Lett.* **102B**, 364.
- Baier, R., and R. Ruckl, 1982, *Nucl. Phys.* **B201**, 1.
- Baier, R., and R. Ruckl, 1983, *Z. Phys. C* **19**, 251.
- Baird, A., *et al.* (H1 Collaboration), 2001, *Nucl. Instrum. Methods Phys. Res., Sect. A* **461**, 461.
- Balitsky, I. I., and V. M. Braun, 1993, *Phys. Lett. B* **314**, 237.
- Balitsky, I. I., and L. N. Lipatov, 1978, *Sov. J. Nucl. Phys.* **28**, 822 [<http://inspirehep.net/search?p=find+j+Sov.J.Nucl.Phys.,28,822>].
- Baranov, S., 1998, *Phys. Lett. B* **428**, 377.
- Baranov, S. P., 2002, *Phys. Rev. D* **66**, 114003.
- Bartel, W., *et al.* (JADE Collaboration), 1986, *Z. Phys. C* **33**, 23.
- Bartels, J., J. R. Ellis, H. Kowalski, and M. Wusthoff, 1999, *Eur. Phys. J. C* **7**, 443.
- Bartels, J., J. R. Forshaw, H. Lotter, and M. Wusthoff, 1996, *Phys. Lett. B* **375**, 301.
- Bartels, J., H. Jung, and A. Kyrieleis, 2002, *Eur. Phys. J. C* **24**, 555.
- Bartels, J., H. Jung, and M. Wusthoff, 1999, *Eur. Phys. J. C* **11**, 111.
- Bartels, J., H. Lotter, and M. Wusthoff, 1996, *Phys. Lett. B* **379**, 239.
- Bartsch, D., 2007, Ph.D. thesis (Universität Bonn), BONN-IR-2007-05.
- Bassler, U., and G. Bernardi, 1995, *Nucl. Instrum. Methods Phys. Res., Sect. A* **361**, 197.
- Bauer, T., R. Spital, D. Yennie, and F. Pipkin, 1978, *Rev. Mod. Phys.* **50**, 261.
- Bearden, I., *et al.* (NA44 Collaboration), 1999, *Nucl. Phys.* **A661**, 387.
- Bearden, I., *et al.*, 2002, *Eur. Phys. J. C* **23**, 237.
- Belavin, A., A. M. Polyakov, A. Schwartz, and Y. Tyupkin, 1975, *Phys. Lett.* **59B**, 85.
- Bentvelsen, S., J. Engelen, and P. Kooijman, 1992, in *Proceedings, Physics at HERA, Hamburg*, edited by W. Buchmueller and G. Ingelman (DESY, Hamburg), Vol. 1, p. 23.
- Berger, E. L., J. C. Collins, D. E. Soper, and G. F. Sterman, 1987, *Nucl. Phys.* **B286**, 704.
- Berger, E. L., and D. L. Jones, 1981, *Phys. Rev. D* **23**, 1521.
- Beringer, J., *et al.* (Particle Data Group), 2012, *Phys. Rev. D* **86**, 010001.
- Bernstein, A., *et al.* (ZEUS Barrel Calorimeter Group), 1993, *Nucl. Instrum. Methods Phys. Res., Sect. A* **336**, 23.
- Bethke, S., 2004, *Nucl. Phys. B, Proc. Suppl.* **135**, 345.
- Bethke, S., *et al.* (JADE Collaboration), 1988, *Phys. Lett. B* **213**, 235.
- Bhadra, S., *et al.*, 1995, *Nucl. Instrum. Methods Phys. Res., Sect. A* **354**, 479.
- Bhadra, S., *et al.*, 1997a, in *Proceedings of the 7th International Conference on Calorimetry in High-Energy Physics (ICCHEP 97), Tucson* (World Scientific, Singapore).
- Bhadra, S., *et al.* (ZEUS FNC Group), 1997b, *Nucl. Instrum. Methods Phys. Res., Sect. A* **394**, 121.
- Biddulph, P., *et al.*, 1994, *Nucl. Instrum. Methods Phys. Res., Sect. A* **340**, 304.
- Binkley, M. E., *et al.*, 1982, *Phys. Rev. Lett.* **48**, 73.
- Binnewies, J., B. A. Kniehl, and G. Kramer, 1995, *Phys. Rev. D* **52**, 4947.
- Binnewies, J., B. A. Kniehl, and G. Kramer, 1997, *Z. Phys. C* **76**, 677.
- Binnewies, J., B. A. Kniehl, and G. Kramer, 1998, *Phys. Rev. D* **58**, 014014.
- Binon, F., *et al.* (IHEP-CERN Collaboration), 1969, *Phys. Lett.* **30B**, 510.
- Bishari, M., 1972, *Phys. Lett.* **38B**, 510.
- Bjorken, J., 1993, *Phys. Rev. D* **47**, 101.
- Blok, B., L. Frankfurt, and M. Strikman, 2010, *Phys. Lett. B* **690**, 159.
- Blumlein, J., and D. Robaschik, 2001, *Phys. Lett. B* **517**, 222.
- Bodwin, G. T., E. Braaten, and G. P. Lepage, 1995, *Phys. Rev. D* **51**, 1125; **55**, 5853(E) (1997).
- Brambilla, N., *et al.*, 2011, *Eur. Phys. J. C* **71**, 1534.
- Brandt, A., S. Erhan, A. Kuzucu, M. Medinnis, N. Ozdes, P. E. Schlein, M. T. Zeyrek, J. G. Zweizig, J. B. Cheze, and J. Zsembery (UA8 Collaboration), 1992, *Phys. Lett. B* **297**, 417.
- Braunschweig, W., *et al.* (TASSO Collaboration), 1990, *Z. Phys. C* **47**, 187.
- Breitweg, J., *et al.* (ZEUS Collaboration), 1997a, *Z. Phys. C* **76**, 599.
- Breitweg, J., *et al.* (ZEUS Collaboration), 1997b, *Phys. Lett. B* **413**, 201.
- Breitweg, J., *et al.* (ZEUS Collaboration), 1997c, *Phys. Lett. B* **414**, 428.
- Breitweg, J., *et al.* (ZEUS Collaboration), 1997d, *Z. Phys. C* **75**, 421.
- Breitweg, J., *et al.* (ZEUS Collaboration), 1998a, *Eur. Phys. J. C* **2**, 77.
- Breitweg, J., *et al.* (ZEUS Collaboration), 1998b, *Eur. Phys. J. C* **1**, 109.
- Breitweg, J., *et al.* (ZEUS Collaboration), 1998c, *Eur. Phys. J. C* **2**, 247.
- Breitweg, J., *et al.* (ZEUS Collaboration), 1998d, *Phys. Lett. B* **421**, 368.
- Breitweg, J., *et al.* (ZEUS Collaboration), 1998e, *Eur. Phys. J. C* **2**, 61.
- Breitweg, J., *et al.* (ZEUS Collaboration), 1999a, *Eur. Phys. J. C* **6**, 603.
- Breitweg, J., *et al.* (ZEUS Collaboration), 1999b, *Eur. Phys. J. C* **6**, 67.
- Breitweg, J., *et al.* (ZEUS Collaboration), 1999c, *Eur. Phys. J. C* **8**, 367.
- Breitweg, J., *et al.* (ZEUS Collaboration), 1999d, *Eur. Phys. J. C* **11**, 251.

- Breitweg, J., *et al.* (ZEUS Collaboration), 1999e, *Eur. Phys. J. C* **6**, 43.
- Breitweg, J., *et al.* (ZEUS Collaboration), 2000a, *Eur. Phys. J. C* **14**, 213.
- Breitweg, J., *et al.* (ZEUS Collaboration), 2000b, *Phys. Lett. B* **472**, 175.
- Breitweg, J., *et al.* (ZEUS Collaboration), 2000c, *Eur. Phys. J. C* **12**, 393.
- Breitweg, J., *et al.* (ZEUS Collaboration), 2001a, *Phys. Lett. B* **507**, 70.
- Breitweg, J., *et al.* (ZEUS Collaboration), 2001b, *Eur. Phys. J. C* **18**, 625.
- Brock, R., *et al.* (CTEQ Collaboration), 1995, *Rev. Mod. Phys.* **67**, 157.
- Brodsky, S. J., V. S. Fadin, V. T. Kim, L. N. Lipatov, and G. B. Pivovarov, 1999, *JETP Lett.* **70**, 155.
- Brodsky, S. J., L. Frankfurt, J. Gunion, A. H. Mueller, and M. Strikman, 1994, *Phys. Rev. D* **50**, 3134.
- Buchmuller, W., T. Gehrmann, and A. Hebecker, 1999, *Nucl. Phys.* **B537**, 477.
- Buchmuller, W., and A. Hebecker, 1995, *Phys. Lett. B* **355**, 573.
- Buchmuller, W., M. McDermott, and A. Hebecker, 1997, *Phys. Lett. B* **410**, 304.
- Burger, J., *et al.*, 1989, *Nucl. Instrum. Methods Phys. Res., Sect. A* **279**, 217.
- Butenschoen, M., and B. A. Kniehl, 2010, *Phys. Rev. Lett.* **104**, 072001.
- Butenschoen, M., and B. A. Kniehl, 2011a, *Phys. Rev. Lett.* **106**, 022003.
- Butenschoen, M., and B. A. Kniehl, 2011b, *Phys. Rev. D* **84**, 051501.
- Butenschoen, M., and B. A. Kniehl, 2012, *Nucl. Phys. B, Proc. Suppl.* **222–224**, 151.
- Butler, S., and C. Pearson, 1963, *Phys. Rev.* **129**, 836.
- Butterworth, J. M., A. R. Davison, M. Rubin, and G. P. Salam, 2008, *Phys. Rev. Lett.* **100**, 242001.
- Butterworth, J. M., J. R. Forshaw, and M. H. Seymour, 1996, *Z. Phys. C* **72**, 637.
- Butterworth, J. M., and M. Wing, 2005, *Rep. Prog. Phys.* **68**, 2773.
- Cacciari, M., 2004, [arXiv:hep-ph/0407187](https://arxiv.org/abs/hep-ph/0407187).
- Cacciari, M., P. Nason, and C. Oleari, 2006, *J. High Energy Phys.* **04**, 006.
- Cacciari, M., G. P. Salam, and G. Soyez, 2008, *J. High Energy Phys.* **04**, 063.
- Caldwell, A., *et al.*, 1992, *Nucl. Instrum. Methods Phys. Res., Sect. A* **321**, 356.
- Camacho, C. M., *et al.* (Jefferson Lab Hall A Collaboration), 2006, *Phys. Rev. Lett.* **97**, 262002.
- Caron, S., 2002, Ph.D. thesis (Rheinisch-Westfälischen Technischen Hochschule Aachen), DESY-THESIS-2002-035.
- Caswell, W., and G. Lepage, 1986, *Phys. Lett.* **167B**, 437.
- Catani, S., Y. L. Dokshitzer, M. H. Seymour, and B. R. Webber, 1993, *Nucl. Phys.* **B406**, 187.
- Catani, S., F. Fiorani, and G. Marchesini, 1990a, *Phys. Lett. B* **234**, 339.
- Catani, S., F. Fiorani, and G. Marchesini, 1990b, *Nucl. Phys.* **B336**, 18.
- Catani, S., and M. H. Seymour, 1997, *Nucl. Phys.* **B485**, 291; **B510**, 503(E) (1998).
- Catani, S., B. R. Webber, Y. L. Dokshitzer, and F. Fiorani, 1992, *Nucl. Phys.* **B383**, 419.
- Chang, C.-H., 1980, *Nucl. Phys.* **B172**, 425.
- Chapin, T., R. Cool, K. A. Goulianos, K. Jenkins, J. Silverman, G. Snow, H. Sticker, S. White, and Y. Chou, 1985, *Phys. Rev. D* **31**, 17.
- Chatrchyan, S., *et al.* (CMS Collaboration), 2011, *J. High Energy Phys.* **09**, 109.
- Chatrchyan, S., *et al.* (CMS Collaboration), 2012a, *J. High Energy Phys.* **02**, 011.
- Chatrchyan, S., *et al.* (CMS Collaboration), 2012b, *J. High Energy Phys.* **08**, 130.
- Chatrchyan, S., *et al.* (CMS Collaboration), 2013a, *Phys. Rev. D* **87**, 012006.
- Chatrchyan, S., *et al.* (CMS Collaboration), 2013b, *J. High Energy Phys.* **04**, 072.
- Chekanov, S., *et al.* (ZEUS Collaboration), 2001a, *Phys. Lett. B* **510**, 36.
- Chekanov, S., *et al.* (ZEUS Collaboration), 2001b, *Phys. Lett. B* **511**, 19.
- Chekanov, S., *et al.* (ZEUS Collaboration), 2001c, *Phys. Lett. B* **516**, 273.
- Chekanov, S., *et al.* (ZEUS Collaboration), 2002a, *Eur. Phys. J. C* **23**, 615.
- Chekanov, S., *et al.* (ZEUS Collaboration), 2002b, *Eur. Phys. J. C* **23**, 13.
- Chekanov, S., *et al.* (ZEUS Collaboration), 2002c, *Eur. Phys. J. C* **24**, 345.
- Chekanov, S., *et al.* (ZEUS Collaboration), 2002d, *Phys. Lett. B* **531**, 9.
- Chekanov, S., *et al.* (ZEUS Collaboration), 2002e, *Phys. Lett. B* **547**, 164.
- Chekanov, S., *et al.* (ZEUS Collaboration), 2002f, *Phys. Rev. D* **65**, 052001.
- Chekanov, S., *et al.* (ZEUS Collaboration), 2003a, *Eur. Phys. J. C* **27**, 531.
- Chekanov, S., *et al.* (ZEUS Collaboration), 2003b, *Eur. Phys. J. C* **26**, 389.
- Chekanov, S., *et al.* (ZEUS Collaboration), 2003c, *Phys. Lett. B* **558**, 41.
- Chekanov, S., *et al.* (ZEUS Collaboration), 2003d, *Nucl. Phys.* **B672**, 3.
- Chekanov, S., *et al.* (ZEUS Collaboration), 2003e, *Eur. Phys. J. C* **27**, 173.
- Chekanov, S., *et al.* (ZEUS Collaboration), 2003f, *Phys. Lett. B* **551**, 226.
- Chekanov, S., *et al.* (ZEUS Collaboration), 2004a, *Phys. Rev. D* **70**, 012008; **74**, 059906(E) (2006).
- Chekanov, S., *et al.* (ZEUS Collaboration), 2004b, *Phys. Lett. B* **583**, 231.
- Chekanov, S., *et al.* (ZEUS Collaboration), 2004c, *Phys. Lett. B* **591**, 7.
- Chekanov, S., *et al.* (ZEUS Collaboration), 2004d, *Nucl. Phys.* **B695**, 3.
- Chekanov, S., *et al.* (ZEUS Collaboration), 2004e, *Phys. Lett. B* **595**, 86.
- Chekanov, S., *et al.* (ZEUS Collaboration), 2004f, *Phys. Lett. B* **578**, 33.
- Chekanov, S., *et al.* (ZEUS Collaboration), 2004g, *Phys. Lett. B* **590**, 143.
- Chekanov, S., *et al.* (ZEUS Collaboration), 2004h, *Eur. Phys. J. C* **38**, 29.
- Chekanov, S., *et al.* (ZEUS Collaboration), 2004i, *Eur. Phys. J. C* **34**, 255.
- Chekanov, S., *et al.* (ZEUS Collaboration), 2004j, *Nucl. Phys.* **B700**, 3.
- Chekanov, S., *et al.* (ZEUS Collaboration), 2005a, *Eur. Phys. J. C* **42**, 1.
- Chekanov, S., *et al.* (ZEUS Collaboration), 2005b, *Nucl. Phys.* **B729**, 492.

- Chekanov, S., *et al.* (ZEUS Collaboration), 2005c, *Eur. Phys. J. C* **44**, 351.
- Chekanov, S., *et al.* (ZEUS Collaboration), 2005d, *Eur. Phys. J. C* **44**, 13.
- Chekanov, S., *et al.* (ZEUS Collaboration), 2005e, *Eur. Phys. J. C* **44**, 183.
- Chekanov, S., *et al.* (ZEUS Collaboration), 2005f, *Phys. Lett. B* **610**, 212.
- Chekanov, S., *et al.* (ZEUS Collaboration), 2005g, *Nucl. Phys.* **B713**, 3.
- Chekanov, S., *et al.* (ZEUS Collaboration), 2005h, *Phys. Lett. B* **610**, 199.
- Chekanov, S., *et al.* (ZEUS Collaboration), 2007a, *Phys. Lett. B* **652**, 1.
- Chekanov, S., *et al.* (ZEUS Collaboration), 2007b, *Eur. Phys. J. C* **51**, 301.
- Chekanov, S., *et al.* (ZEUS Collaboration), 2007c, *Eur. Phys. J. C* **52**, 813.
- Chekanov, S., *et al.* (ZEUS Collaboration), 2007d, *Nucl. Phys.* **B767**, 1.
- Chekanov, S., *et al.* (ZEUS Collaboration), 2007e, *PMC Phys. A* **1**, 6.
- Chekanov, S., *et al.* (ZEUS Collaboration), 2007f, *Phys. Rev. D* **76**, 072011.
- Chekanov, S., *et al.* (ZEUS Collaboration), 2007g, *Nucl. Phys.* **B765**, 1.
- Chekanov, S., *et al.* (ZEUS Collaboration), 2007h, *Phys. Lett. B* **649**, 12.
- Chekanov, S., *et al.* (ZEUS Collaboration), 2007i, *Nucl. Phys.* **B776**, 1.
- Chekanov, S., *et al.* (ZEUS Collaboration), 2007j, *Nucl. Phys.* **B786**, 181.
- Chekanov, S., *et al.* (ZEUS Collaboration), 2007k, *J. High Energy Phys.* **07**, 074.
- Chekanov, S., *et al.* (ZEUS Collaboration), 2007l, *Eur. Phys. J. C* **50**, 299.
- Chekanov, S., *et al.* (ZEUS Collaboration), 2007m, *Eur. Phys. J. C* **49**, 511.
- Chekanov, S., *et al.* (ZEUS Collaboration), 2007n, *Eur. Phys. J. C* **50**, 283.
- Chekanov, S., *et al.* (ZEUS Collaboration), 2008a, *Phys. Rev. D* **78**, 072001.
- Chekanov, S., *et al.* (ZEUS Collaboration), 2008b, *Nucl. Phys.* **B800**, 1.
- Chekanov, S., *et al.* (ZEUS Collaboration), 2008c, *Eur. Phys. J. C* **55**, 177.
- Chekanov, S., *et al.* (ZEUS Collaboration), 2008d, *J. High Energy Phys.* **06**, 061.
- Chekanov, S., *et al.* (ZEUS Collaboration), 2008e, *Phys. Rev. Lett.* **101**, 112003.
- Chekanov, S., *et al.* (ZEUS Collaboration), 2008f, *Nucl. Phys.* **B792**, 1.
- Chekanov, S., *et al.* (ZEUS Collaboration), 2009a, *J. High Energy Phys.* **05**, 108.
- Chekanov, S., *et al.* (ZEUS Collaboration), 2009b, *Nucl. Phys.* **B816**, 1.
- Chekanov, S., *et al.* (ZEUS Collaboration), 2009c, *J. High Energy Phys.* **06**, 074.
- Chekanov, S., *et al.* (ZEUS Collaboration), 2009d, *J. High Energy Phys.* **04**, 133.
- Chekanov, S., *et al.* (ZEUS Collaboration), 2009e, *J. High Energy Phys.* **02**, 032.
- Chekanov, S., *et al.* (ZEUS Collaboration), 2009f, *J. High Energy Phys.* **12**, 007.
- Chekanov, S., *et al.* (ZEUS Collaboration), 2009g, *J. High Energy Phys.* **04**, 082.
- Chekanov, S., *et al.* (ZEUS Collaboration), 2009h, *Phys. Lett. B* **682**, 8.
- Chekanov, S., *et al.* (ZEUS Collaboration), 2009i, *Eur. Phys. J. C* **60**, 25.
- Chekanov, S., *et al.* (ZEUS Collaboration), 2009j, *Eur. Phys. J. C* **60**, 25.
- Chekanov, S., *et al.* (ZEUS Collaboration), 2009k, *Eur. Phys. J. C* **63**, 527.
- Chekanov, S., *et al.* (ZEUS Collaboration), 2010a, *Nucl. Phys.* **B831**, 1.
- Chekanov, S., *et al.* (ZEUS Collaboration), 2010b, *Eur. Phys. J. C* **65**, 65.
- Chekanov, S., *et al.* (ZEUS Collaboration), 2010c, *Nucl. Phys.* **B827**, 1.
- Chekanov, S., *et al.* (ZEUS Collaboration), 2010d, *Phys. Lett. B* **687**, 16.
- Chekanov, S., *et al.* (ZEUS Collaboration), 2010e, *Phys. Lett. B* **687**, 16.
- Chekanov, S., *et al.* (ZEUS Collaboration), 2010f, *J. High Energy Phys.* **05**, 085.
- Chekanov, S., *et al.* (ZEUS Collaboration), 2012, *Phys. Rev. D* **85**, 052008.
- Chew, G. F., and S. C. Frautschi, 1961, *Phys. Rev. Lett.* **7**, 394.
- Chew, G. F., S. C. Frautschi, and S. Mandelstam, 1962, *Phys. Rev.* **126**, 1202.
- Cho, P. L., and A. K. Leibovich, 1996a, *Phys. Rev. D* **53**, 150.
- Cho, P. L., and A. K. Leibovich, 1996b, *Phys. Rev. D* **53**, 6203.
- Choi, S., *et al.* (AMY Collaboration), 1995, *Phys. Lett. B* **355**, 406.
- Chyla, J., J. Cvach, K. Sedlak, and M. Tasevsky, 2005, *Eur. Phys. J. C* **40**, 469.
- Ciafaloni, M., 1988, *Nucl. Phys.* **B296**, 49.
- Collins, J. C., 1998, *Phys. Rev. D* **57**, 3051; **61**, 019902(E) (1999).
- Collins, J. C., L. Frankfurt, and M. Strikman, 1997, *Phys. Rev. D* **56**, 2982.
- Corcella, G., I. G. Knowles, G. Marchesini, S. Moretti, K. Odagiri, P. Richardson, M. H. Seymour, and B. R. Webber, 2001, *J. High Energy Phys.* **01**, 010.
- Cornet, F., P. Jankowski, and M. Krawczyk, 2004, *Phys. Rev. D* **70**, 093004.
- Cox, B. E., and J. R. Forshaw, 2002, *Comput. Phys. Commun.* **144**, 104.
- Cronin, J., H. J. Frisch, M. Shochet, J. Boymond, P. Piroué, and R. Sumner, 1975, *Phys. Rev. D* **11**, 3105.
- Cudell, J. R., K. Kang, and S. K. Kim, 1997, *Phys. Lett. B* **395**, 311.
- Danilov, M., and R. Mizuk, 2008, *Phys. At. Nucl.* **71**, 605.
- Dederichs, K. H., and M. A. Faessler, 1989, *Phys. Lett. B* **232**, 405.
- de Florian, D., R. Sassot, and M. Stratmann, 2007a, *Phys. Rev. D* **75**, 114010.
- de Florian, D., R. Sassot, and M. Stratmann, 2007b, *Phys. Rev. D* **76**, 074033.
- Denby, B. H., *et al.*, 1984, *Phys. Rev. Lett.* **52**, 795.
- Derrick, M., D. Gacek, N. Hill, B. Musgrave, R. Noland, E. Petereit, J. Repond, R. Stanek, and K. Sugano, 1991, *Nucl. Instrum. Methods Phys. Res., Sect. A* **309**, 77.
- Derrick, M., *et al.* (ZEUS Collaboration), 1992, *Phys. Lett. B* **297**, 404.
- Derrick, M., *et al.* (ZEUS Collaboration), 1993, *Phys. Lett. B* **315**, 481.
- Derrick, M., *et al.* (ZEUS Collaboration), 1994a, *Phys. Lett. B* **322**, 287.

- Derrick, M., *et al.* (ZEUS Collaboration), 1994b, *Phys. Lett. B* **332**, 228.
- Derrick, M., *et al.* (ZEUS Collaboration), 1995a, *Phys. Lett. B* **348**, 665.
- Derrick, M., *et al.* (ZEUS Collaboration), 1995b, *Z. Phys. C* **67**, 93.
- Derrick, M., *et al.* (ZEUS Collaboration), 1995c, *Phys. Lett. B* **346**, 399.
- Derrick, M., *et al.* (ZEUS Collaboration), 1995d, *Z. Phys. C* **67**, 227.
- Derrick, M., *et al.* (ZEUS Collaboration), 1996a, *Z. Phys. C* **70**, 1.
- Derrick, M., *et al.* (ZEUS Collaboration), 1996b, *Phys. Lett. B* **369**, 55.
- Derrick, M., *et al.* (ZEUS Collaboration), 1997, *Z. Phys. C* **73**, 253.
- Devenish, R., and A. Cooper-Sarkar, 2004, *Deep Inelastic Scattering* (Oxford University Press, Oxford), p. 403.
- Diakonov, D., V. Petrov, and M. V. Polyakov, 1997, *Z. Phys. A* **359**, 305.
- Diehl, M., 2003, *Phys. Rep.* **388**, 41.
- Dissertori, G., I. Knowles, and M. Schmelling, 2003, *International Series of Monographs on Physics* (Oxford University Press, New York), Vol. 115, p. 1.
- Dokshitzer, Y. L., 1977, *Sov. Phys. JETP* **46**, 641 [<http://inspirehep.net/search?p=find+j+Sov.Phys.Jetp,46,641>].
- Dokshitzer, Y. L., V. A. Khoze, and T. Sjostrand, 1992, *Phys. Lett. B* **274**, 116.
- Dokshitzer, Y. L., A. Lucenti, G. Marchesini, and G. Salam, 1998, *Nucl. Phys.* **B511**, 396; **B593**, 729(E) (2001).
- Dokshitzer, Y. L., G. Marchesini, and G. Salam, 1999, *Eur. Phys. J. direct C* **1**, 3 [<http://inspirehep.net/search?p=find+eprint+HEP-PH/9812487>].
- Dokshitzer, Y. L., G. Marchesini, and B. Webber, 1996, *Nucl. Phys.* **B469**, 93.
- Dokshitzer, Y. L., and B. Webber, 1995, *Phys. Lett. B* **352**, 451.
- Dokshitzer, Y. L., and B. Webber, 1997, *Phys. Lett. B* **404**, 321.
- Donnachie, A., and P. Landshoff, 1984, *Nucl. Phys.* **B244**, 322.
- Donnachie, A., and P. Landshoff, 1992, *Phys. Lett. B* **296**, 227.
- Donnachie, A., and P. Landshoff, 1998, *Phys. Lett. B* **437**, 408.
- Donnachie, A., and P. V. Landshoff, 1987, *Phys. Lett. B* **191**, 309; **198**, 590(E) (1987).
- Dorfan, D., J. Eades, L. Lederman, W. Lee, and C. Ting, 1965, *Phys. Rev. Lett.* **14**, 1003.
- Dzierba, A. R., C. A. Meyer, and A. P. Szczepaniak, 2005, *J. Phys. Conf. Ser.* **9**, 192.
- Edin, A., G. Ingelman, and J. Rathsman, 1996, *Phys. Lett. B* **366**, 371.
- Eick, W., *et al.*, 1997, *Nucl. Instrum. Methods Phys. Res., Sect. A* **386**, 81.
- Ellis, R. K., W. J. Stirling, and B. Webber, 2003, *QCD and Collider Physics* (Cambridge University Press, Cambridge, England).
- Ellis, S. D., Z. Kunszt, and D. E. Soper, 1992, *Phys. Rev. Lett.* **69**, 3615.
- Ellis, S. D., and D. E. Soper, 1993, *Phys. Rev. D* **48**, 3160.
- Enberg, R., J. R. Forshaw, L. Motyka, and G. Poludniowski, **2003**, *J. High Energy Phys.* **09**, 008.
- Enberg, R., G. Ingelman, and L. Motyka, 2002, *Phys. Lett. B* **524**, 273.
- Enberg, R., L. Motyka, and G. Poludniowski, 2002, *Eur. Phys. J. C* **26**, 219.
- Faiman, D., H. Lipkin, and H. Rubinstein, 1975, *Phys. Lett.* **59B**, 269.
- Feinberg, E., and I. Pomerančuk, 1956, *II Nuovo Cimento Suppl.* **3**, 652.
- Feynman, R. P., 1972, *Photon-Hadron Interactions* (Benjamin, New York).
- Fontannaz, M., J. P. Guillet, and G. Heinrich, 2001, *Eur. Phys. J. C* **21**, 303.
- Fontannaz, M., J. P. Guillet, and G. Heinrich, 2002, *Eur. Phys. J. C* **26**, 209.
- Fontannaz, M., and G. Heinrich, 2004, *Eur. Phys. J. C* **34**, 191.
- Forshaw, J. R., G. Kerley, and G. Shaw, 1999, *Phys. Rev. D* **60**, 074012.
- Forshaw, J. R., and G. Poludniowski, 2003, *Eur. Phys. J. C* **26**, 411.
- Forshaw, J. R., and M. Ryskin, 1995, *Z. Phys. C* **68**, 137.
- Forshaw, J. R., R. Sandapen, and G. Shaw, 2004, *Phys. Rev. D* **69**, 094013.
- Forshaw, J. R., and M. H. Seymour, **1999**, *J. High Energy Phys.* **09**, 009.
- Forshaw, J. R., and P. Sutton, 1998, *Eur. Phys. J. C* **1**, 285 [<http://inspirehep.net/search?p=find+j+Eur.Phys.J.,C1,285>].
- Foster, B., *et al.*, 1993, *Nucl. Phys. B, Proc. Suppl.* **32**, 181.
- Foster, B., *et al.*, 1994, *Nucl. Instrum. Methods Phys. Res., Sect. A* **338**, 254.
- Frankfurt, L., A. Freund, and M. Strikman, 1998, *Phys. Rev. D* **58**, 114001.
- Frankfurt, L., V. Guzey, M. McDermott, and M. Strikman, 2001, [arXiv:hep-ph/0104252](http://arxiv.org/abs/hep-ph/0104252).
- Frankfurt, L., W. Koepf, and M. Strikman, 1996, *Phys. Rev. D* **54**, 3194.
- Frankfurt, L., W. Koepf, and M. Strikman, 1997, *Phys. Lett. B* **405**, 367.
- Frankfurt, L., M. McDermott, and M. Strikman, **2001**, *J. High Energy Phys.* **03**, 045.
- Frankfurt, L., M. Strikman, and M. Zhalov, 2008, *Phys. Lett. B* **670**, 32.
- Frixione, S., 1997, *Nucl. Phys.* **B507**, 295.
- Frixione, S., Z. Kunszt, and A. Signer, 1996, *Nucl. Phys.* **B467**, 399.
- Frixione, S., M. L. Mangano, P. Nason, and G. Ridolfi, 1993, *Phys. Lett. B* **319**, 339.
- Frixione, S., M. L. Mangano, P. Nason, and G. Ridolfi, 1995, *Phys. Lett. B* **348**, 633.
- Frixione, S., P. Nason, and G. Ridolfi, 1995, *Nucl. Phys.* **B454**, 3.
- Frixione, S., and G. Ridolfi, 1997, *Nucl. Phys.* **B507**, 315.
- Frixione, S., and B. R. Webber, **2002**, *J. High Energy Phys.* **06**, 029.
- Gavalian, G., *et al.* (CLAS Collaboration), 2009, *Phys. Rev. C* **80**, 035206.
- Gehrmann-De Ridder, A., T. Gehrmann, and E. Poulsen, 2006a, *Phys. Rev. Lett.* **96**, 132002.
- Gehrmann-De Ridder, A., T. Gehrmann, and E. Poulsen, 2006b, *Eur. Phys. J. C* **47**, 395.
- Gehrmann-De Ridder, A., G. Kramer, and H. Spiesberger, 2000, *Nucl. Phys.* **B578**, 326.
- Gibbs, M., A. Ringwald, and F. Schrempp, 1995, [arXiv:hep-ph/9506392](http://arxiv.org/abs/hep-ph/9506392).
- Ginzburg, I., S. Panfil, and V. Serbo, 1987, *Nucl. Phys.* **B284**, 685.
- Girod, F., *et al.* (CLAS Collaboration), 2008, *Phys. Rev. Lett.* **100**, 162002.
- Gladilin, L., 1999, [arXiv:hep-ex/9912064](http://arxiv.org/abs/hep-ex/9912064).
- Glazov, A. A., 1998, Ph.D. thesis (Humboldt University, Berlin) DESY-THESIS-1998-005.
- Gluck, M., E. Reya, and I. Schienbein, 1999, *Eur. Phys. J. C* **10**, 313.
- Gluck, M., E. Reya, and M. Stratmann, 1996, *Phys. Rev. D* **54**, 5515.
- Goldhaber, G., W. B. Fowler, S. Goldhaber, and T. Hoang, 1959, *Phys. Rev. Lett.* **3**, 181.
- Goldhaber, G., S. Goldhaber, W.-Y. Lee, and A. Pais, 1960, *Phys. Rev.* **120**, 300.
- Golec-Biernat, K. J., and A. Luszczak, 2007, *Phys. Rev. D* **76**, 114014.
- Golec-Biernat, K. J., and M. Wusthoff, 1998, *Phys. Rev. D* **59**, 014017.
- Golec-Biernat, K. J., and M. Wusthoff, 1999, *Phys. Rev. D* **60**, 114023.
- Good, M. L., and W. D. Walker, 1960, *Phys. Rev.* **120**, 1857.

- Gordon, L. E., and J. K. Storrow, 1992, *Phys. Lett. B* **291**, 320.
- Gordon, L. E., and J. K. Storrow, 1994, *Z. Phys. C* **63**, 581.
- Gotsman, E., A. Kormilitzin, E. Levin, and U. Maor, 2007, *Eur. Phys. J. C* **52**, 295.
- Gotsman, E., E. Levin, U. Maor, and E. Naftali, 2002, *Phys. Lett. B* **532**, 37.
- Goulianos, K. A., 1983, *Phys. Rep.* **101**, 169.
- Graudenz, D., 1997, [arXiv:hep-ph/9710244](https://arxiv.org/abs/hep-ph/9710244).
- Gribov, L. V., E. M. Levin, and M. G. Ryskin, 1983, *Phys. Rep.* **100**, 1.
- Gribov, V., 1970, *Sov. Phys. JETP* **30**, 709 [<http://inspirehep.net/search?p=find+j+Sov.Phys.Jetp,30,709>].
- Gribov, V. N., and L. N. Lipatov, 1972, *Sov. J. Nucl. Phys.* **15**, 438 [<http://inspirehep.net/search?p=find+j+Sov.J.Nucl.Phys.,15,438>].
- Gross, D., and F. Wilczek, 1973a, *Phys. Rev. D* **8**, 3633.
- Gross, D., and F. Wilczek, 1973b, *Phys. Rev. Lett.* **30**, 1343.
- H1 Collaboration, 1992, <http://h1.desy.de/e104552/e104555/>.
- Harnew, N., G. P. Heath, M. D. Jeffs, J. Nash, G. L. Salmon, P. D. Shield, D. J. White, and F. F. Wilson, 1989, *Nucl. Instrum. Methods Phys. Res., Sect. A* **279**, 290.
- Harris, B. W., and J. F. Owens, 1997, *Phys. Rev. D* **56**, 4007.
- Harris, B. W., and J. Smith, 1995a, *Nucl. Phys.* **B452**, 109.
- Harris, B. W., and J. Smith, 1995b, *Phys. Lett. B* **353**, 535.
- Harris, B. W., and J. Smith, 1998, *Phys. Rev. D* **57**, 2806.
- Hebecker, A., and T. Teubner, 2001, *Phys. Lett. B* **498**, 16.
- Henning, S., *et al.* (British-Scandinavian-MIT Collaboration), 1978, *Lett. Nuovo Cimento Soc. Ital. Fis.* **21**, 189.
- Hicks, K., 2005a, *J. Phys. Conf. Ser.* **9**, 183.
- Hicks, K. H., 2005b, *Prog. Part. Nucl. Phys.* **55**, 647.
- Hicks, K. H., 2012, *Eur. Phys. J. H* **37**, 1.
- Hoeger, K. C., 1992, in *Proceedings, Physics at HERA, Hamburg*, edited by W. Buchmueller and G. Ingelman (DESY, Hamburg), Vol. 1, p. 43.
- Holtmann, H., G. Levman, N. N. Nikolaev, A. Szczurek, and J. Speth, 1994, *Phys. Lett. B* **338**, 363.
- Iancu, E., K. Itakura, and S. Munier, 2004, *Phys. Lett. B* **590**, 199.
- Ingelman, G., and P. E. Schlein, 1985, *Phys. Lett.* **152B**, 256.
- Ivanov, I., N. Nikolaev, and A. Savin, 2006, *Phys. Part. Nucl.* **37**, 1.
- Jacquet, F., and A. Blondel, 1979, in *Proceedings, Study Of An E P Facility For Europe, Hamburg*, edited by U. Amaldi (DESY, Hamburg), p. 391.
- Jaffe, R. L., 1977, *Phys. Rev. D* **15**, 281.
- Jimenez-Delgado, P., and E. Reya, 2009, *Phys. Rev. D* **79**, 074023.
- Jung, H., 1995, *Comput. Phys. Commun.* **86**, 147.
- Jung, H., 2002, *Comput. Phys. Commun.* **143**, 100.
- Jung, H., and G. P. Salam, 2001, *Eur. Phys. J. C* **19**, 351.
- Juricic, I., *et al.* (MARK II Collaboration), 1989, *Phys. Rev. D* **39**, 1.
- Kaidalov, A., V. Khoze, A. Martin, and M. Ryskin, 2003, *Phys. Lett. B* **567**, 61.
- Kaidalov, A., V. Khoze, A. Martin, and M. Ryskin, 2006, *Eur. Phys. J. C* **47**, 385.
- Kaidalov, A., V. Khoze, A. Martin, and M. Ryskin, 2010, *Eur. Phys. J. C* **66**, 373.
- Kaidalov, A. B., 1979, *Phys. Rep.* **50**, 157.
- Kartvelishvili, V., A. Likhoded, and V. Petrov, 1978, *Phys. Lett.* **78B**, 615.
- Khachatryan, V., *et al.* (CMS Collaboration), 2010, *Eur. Phys. J. C* **70**, 555.
- Khachatryan, V., *et al.* (CMS Collaboration), 2011, *J. High Energy Phys.* **05**, 029.
- Khoze, V., A. Martin, and M. Ryskin, 2006, *Eur. Phys. J. C* **48**, 797.
- Klasen, M., and G. Kramer, 1997, *Z. Phys. C* **76**, 67.
- Klasen, M., and G. Kramer, 2009, *Phys. Rev. D* **80**, 074006.
- Klein, M., and R. Yoshida, 2008, *Prog. Part. Nucl. Phys.* **61**, 343.
- Klempt, E., and A. Zaitsev, 2007, *Phys. Rep.* **454**, 1.
- Knieh, B. A., G. Kramer, and B. Potter, 2000, *Phys. Rev. Lett.* **85**, 5288.
- Knieh, B. A., G. Kramer, and M. Spira, 1997, *Z. Phys. C* **76**, 689.
- Korotkov, V., *et al.* (BBCNC Collaboration), 1993, *Z. Phys. C* **60**, 37.
- Kowalski, H., L. Motyka, and G. Watt, 2006, *Phys. Rev. D* **74**, 074016.
- Kowalski, H., and D. Teaney, 2003, *Phys. Rev. D* **68**, 114005.
- Kramer, M., 1996, *Nucl. Phys.* **B459**, 3.
- Krawczyk, M., and A. Zembrzski, 2001, *Phys. Rev. D* **64**, 114017.
- Kretzer, S., 2000, *Phys. Rev. D* **62**, 054001.
- Krueger, K. (H1 Collaboration), 2009, *Proc. Sci. EPS-HEP2009*, 079.
- Kumericki, K., and D. Mueller, 2010, *Nucl. Phys.* **B841**, 1.
- Kuraev, E. A., L. N. Lipatov, and V. S. Fadin, 1976, *Sov. Phys. JETP* **44**, 443 [<http://inspirehep.net/search?p=find+j+Sov.Phys.Jetp,44,443>].
- Kuraev, E. A., L. N. Lipatov, and V. S. Fadin, 1977, *Sov. Phys. JETP* **45**, 199 [<http://inspirehep.net/search?p=find+j+Sov.Phys.Jetp,45,199>].
- Landshoff, P., and J. Polkinghorne, 1978, *Phys. Rev. D* **18**, 3344.
- Li, Y., *et al.* (AMY Collaboration), 1990, *Phys. Rev. D* **41**, 2675.
- Lipatov, A., and N. Zotov, 2003, *Eur. Phys. J. C* **27**, 87.
- Lipatov, A. V., and N. P. Zotov, 2005, *Phys. Rev. D* **72**, 054002.
- Lipatov, L. N., 1975, *Sov. J. Nucl. Phys.* **20**, 94 [<http://inspirehep.net/search?p=find+j+Sov.J.Nucl.Phys.,20,94>].
- Lipkin, H. J., 1987, *Phys. Lett. B* **195**, 484.
- Lohrmann, E., 2011, [arXiv:1112.3757](https://arxiv.org/abs/1112.3757).
- Lonnblad, L., 1995, *Z. Phys. C* **65**, 285.
- Lotter, H., 1997, *Phys. Lett. B* **406**, 171.
- Low, F., 1975, *Phys. Rev. D* **12**, 163.
- Lukaszk, L., and B. Nicolescu, 1973, *Lett. Nuovo Cimento Soc. Ital. Fis.* **8**, 405.
- Marchesini, G., 1995, *Nucl. Phys.* **B445**, 49.
- Marchesini, G., B. R. Webber, G. Abbiendi, I. G. Knowles, M. H. Seymour, and L. Stanco, 1992, *Comput. Phys. Commun.* **67**, 465.
- Marquet, C., R. B. Peschanski, and G. Soyez, 2007, *Phys. Rev. D* **76**, 034011.
- Martin, A., C. Nockles, M. G. Ryskin, and T. Teubner, 2008, *Phys. Lett. B* **662**, 252.
- Martin, A., M. Ryskin, and G. Watt, 2007, *Phys. Lett. B* **644**, 131.
- Martin, A. D., R. G. Roberts, W. J. Stirling, and R. S. Thorne, 2005, *Eur. Phys. J. C* **39**, 155.
- Martin, A. D., M. Ryskin, and T. Teubner, 1997, *Phys. Rev. D* **55**, 4329.
- Martin, A. D., M. Ryskin, and T. Teubner, 2000, *Phys. Rev. D* **62**, 014022.
- Martin, A. D., W. J. Stirling, R. S. Thorne, and G. Watt, 2009, *Eur. Phys. J. C* **63**, 189.
- Massam, T., T. Muller, B. Righini, M. Schneegans, and A. Zichichi, 1965, *Nuovo Cimento* **39**, 10.
- Miettinen, H. I., and J. Pumplin, 1978, *Phys. Rev. D* **18**, 1696.
- Mirkes, E., and D. Zeppenfeld, 1996, *Phys. Lett. B* **380**, 205.
- Moch, S., A. Ringwald, and F. Schrempp, 1997, *Nucl. Phys.* **B507**, 134.
- Mueller, A. H., 1970, *Phys. Rev. D* **2**, 2963.
- Mueller, A. H., 1990, *Nucl. Phys.* **B335**, 115.
- Mueller, A. H., and W.-K. Tang, 1992, *Phys. Lett. B* **284**, 123.
- Nagy, Z., and Z. Trocsanyi, 2001, *Phys. Rev. Lett.* **87**, 082001.
- Nason, P., 2004, *J. High Energy Phys.* **11**, 040.
- Navin, S., 2010, [arXiv:1005.3894](https://arxiv.org/abs/1005.3894).
- Newman, P., and M. Ruspia, 2009, [arXiv:0903.2957](https://arxiv.org/abs/0903.2957).
- Newman, P. R., 2005, [arXiv:hep-ex/0511047](https://arxiv.org/abs/hep-ex/0511047).
- Nicholls, T., M. Charlet, J. Coughlan, E. Elsen, D. Hoffmann, H. Krehbiell, H.-C. Schultz-Coulon, J. Schutt, and F. Sefkow, 1998, *IEEE Trans. Nucl. Sci.* **45**, 810.

- Nikolaev, N., and B. G. Zakharov, 1992, *Z. Phys. C* **53**, 331.
- Nikolaev, N. N., and B. Zakharov, 1991, *Z. Phys. C* **49**, 607.
- Nikolaev, N. N., B. Zakharov, and V. Zoller, 1996, *Phys. Lett. B* **366**, 337.
- Nisius, R., 2000, *Phys. Rep.* **332**, 165.
- Nussinov, S., 1975, *Phys. Rev. Lett.* **34**, 1286.
- Okorokov, V., 2012, *Int. J. Mod. Phys. A* **27**, 1250037.
- Perez, E., and E. Rizvi, 2013, *Rep. Prog. Phys.* **76**, 046201.
- Petersen, A., *et al.*, 1988, *Phys. Rev. D* **37**, 1.
- Peterson, C., D. Schlatter, I. Schmitt, and P. M. Zerwas, 1983, *Phys. Rev. D* **27**, 105.
- Pitzl, D., *et al.*, 2000, *Nucl. Instrum. Methods Phys. Res., Sect. A* **454**, 334.
- Polini, A., *et al.*, 2007, *Nucl. Instrum. Methods Phys. Res., Sect. A* **581**, 656.
- Politzer, H. D., 1973, *Phys. Rev. Lett.* **30**, 1346.
- Politzer, H. D., 1974, *Phys. Rep.* **14**, 129.
- Poludniowski, G., R. Enberg, J. R. Forshaw, and L. Motyka, **2003**, *J. High Energy Phys.* **12**, 002.
- Potter, B., 1999, *Comput. Phys. Commun.* **119**, 45.
- Rathsman, J., 1999, *Phys. Lett. B* **452**, 364.
- Regge, T., 1959, *Nuovo Cimento* **14**, 951.
- Regge, T., 1960, *Nuovo Cimento* **18**, 947.
- Rezaeian, A. H., M. Siddikov, M. Van de Klundert, and R. Venugopalan, 2013, *Phys. Rev. D* **87**, 034002.
- Ringwald, A., and F. Schrempp, 1994, [arXiv:hep-ph/9411217](https://arxiv.org/abs/hep-ph/9411217).
- Ringwald, A., and F. Schrempp, 1998, *Phys. Lett. B* **438**, 217.
- Ringwald, A., and F. Schrempp, 1999, *Phys. Lett. B* **459**, 249.
- Ringwald, A., and F. Schrempp, 2000, *Comput. Phys. Commun.* **132**, 267.
- Ringwald, A., and F. Schrempp, 2001, *Phys. Lett. B* **503**, 331.
- Royon, C., L. Schoeffel, J. Bartels, H. Jung, and R. B. Peschanski, 2001, *Phys. Rev. D* **63**, 074004.
- Ryskin, M., 1993, *Z. Phys. C* **57**, 89.
- Ryskin, M., A. Martin, and V. Khoze, 2011, *Eur. Phys. J. C* **71**, 1617.
- Salam, G. P., and G. Soyez, **2007**, *J. High Energy Phys.* **05**, 086.
- Schael, S., *et al.* (ALEPH Collaboration), 2006, *Phys. Lett. B* **639**, 192.
- Schilling, K., and G. Wolf, 1973, *Nucl. Phys.* **B61**, 381.
- Sefkow, F., E. Elsen, H. Krehbiel, U. Straumann, and J. Coughlan, 1995, *IEEE Trans. Nucl. Sci.* **42**, 900.
- Seymour, M. H., 1994, *Nucl. Phys.* **B421**, 545.
- Seymour, M. H., 1996, *Phys. Lett. B* **378**, 279.
- Shambroom, W., *et al.*, 1982, *Phys. Rev. D* **26**, 1.
- Sjostrand, T., 1994, *Comput. Phys. Commun.* **82**, 74.
- Sjostrand, T., S. Mrenna, and P. Skands, **2006**, *J. High Energy Phys.* **05**, 026.
- Sjostrand, T., P. Edén, C. Friberg, L. Lönnblad, G. Miu, S. Mrenna, and E. Norrbin, 2001, *Comput. Phys. Commun.* **135**, 238.
- Slominski, W., H. Abramowicz, and A. Levy, 2006, *Eur. Phys. J. C* **45**, 633.
- Smith, W. H., K. Tokushuku, and L. W. Wiggers, 1992, in *Proceedings of the 10th International Conference on Computing in High Energy Physics (CHEP 92), Annecy, France* (CERN, Geneva).
- Steinhart, J., 1999, Ph.D. thesis (Hamburg University), DESY-THESIS-1999-029.
- Streng, K. H., T. F. Walsh, and P. M. Zerwas, 1979, *Z. Phys. C* **2**, 237.
- Strottman, D., 1979, *Phys. Rev. D* **20**, 748.
- Szczurek, A., N. N. Nikolaev, and J. Speth, 1998, *Phys. Lett. B* **428**, 383.
- Thacker, B., and G. P. Lepage, 1991, *Phys. Rev. D* **43**, 196.
- 't Hooft, G., 1976a, *Phys. Rev. D* **14**, 3432; **18**, 2199(E) (1978).
- 't Hooft, G., 1976b, *Phys. Rev. Lett.* **37**, 8.
- Toll, T., 2010, Ph.D. thesis (Hamburg University), DESY-THESIS-2010-004.
- Trentadue, L., and G. Veneziano, 1994, *Phys. Lett. B* **323**, 201.
- Uematsu, T., and T. Walsh, 1981, *Phys. Lett.* **101B**, 263.
- Van Esch, P., *et al.*, 2000, *Nucl. Instrum. Methods Phys. Res., Sect. A* **446**, 409.
- von Weizsacker, C. F., 1934, *Z. Phys.* **88**, 612.
- Voss, G., and B. Wiik, 1994, *Annu. Rev. Nucl. Part. Sci.* **44**, 413.
- Williams, E. J., 1934, *Phys. Rev.* **45**, 729.
- Wing, M. (ZEUS Collaboration), 2002, [arXiv:hep-ex/0206036](https://arxiv.org/abs/hep-ex/0206036).
- Wolf, G., 2010, *Rep. Prog. Phys.* **73**, 116202.
- Wusthoff, M., 1997, *Phys. Rev. D* **56**, 4311.
- Yao, W., *et al.* (Particle Data Group), 2006, *J. Phys. G* **33**, 1.
- Zembruski, A., and M. Krawczyk, 2003, [arXiv:hep-ph/0309308](https://arxiv.org/abs/hep-ph/0309308).
- ZEUS Collaboration, 1992, http://www-zeus.desy.de/zeus_papers/zeus_papers.html.
- ZEUS Collaboration, 1993, *The ZEUS Detector*, edited by U. Holm, Status Report (unpublished), DESY, <http://www-zeus.desy.de/bluebook/bluebook.html>.
- Zotov, N., and V. Tsarev, 1988, *Sov. Phys. Usp.* **31**, 119.